Herausgeber
Tom Lahmer Timon Rabczuk Carsten Könke

ISM-Bericht ISSN: 1610-7381
Institut für Strukturmechanik
Fakultät Bauingenieurwesen
Bauhaus-Universität Weimar
Marienstraße 15
D-99423 Weimar
Germany

Tel. +49 (0)3643/584504
Fax. +49 (0)3643/584514

http://www.uni-weimar.de/Bauing/ism

Reference Surface-Based System Identification

(Referenzflächen-basierte Systemidentifikation)

DISSERTATION

zur Erlangung des akademischen Grades

Doktor-Ingenieur (Dr.-Ing.)

an der Fakultät Bauingenieurwesen

der Bauhaus-Universität Weimar

vorgelegt von

Sofyan Ahmad
geb. am 18.08.1975 in Sigli, Indonesien

Weimar, Mai 2013

Gutachter:

Prof. Dr.-Ing. habil. Carsten Könke
Prof. Dr.techn. Christian Bucher
Prof. Dr.-Ing. Frank Wuttke

Tag der Disputation: 5. September 2013

To my beloved wife, Odra
&
to my dearest daughters, Nafeiza and Naira.

Acknowledgements

Foremost, I would like to express my deepest appreciation and gratitude to my supervisor Professor Carsten Könke, for his encouragement, guidance, and support from the initial to the final stages of my research work. I would also like to thank Dr. Volkmar Zabel for his assistance during my work. I appreciate his contributions of time, ideas and openness in discussions.

I am indebted to Professor Bucher for his constructive feedback, and insightful discussions in Weimar and Wien. My sincere thanks go to Professor Tom Lahmer, for his support and time for discussion about model approximation.

I would like to thank all my colleagues and friends at ISM. Special thanks go to Simon Höll, Albrecht Schmidt, Dr. Maik Brehm, Dr. Torsten Luther and Daniel Arnold. They helped me to deal with German scripts, numerical methods, and computer problems.

Lastly, I would like to express my biggest gratitude to my family, particularly to my parents for their constant supports and encouragement.

Sofyan Ahmad

Weimar, May 2013

Abstract

Environmental and operational variables and their impact on structural responses have been acknowledged as one of the most important challenges for the application of the ambient vibration-based damage identification in structures. The damage detection procedures may yield poor results, if the impacts of loading and environmental conditions of the structures are not considered.

The reference-surface-based method, which is proposed in this thesis, is addressed to overcome this problem. In the proposed method, meta-models are used to take into account significant effects of the environmental and operational variables. The usage of the approximation models, allows the proposed method to simply handle multiple non-damaged variable effects simultaneously, which for other methods seems to be very complex. The input of the meta-model are the multiple non-damaged variables while the output is a damage indicator.

The reference-surface-based method diminishes the effect of the non-damaged variables to the vibration based damage detection results. Hence, the structure condition that is assessed by using ambient vibration data at any time would be more reliable. Immediate reliable information regarding the structure condition is required to quickly respond to the event, by means to take necessary actions concerning the future use or further investigation of the structures, for instance shortly after extreme events such as earthquakes.

The critical part of the proposed damage detection method is the learning phase, where the meta-models are trained by using input-output relation of observation data. Significant problems that may encounter during the learning phase are outlined and some remedies to overcome the problems are suggested.

The proposed damage identification method is applied to numerical and experimental models. In addition to the natural frequencies, wavelet energy and stochastic subspace damage indicators are used.

Kurzfassung

Umwelt- oder betriebsbedingte Veränderungen von Strukturen und deren Auswirkungen auf das Antwortverhalten stellen große Herausforderungen für die Anwendung von Schadensdetektion basierend auf ambient angeregten Schwingungen dar. Die Schadensdetektionsverfahren können zu schlechten Ergebnissen führen, wenn die Last- und Umgebungsbedingungen der Strukturen nicht berücksichtigt werden.

In dieser Arbeit wird eine auf Referenzflächen basierende Methode vorgeschlagen, die das Ziel hat dieses Problem zu überwinden. In dem vorgeschlagenen Verfahren werden Metamodelle genutzt, um signifikante Effekte der Umwelt- und Betriebsbedingungen zu berücksichtigen. Die Verwendung von Approximationsmodellen erlaubt Effekte, die nicht zur Schädigung führen, simultan zu betrachten, was sich bei anderen Identifikationsmethoden als schwierig erweist. Diese Metamodelle besitzen als Eingangsgrößen schädigungsirrelevante Variablen, während ein Schadensindikator die Ausgangsgröße ist.

Die auf Referenzflächen basierende Methode verringert den Einfluss von schadensirrelevanten Veränderungen auf die Ergebnisse der auf Schwingungen basierten Schadensdetektion. Daher wird der ermittelte Strukturzustand verlässlicher bewertet, wenn kontinuierlich ambient angeregte Schwingungsdaten (bei unterschiedlichen Umgebungszuständen) beurteilt werden. Es werden instantan verlässliche Informationen über den Zustand der Struktur benötigt, um z.B. schnell nach extremen Ereignissen wie Erdbeben über die weitere Nutzung oder die intensivere Untersuchung der Struktur entscheiden zu können.

Die kritische Phase der vorgeschlagenen Schadensdetektionsmethode ist die Lernphase, bei der die Metamodelle durch Eingangs-Ausgangs-Beziehungen der Beobachtungsdaten trainiert werden. Es werden relevante Probleme, die während der Lernphase entstehen können, aufgezeigt und es werden einige Abhilfen vorgeschlagen, um diese Probleme zu beseitigen. Die vorgestellte Schadensdetektion wurde auf numerische und experimentelle Modelle angewendet. Zusätzlich zu den Eigenfrequenzen wurden Wavelet-Energien und Schadensindikatoren, die auf stochastischen Unterräume basieren, genutzt.

Contents

List of Figures

Nomenclature

Abbreviations

ANN Artificial neural networks

DoE Design of experiments

DP Damage detection points

LHS Latin hypercube sampling

MAC Modal assurance criteria

MLS Moving least squares

MSCC Mode shape correlation coefficient

MSE Mean squared error

MSF Modal scale factor

NMD Normalized mode difference

RBF Radial basis function

RSM Response surface methodology

SSI Stochastic subspace identification

Vibration-based Damage Indicator

$[\Phi]$ Eigenvectors

$[C_2]$ Damping matrix

$[K]$ Stiffness matrix

$[M]$ Mass matrix

$\ddot{q}(t)$ Acceleration

$\dot{q}(t)$ Velocity

ψ Mother wavelet

$\psi_{a,b}$ Dilated and translated mother wavelet in continuous wavelet analysis

$\psi_{m,n}$ Dilated and translated mother wavelet in discrete wavelet analysis

φ Scaling function

$\varphi_{m,n}$ Dilated and translated scaling function

$\{\omega\}$ Eigen frequency

a Scaling parameter in continuous wavelet analysis

b Translation parameter in continuous wavelet analysis

$C_{m,n}$ Wavelet approximation coefficients

$D_{m,n}$ Wavelet detail coefficients

$f(\omega)$ Fourier transform of a function $f(t)$

$F(t)$ External force

$f_w(\omega, \tau)$ Windowed Fourier transform of a function $f(t)$

M Highest wavelet decomposition level

t Time variable

V_m, W_m Subspaces of a multi-scale analysis

$q(t)$ Displacement

Experimental Structural Dynamics

$\hat{q}$ Estimate value of q

λ Eigenvalue

Φ Eigenvector matrix

ϕ Eigenvector of a mode shape

ϕ_A Eigenvector of a numerical or analytical mode shape

ϕ_X Eigenvector of an experimental mode shape

ψ Orthogonal eigenvectors

Ψ_0^2 Variance of stationary Gaussian measurement white noise N

E Expected value

f_{Nyq} Nyquist frequency

f_s Sampling frequency

I identity matrix

N Stationary Gaussian measurement white noise

Q Fisher information matrix

q Target modal response

y Sensor response vector

Δt Time step

Response Surface Methodology

α Shape parameter

β Regression coefficients

$\hat{y}$ Approximation response value

λ Regularization parameter

Ψ Gram matrix

ε Approximate error

φ Basis function

c Interpolation coefficients

D Influence radius

m Polynomial order

r	The distance between approximated point and support points
R^2	Coefficient of determination
R^2_{adj}	Adjusted coefficient of determination

Chapter 1

Introduction

1.1 Motivation

The application of structural health monitoring in civil engineering is motivated by two major aspects, life safety and economic benefits. The chance to avoid a sudden collapse of bridges, buildings, etc., increases by having continuous inspection of their health condition. An appropriate repair or rehabilitation can prevent a rapid degradation of the structural performance due to damages and optimize the maintenance cost. Damage, in this context, can be defined as changes in the material or geometrical properties of the system that can reduce their structural performance. Some examples of common damages are cracks and spalling in concrete or corrosion in steel elements. However, a change in boundary condition or system connectivity of the structure is also classified as damage. A loose bolt or rivet, for instance, will reduce the structural stiffness and stability, and can lead to higher displacements or structural instability. Moreover, it could promote damages in other structure's components.

Ideally, damage in a structure should be handled properly and immediately during its initiation period. Late or inappropriate handling of damage tends to propagate and promotes more serious effects on the structure, and has a strong impact on the maintenance cost and human risk accordingly. Therefore, discovering the damage in an early state before it has been fully developed is very important. A piece of information about the presence of damage in structure guides the owner to perform further actions in order to prevent an acceleration of the structural deterioration.

Periodic maintenance has a strong impact on the reliability, maintenance cost and service

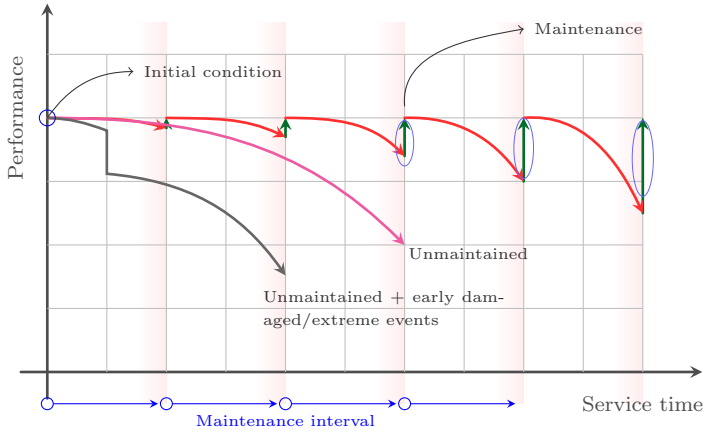

Figure 1.1: Degradation of performance with respect to service time

life of a structure. Figure 1.1 illustrates the performance and service life comparison between a structure that has regular maintenance and structure without any maintenance. The performance of the unmaintained structure decreases significantly over time and possibly cannot reach its service life target without extensive rehabilitation. On the other hand, the well-maintained structure preserves its level of performance by assigning necessary repairs. In this case, a periodic non-destructive test is scheduled to deal with damage issues and then repairs are planned according to the test result. However, it should be noted that there is a trade-off between investigation frequency and maintenance cost. A more frequent periodic investigation increases the probability to find damages in their early state. However, more tests lead to higher cost, time consumption and user inconvenience.

Basically, regular periodic investigations can deal with ordinary events such as damage due to aging. However, early damages may immediately take place due to factors such as inappropriate design assumption, elements connectivity, material imperfection, and overloading. This kind of damage is difficult to predict and the maintenance should not be delayed until the next scheduled investigation. Furthermore, extreme events such as earthquake or blast loading may occur anytime. For important structures such as bridges and public buildings, the site investigation and maintenance has a strong impact on the economic mobility of the community. Hence, the assessment of the load carrying capacity of these structures following extreme events is of vital importance for decisions about on the repair and rehabilitation actions for the structure's future use.

The structural performance can be assessed anytime by applying a long term monitoring system to the structures. The monitoring system can be customized to work automatically on a regular basis. It can be used also to assess the conditions on certain occasions, for

example, following an extreme event such as an earthquake. In this context, the vibration-based damage identification approach becomes common in practice. Damages change the vibration characteristics of structures. Based on this concept, several damage detection methods have been developed by different research groups within the last decades. Many damage indicators such as eigen frequency and modal displacement have been applied with various success.

New advances in the system identification of a mechanical structure allow the vibration-based damage identification method to utilize ambient excitations. The modal properties are extracted by using output only data, where the excitation forces are not measured. However, vibration responses of most civil engineering structures are also significantly affected by its operational or environmental conditions. The system identification of a structure may yield different results if the operational and environmental conditions are different.

The dynamic response of a bridge due to passing vehicles for instance is significantly affected by vehicle characteristics such as speed, axle configuration, and weight. Furthermore, temperature changes alter some material properties of the structure's components that may lead to different dynamic responses. Many papers report that ambient temperature has a significant effect on the results of the modal frequency measurement of structures e.g. in [Cornwell *et al.*, 1999b], [Sohn *et al.*, 1999] and [Peeters & De Roeck, 2001]. In this situation, the abnormality that is recognized by observing the dynamic responses becomes obscure, and it is not clear whether it has been caused by damages or environmental effects only. The reliability of structural health monitoring systems that do not include significant operational and environmental conditions will be questioned. The structural health monitoring systems will not be accepted in practical applications unless robust techniques are developed to explicitly account for environmental and operational conditions, [Sohn, 2008]. The environmental and operational variables are often called non-damaged variables.

Some strategies could be developed to reduce the impact of non-damaged parameters on the result of the vibration-based damage identification method. One strategy is to use damage indicators that are less sensitive to non-damaged parameters. Basically, the damage indicators that are sensitive to damages are also often sensitive to non-damaged variables. Another strategy is to perform post-processing on the damage identification results, in order to subtract the effect of the environmental variable such as temperature. However, this approach seems to be more complex if multiple non-damaged variables are

considered. This thesis proposes an approximation strategy to take into account non-damaged variables that have significant impacts on the dynamic response of structures.

1.2 Aim and Scope of Work

This thesis proposes the reference surface-based method for system identification of structures. The proposed method is a combination of the vibration-based damage identification and the response surface methodology. It allows to accommodate the influence of environmental and operational conditions on structures into the damage detection procedure. In the proposed damage identification method, multiple non-damaged variables can be easily handled, while this seems to be very complex for other methods.

The main focus of this research is to observe the capability of the reference surface-based system identification method to assess the health condition of structures with a given operational and environmental condition. The healthy condition of the structure is described by a meta-model, the reference surface model. Damage detection is done by comparing the recent response to the reference surface model.

The study begins by observing the vibration-based damage indicators that can be applied to the reference surface-based method. Instead of eigen frequency, wavelet-based and stochastic subspace identification damage indicators are used. Meanwhile, global polynomial regression, radial basis function, moving least squares, and artificial neural networks approximation methods are used to build the reference surface models.

The reference surface-based system identification method is applied to numerical and experimental models. A train passing over a concrete filler beam bridge model is used as numerical model. In this simulation study, the temperature and train speed are chosen as environmental and operational conditions, respectively. An elastically supported steel IPE-80 beam is chosen as the experimental model. Three non-damaged variables are considered, all of which support stiffness, impulse force, and additional mass.

1.3 Outline of The Thesis

In Chapter 2, several vibration-based damage indicators are briefly presented. First, modal-based damage indicators are described. Second, wavelet-based damage indicators

are discussed. Finally, the stochastic subspace damage indicator is discussed. The advantages and drawbacks of these damage indicators are highlighted.

Chapter 3 elaborates several important aspects in experimental structural dynamics in order to obtain as much information as possible from a dynamic testing. At the beginning, the sampling rate will be discussed, followed by an elaboration of methods used to find the best location to place the reference sensor. Methods that can be used to compare numerical and experimental modal analysis results are also discussed in this chapter.

Chapter 4 presents the design of experiments and scattered data approximation methods. This chapter also provides a brief description of the model selection, model validation, and sensitivity analysis.

Chapter 5 introduces the basic concept of the reference surface-based system identification. The backgrounds, advantages and detail procedures of the proposed damage detection method are briefly elaborated.

Chapter 6 presents the application of the proposed damage identification method to a numerical Finite Element model. The Finite Element model is a filled concrete beam railway bridge that is excited by the passing of ICE-3 train model. The temperature and train speed are varied in order to introduce the environmental and operational conditions, respectively.

In Chapter 7, the proposed damage identification method is applied to a physical structure. The experimental model is a 3300 mm length IPE-80 steel beam. The beam is supported by two springs. The variation of surrounding temperature considered as the first non-damaged variable. It is taken into account by modifying the spring stiffness. An additional mass is attached to the beam to introduce the second non-damaged variable. The third non-damaged variable is the amplitude of impulse force.

Chapter 8 summarizes some important results of the proposed method. Furthermore, some limitation and restriction of the method also pointed out. Finally, possible future developments and improvements of the reference surface-based system identification method are highlighted.

Chapter 2

Vibration-based Damage Indicators

2.1 Introduction

An important breakthrough in long-term structural health monitoring was the application of vibration data for damage identification. Given recent developments, it is now possible to perform damage identification procedure using output data only, and information of the excitation forces is not required. In this case, dynamic response signals resulting from ambient excitations (e.g., traffic, pedestrian walks, and wind) are used. The measurement, signal processing, and damage indicator extraction can be integrated and programmed to work automatically according to a regular schedule or shortly after extreme events. Moreover, data acquisition systems can be connected to the internet or a wireless device that allows the monitoring system to be controlled from a place far from the location of structures. The vibration-based damage identification method seems to be a good approach for the modern concept of a long-term structural health monitoring system.

The vibration-based damage identification method emerged in the 1970s in the offshore oil industry. Basically, it was addressed to the structural reliability assessment of offshore platforms. In this context, the use of the vibration-based damage identification method is motivated by a specific reason; the location of damages in the structure is unknown and often inaccessible. In this situation, local inspections are costly and nearly impossible. Several studies have addressed this topic, for instance [Vandiver, 1977], [Begg *et al.*, 1976], and [Wojnarowski *et al.*, 1977]. In the 1980s, the vibration-based damage identification concept was also applied to civil engineering fields. Modal properties were used to distinguish damaged and undamaged conditions in civil engineering structures, such as bridges, buildings, etc. A general overview about the development of the vibration-based damage

identification can be found in [Doebling *et al.*, 1998].

The basic concept of the vibration-based damage identification method is quite simple; changes in physical or material properties of structures lead to alterations in dynamic properties and response signals. Damages in a structure constitute reductions in physical properties (e.g., cross-sectional area), material properties (e.g., Young's modulus), and the stiffness of connection systems (e.g., tightness of bolts). These reductions lead to alterations in global stiffness, masses, and damping of the structures. A quantity that can be used to identify the existence of damage in a structure is called a damage indicator, [Rytter, 1993]. Several damage indicators have been proposed to be applied in the vibration-based damage identification method. Section 2.2, 2.3, and 2.4 briefly describe some of these damage indicators.

2.2 Modal-Based Damage Indicator

The modal-based damage indicator is probably the most commonly used indicator for vibration-based damage identification of structures. The presence of damage alters the modal properties of the structures. The alteration can be observed through natural frequencies and mode shapes.

The equation of motion of a viscously damped system can be written as

$$[M]\{\ddot{q}(t)\} + [C_2]\{\dot{q}(t)\} + [K]\{q(t)\} = \{F(t)\}, \tag{2.1}$$

where $[M]$, $[C_2]$, and $[K]$ are mass, damping, and stiffness matrices, respectively. $[C_2]$ is used instead of $[C]$ to avoid confusion in other subsections. The displacement, velocity, and acceleration vectors are $\{q(t)\}$, $\{\dot{q}(t)\}$, and $\{\ddot{q}(t)\}$, respectively. $\{F(t)\}$ represents the excitation forces. The modal characteristics of undamped or lightly-damped systems can be determined by solving the following eigenvalue equation

$$([K] - \{\omega^2\}[M])[\Phi] = 0, \tag{2.2}$$

where $\{\omega\}$ and $[\Phi]$ are eigen frequencies and eigenvectors, respectively. Several algorithms can be used to solve the eigenvalue problem, for instance QR method, Rayleigh-Ritz method, Jacobi iteration method, and subspace iteration methods. Detailed description about these methods can be found in many standard books about structural dynamics or Finite Element analysis, e.q. [Bathe, 1982].

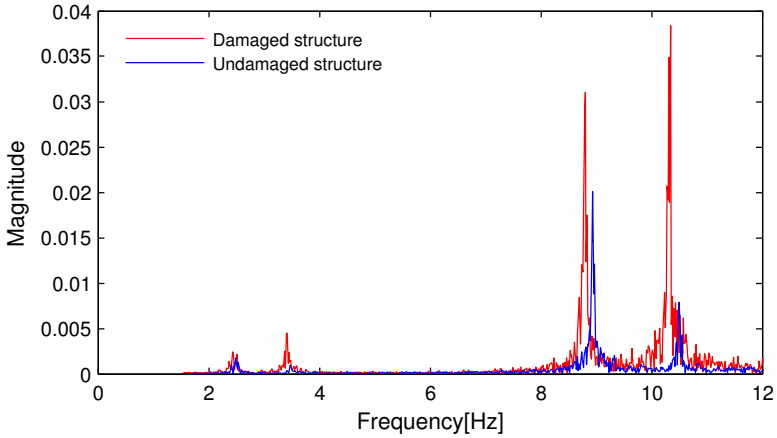

Figure 2.1: Frequency shifted due to damage in structure.

The modal parameters of a physical model are obtained by performing a so-called experimental modal analysis or modal testing. Time history of measured response signals can be transformed into frequency domain to obtain the frequency content of signals. However, greater effort is required to identify the mode shapes.

2.2.1 Natural Frequency

The natural frequency is the most widely used indicator for vibration-based damage identification; it is relatively simple and cheap to acquire. The natural frequencies content of a structure can be observed from a single response signal. However, a significant damage may cause only a small change in natural frequencies. A review of the use of natural frequencies for damage identification is presented in [Salawu, 1997].

Figure 2.1 illustrates the frequency response plot comparison of a damaged and undamaged structure. The damage shifts the peaks of the frequency response plot. The shift may not be the same for all eigen modes; higher frequency mode usually shows larger changes compared to the lower ones. Damage is a local phenomenon, whereby it may be easily captured by higher frequency modes that associate with local responses. The lower modes tend to present global responses of the structures. It is often not sensitive to small local changes.

2.2.2 Modal Displacement

Modal displacement can deliver clearer differences between damaged and undamaged conditions of a structure when compared to the eigen frequency. Mode shapes introduce spatial information about the damage. A higher frequency mode shape may be more sensitive to damage when compared to lower ones. However, the sensitivity of the modal displacement damage indicator also depends on the geometry of the structure, the monitoring point, and the damage location, and damage severity. The usage of a dense sensor arrays increases the probability of capturing local mode shapes associated with the damage.

Instead of comparing mode shapes, some researchers suggest using the derivative of the mode shape as a damage indicator. The curvature mode shape damage indicator has been suggested by [Pandey *et al.*, 1991]. The curvature values are computed from modal displacement using central difference method. Changes in modal strain energy have been used for damage indicator by [Stubbs *et al.*, 1992] and [Cornwell *et al.*, 1999a].

2.3 Wavelet-Based Damage Indicator

The wavelet transform is a tool that cuts up data or functions or operators into different frequency components, and then studies each component with a resolution matched to its scale [Daubechies, 1992]. Time-frequency decomposition gives the wavelet transform advantages over the traditional Fourier transform in analyzing non-stationary signals. The wavelet transform is analogous to short-time Fourier transform with different window sizes. It allows performing a local analysis to a signal and reveals some of its hidden aspects. Therefore, it makes sense to apply the wavelet transform to the vibration-based damage identification method.

The application of the wavelet transform in structural damage identification has been proposed by many researchers. For instance, [Sun & Chang, 2002] used the wavelet packet transform to develop a so-called statistical pattern classification for structural health monitoring. The wavelet transform was combined with the Shannon entropy to detect and locate damage in a simple supported steel beam, [Ren & Sun, 2008]. [Zabel, 2003] applied the wavelet analysis to identify damage in a reinforced concrete beam. [Brehm & Zabel, 2008] reported that the results of numerical study show that wavelet energy and wavelet entropy damage indicators are much more sensitive in comparison to natural frequency or modal displacement.

The following subsection presents some theoretical background about the wavelet transform. This is followed by a description of wavelet energy and wavelet entropy damage indicators. The wavelet energy damage indicator is applied to a numerical Finite Element and experimental models and will be presented in Chapter 6 and Chapter 7.

2.3.1 Wavelet Analysis

The history of wavelet transform was started in 1909 when Alfred Haar introduced rectangular basis functions. However, the term wavelet was firstly used by Jean Morlet to describe the resulting waveforms of varying window width in short-time Fourier transform [Gao & Yan, 2009]. The theoretical formulation of wavelet transform was first published in [Grossmann & Morlet, 1984]. The important breakthrough in wavelet analysis emerged in the late 1990s. Stephane Mallat proposed the multiresolution analysis to construct wavelet bases. Around the same times, Ingrid Daubechies introduced a so-called Daubechies wavelet base. The theory of wavelet transform is described in many literature, for example, [Newland, 1993], [Daubechies, 1992], and [Zabel, 2003]. For the purpose of this study, theoretical background of wavelet analysis is presented in this subsection.

The most widely used signal processing tool is probably the Fourier transform. It converts a function $f(t)$ from time domain into frequency domain as follows

$$f(\omega) = \frac{1}{\sqrt{2\pi}} \int_{-\infty}^{\infty} f(t) e^{-i\omega t} dt. \tag{2.3}$$

The Fourier transform provides information about the frequency content of a signal but it does not provides information concerning time localization. Therefore the Fourier transform is not suitable for observing non-stationary or time-varying signals. The short-time Fourier transform was introduced to overcome the limitation of the Fourier transform [Gabor, 1946]. It employs a window function $w(\tau)$ to extract signal in window position; as such, it is called windowed Fourier transform. The signal within the window is analyzed by using the Fourier transform to obtain the time-frequency information. Subsequently, the window is slid along the time line to analyze the signal in other positions. The choice of the window function affects the time and frequency resolution of the results. The windowed Fourier transform is described as

$$f_w(\omega, \tau) = \frac{1}{\sqrt{2\pi}} \int_{-\infty}^{\infty} w(t-\tau) f(t) e^{-i\omega t} dt. \tag{2.4}$$

Similar to the windowed Fourier transform in, the wavelet approach transforms the signal by multiplying it with a function of two variables. However, in contrast to the short-time Fourier transform technique where the window size is fixed, the wavelet enables variable window size in analyzing different frequency components in a signal [Mallat, 1998]. The continuous wavelet transform of a signal $f(t)$ can be expressed as

$$W_{\psi}^{f}(a,b) = |a|^{-1/2} \int_{-\infty}^{\infty} f(t)\psi^{*}\left(\frac{t-b}{a}\right) \mathrm{d}t, \tag{2.5}$$

where ψ^* denotes the complex conjugate of ψ. In the Equation (2.5), the function $f(t)$ is multiplied by a function of two variables,

$$\psi_{a,b}(t) = |a|^{-1/2}\, \psi\left(\frac{t-b}{a}\right). \tag{2.6}$$

The term wavelet is used to describe the function $\psi_{a,b}$, which is actually the dilated (stretched or compressed) and translated versions of the mother wavelet ψ. The variable a represents the scaling parameter that determines the time and frequency resolution of the scaled base wavelet. The variable b is the shifting parameter, which translates the scaled base wavelet along the time axis. It is assumed that the mean value of the function ψ is zero,

$$\int_{-\infty}^{\infty} \psi(t)dt = 0. \tag{2.7}$$

Several types of wavelet families are known, such as Mexican Hat, Meyer, Haar, Morlet and Daubechies. Figure 2.2 shows examples of mother wavelets.

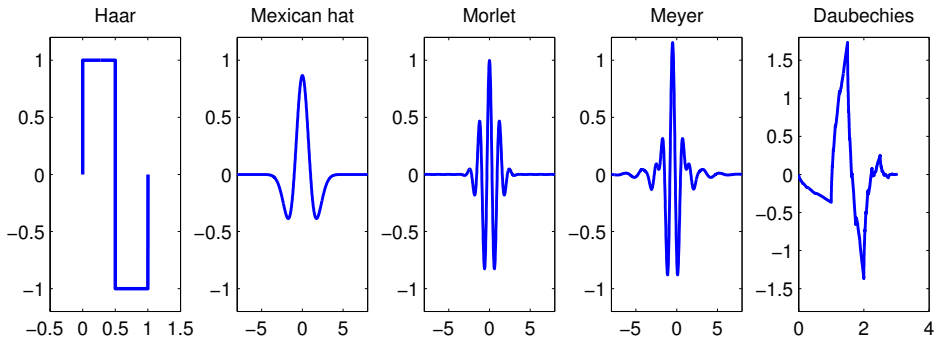

Figure 2.2: Different types of mother wavelets

In most applications, only samples or discrete values of a signal are available. In this case, the parameter a and b in the Equation (2.6) become discrete values,

$$a = {a_0}^m, \qquad b = n\, b_0\, {a_0}^m, \tag{2.8}$$

where $m, n \in \mathbb{Z}$, $a_0 > 1$, and $b_0 > 0$ [Daubechies, 1992]. By substituting these constants, the equation Equation (2.6) becomes

$$\psi_{m,n}(t) = a_0^{-\frac{m}{2}} \psi \left(\frac{t - n\, b_0\, {a_0}^m}{{a_0}^m} \right) = a_0^{-\frac{m}{2}} \psi \left(a_0^{-m} t - n\, b_0 \right). \tag{2.9}$$

A well-known group of discrete wavelets is given by the dyadic wavelet. They are formed by setting $a_0 = 2$ and $b_0 = 1$. By considering these values, Equation (2.9) becomes

$$\psi_{m,n}(t) = 2^{-\frac{m}{2}} \psi \left(2^{-m} t - n \right). \tag{2.10}$$

The numerical implementation of the discrete wavelet transform is done by means of the fast wavelet transform, which is a set of algorithms developed by [Mallat, 1989]. The algorithm is based on the multiresolution analysis concept. In the multiresolution analysis, the space $L^2(\mathbb{R})$ consists of a sequence of nested subspaces,

$$\{0\} \subset \cdots \subset V_2 \subset V_1 \subset V_0 \subset V_{-1} \subset V_{-2} \subset \cdots \subset L^2(\mathbb{R}). \tag{2.11}$$

A given signal f in the subspace V_{-1} in $L^2(\mathbb{R})$ is separated into high and low frequency parts. The low frequency part is an orthogonal projection $P_0 f$ onto lower space V_0 in V_{-1}. The complement of V_0 concerning V_{-1} is the space W_0, whereas the projection of f onto W_0 is $Q_0 f$.

$$f = P_0 f + Q_0 f, \quad V_{-1} = V_0 \oplus W_0. \tag{2.12}$$

In this context, the low frequency part is called approximate part and the high frequency part is called detailed information or wavelet. The approximate part in V_0 can be further decomposed to obtain the approximate and detailed information for the next level (V_1 and W_1). The decomposition process can be repeated until the required scale is reached. The multiresolution analysis is illustrated in figure Figure 2.3.

Therefore, a signal f in $L^2(\mathbb{R})$ can be described by the following decomposition until a scale M,

$$f = P_M f + \sum_{k=-\infty}^{M} Q_k f, \quad f \in L^2(\mathbb{R}). \tag{2.13}$$

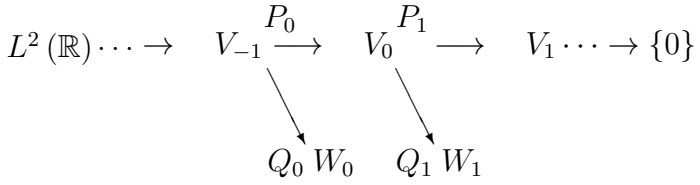

Figure 2.3: Scheme of a multi-scale analysis

The orthogonal decomposition of $L^2(\mathbb{R})$ is

$$L^2(\mathbb{R}) = V_M \oplus \bigoplus_{k=-\infty}^{M} W_k. \tag{2.14}$$

If a signal f belongs to a subspace V_m, Equations (2.13) and (2.14) become:

$$f^m = P_M f + \sum_{k=m+1}^{M} Q_k f, \quad M > m. \tag{2.15}$$

$$V_m = V_M \oplus \bigoplus_{k=m+1}^{M} W_k, \quad M > m. \tag{2.16}$$

The multi-scale analysis in the context of the orthogonal wavelet transform assumes the existence of a scaling function φ,

$$\varphi_{m,n} = 2^{-\frac{m}{2}} \varphi\left(2^{-m}t - n\right). \tag{2.17}$$

The scaling function φ satisfies the scaling condition:

$$\varphi(t) = \sqrt{2} \sum_{k \in \mathbb{Z}} a_k \varphi(2t - k), \quad a_k \in \mathbb{R} \tag{2.18}$$

Based on such a scaling function φ, a mother wavelet ψ can be written:

$$\psi(t) = \sqrt{2} \sum_{k \in \mathbb{Z}} b_k \varphi(2t - k), \quad b_k \in \mathbb{R}, \tag{2.19}$$

where φ and ψ hold the following properties,

$$\int_{-\infty}^{\infty} \varphi(t)dt = 1, \quad \int_{-\infty}^{\infty} \psi(t)dt = 0. \tag{2.20}$$

$$\langle \varphi_{m,k}, \varphi_{m,l} \rangle = \delta_{k,l} \tag{2.21}$$

$$\langle \psi_{m,n}, \psi_{k,l} \rangle = \delta_{m,k}\delta_{n,l} \tag{2.22}$$

$$\langle \varphi_{m,n}, \psi_{k,l} \rangle = 0 \qquad \forall\, m \geq k. \tag{2.23}$$

The symbol $\delta_{k,l}$ is the Kronecker-Delta and follows the condition,

$$\delta_{kl} = \begin{cases} 1, & k = l \\ 0, & k \neq l \end{cases} \quad . \tag{2.24}$$

The coefficients a_k and b_k follow the conditions

$$\sum_{k\in\mathbb{Z}} a_k = \sqrt{2}, \quad \sum_{k\in\mathbb{Z}} b_k = 0. \tag{2.25}$$

By using the fast wavelet transform, a signal $f(t) \in V_0 \subset L^2(\mathbb{R})$ defined by Equation (2.12) and (2.13) can be decomposed as

$$f(t) = \sum_{k\in\mathbb{Z}} C_{M,k}\varphi_{M,k} + \sum_{m=1}^{M}\sum_{k\in\mathbb{Z}} D_{m,k}\psi_{m,k}, \tag{2.26}$$

where $C_{m,n}$ and $D_{m,n}$ are approximation and detailed coefficients, respectively, which are calculated using the following equations:

$$C_{m,n} = \sum_{k\in\mathbb{Z}} a_{k-2n}C_{m-1,k}, \quad D_{m,n} = \sum_{k\in\mathbb{Z}} b_{k-2n}C_{m-1,k}. \tag{2.27}$$

Figure 2.4 illustrates the wavelet decomposition of a signal. The original signal is decomposed to obtain the approximation and detailed components of level 1. The Approximation part of level 1 is further decomposed to obtain the signal in level 2. The process can be continued until the target level is reached.

The algorithm of the fast wavelet transform is based on multiresolution analysis proposed by Mallat [Mallat, 1989]. This algorithm has been implemented in the SLang software package [Dynardo GmbH & Bauhaus University Weimar, 2009] and is used in this study.

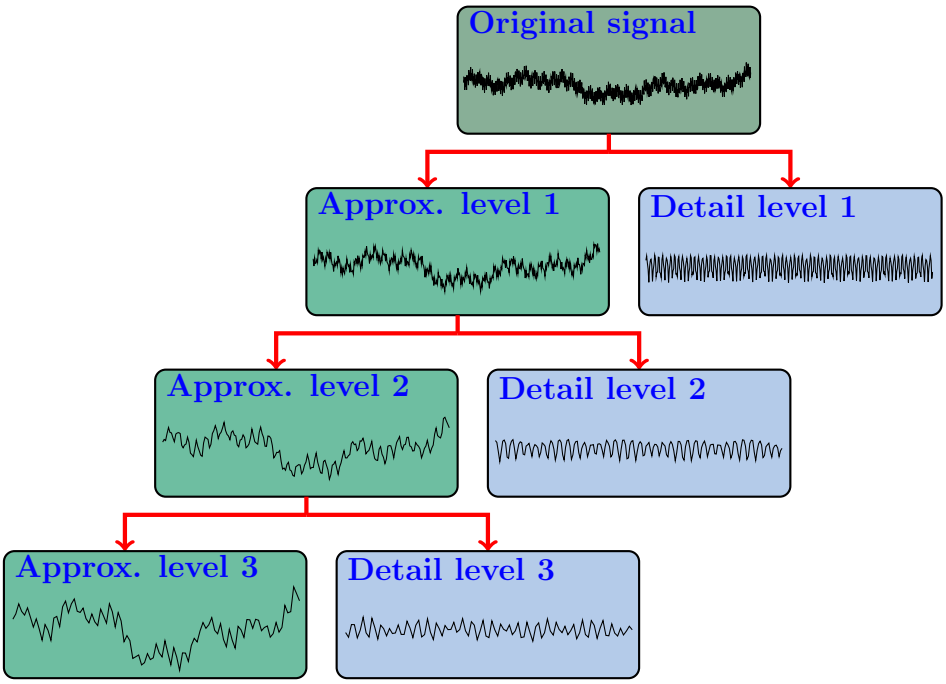

Figure 2.4: Wavelet decomposition

2.3.2 Wavelet Energy Damage Indicator

In signal processing, the energy E_s of a continuous-time signal $x(t)$ is defined as

$$E_s = \int_{-\infty}^{\infty} |x(t)|^2 \, \mathrm{d}t. \tag{2.28}$$

The concept of energy in signal processing can be applied for the wavelet analysis. Based on Equation (2.26), the total energy of the decomposition signal up to level M can be written as

$$\Pi_0 = \sum_k 2^M C_{M,k}^2 + \sum_{m=1}^{M} \sum_k 2^m D_{m,k}^2. \tag{2.29}$$

In Equation (2.29), C and D indicate the approximation and detailed coefficients of respective wavelet decomposition. M and m are the highest and current decomposition levels, respectively. The factor 2^m ensures the same energy under different wavelet levels. The absolute wavelet energy of the approximation and detailed parts of a level m is given by Equations (2.30) and (2.31), respectively.

$$\Pi_{C,m} = 2^m \sum_k C_{m,k}^2 \tag{2.30}$$

$$\Pi_{D,m} = 2^m \sum_k D_{m,k}^2. \tag{2.31}$$

The wavelet energy ratio at level m is

$$\Pi_m^r = \frac{\Pi_{C,m}}{\Pi_0} \quad \text{or} \quad \Pi_m^r = \frac{\Pi_{D,m}}{\Pi_0} \quad \text{with} \quad \Pi_0 \neq 0, \tag{2.32}$$

where Π_0 is the total wavelet energy. Π_m^r is wavelet energy ratio of the approximations or detailed parts at level m.

2.3.3 Entropy of Relative Wavelet Energy Damage Indicator

In signal processing or information theory, the entropy appears as a measure of the degree of order/disorder of a signal. It provides useful information regarding the physical process associated with the signal. The damage that presents in the structure results in changes in the signal entropy. According to [Shannon & Weaver, 1949], the total entropy of the relative wavelet energy can be written as

$$S = -\sum_{m=1}^{M} \Pi_m^r \ln \Pi_m^r. \tag{2.33}$$

The entropy of one single wavelet level m is

$$S_m = -\Pi_m^r \ln \Pi_m^r, \tag{2.34}$$

where Π_m^r is the relative wavelet energy at level m.

2.4 Stochastic Subspace Identification

The stochastic subspace identification (SSI) has become a common approach for modal parameters identification of mechanical systems, especially in civil engineering structures. The SSI approach became very popular due to the fact that it does not require information about excitation forces. In this output only data approach, a cheap daily available natural excitation, such as wind, waves, or vehicles can be used. The conventional modal parameter identification methods require both excitation and response signals. The use of

artificial excitation sources, such as shaker and drop weights for large structures is often impractical and expensive. It also creates disturbances for the structure's user.

Actually, the concept and applications of subspace model for modal parameter identification have been discussed in many publications in the early 1990s, for example [Prevosto *et al.*, 1991] and [Viberg, 1995]. However, the most important breakthrough for this approach happened in 1996, when Peter Van Overschee and Bart De Moor published their book [Overschee & Moor, 1996]. This book not only presents the mathematical background of subspace identification, it also provides a set of files that allow readers to try the algorithm. Since then, many works on stochastic subspace identification application have been published. A comprehensive review and elaboration about the application of SSI for modal parameter identification can be found in [Peeters, 2000].

The stochastic subspace identification is used to extract modal parameters of structures. Meanwhile, the presence of damages changes the modal parameters of structures. Hence, it makes sense to derive a damage indicator by using the stochastic subspace identification approach. [Basseville *et al.*, 2000] and [Mengelkamp, 2003] present insightful explanations about the application of SSI algorithm for damage identification. The theoretical background of the state-space model and SSI damage indicator are presented in the next two subsections.

2.4.1 State-Space Model

The conventional formulation of the equation of motion for a viscously damped system can be written as

$$[M]\{\ddot{q}(t)\} + [C_2]\{\dot{q}(t)\} + [K]\{q(t)\} = \{F(t)\} = [B_2]\{u(t)\}, \tag{2.35}$$

where $[M]$, $[C_2]$ and $[K]$ are mass, damping and stiffness matrices, respectively. $\{q(t)\}$ is the displacement vector at continuous time t. The excitation force vector $\{F(t)\}$ can be represented by real matrices $[B_2]$ and $\{u(t)\}$, which specify locations and values of acting forces, respectively. The equation of motion in Equation (2.35) can be transferred into a system of first order differential equation, by adding the identity $[M]\{\dot{q}(t)\} = [M]\{\dot{q}(t)\}$.

$$\underbrace{\begin{bmatrix} [C_2] & [M] \\ [M] & [0] \end{bmatrix}}_{[P]} \underbrace{\begin{Bmatrix} \{\dot{q}(t)\} \\ \{\ddot{q}(t)\} \end{Bmatrix}}_{\{\dot{x}(t)\}} + \begin{bmatrix} [K] & [0] \\ [0] & [-M] \end{bmatrix} \underbrace{\begin{Bmatrix} \{q(t)\} \\ \{\dot{q}(t)\} \end{Bmatrix}}_{\{x(t)\}} = \begin{bmatrix} [B_2] \\ [0] \end{bmatrix} \{u(t)\} \tag{2.36}$$

The inverse of $[P]$ can be computed as

$$[P]^{-1} = \begin{bmatrix} [0] & [M]^{-1} \\ [M]^{-1} & -[M]^{-1}[C_2][M]^{-1} \end{bmatrix}. \tag{2.37}$$

Equation (2.36) can be normalized by pre-multiplying it with $[P]^{-1}$ to obtain:

$$\{\dot{x}(t)\} = \underbrace{\begin{bmatrix} [0] & [I] \\ -[M]^{-1}[K] & -[M]^{-1}[C_2] \end{bmatrix}}_{[A_c]} \{x(t)\} + \underbrace{\begin{bmatrix} [0] \\ -[M]^{-1}[B_2] \end{bmatrix}}_{[B_c]} \{u(t)\}. \tag{2.38}$$

$$\{\dot{x}(t)\} = [A_c]\{x_{(t)}\} + [B_c]\{u_{(t)}\}. \tag{2.39}$$

Equation (2.39) is called the state equation in control theory. Meanwhile, the response vector $\{y(t)\} \in \mathbb{R}$ containing all structural responses that are measured in a test can be described as

$$\{y(t)\} = [C_a]\{\ddot{q}(t)\} + [C_v]\{\dot{q}(t)\} + [C_d]\{q(t)\}. \tag{2.40}$$

The matrices $[C_a]$, $[C_v]$ and $[C_d] \in \mathbb{R}$ describe the sensor positions to measure the accelerations, velocities, and displacements, respectively. These matrices basically consist of zeros and ones, which correspond to the measurement points selection from the degrees of freedom of the finite element model. The acceleration vector $\{\ddot{q}(t)\}$ in Equation (2.40) is substituted by $\{\ddot{q}(t)\}$ from Equation (2.35) to obtain:

$$\begin{aligned} \{y(t)\} = & \underbrace{\begin{bmatrix} ([C_d] - [C_a][M]^{-1}[K]) & ([C_v] - [C_a][M]^{-1}[C_2]) \end{bmatrix}}_{[C_c]} \underbrace{\begin{Bmatrix} \{q(t)\} \\ \{\dot{q}(t)\} \end{Bmatrix}}_{\{x(t)\}} \\ & + \underbrace{[C_a][M]^{-1}[B_2]}_{[D_c]}\{u(t)\}. \end{aligned} \tag{2.41}$$

$$\{y(t)\} = [C_c]\{x(t)\} + [D_c]\{u(t)\} \tag{2.42}$$

Equation (2.42) is called the observation equation. Matrices $[C_c]$ and $[D_c]$ are the output matrix and transmission matrix, respectively. The continuous-time state-space model can be written by combining the state equation (2.39) and the observation equation (2.42):

$$\begin{aligned}\{\dot{x}(t)\} &= [A_c]\{x(t)\} + [B_c]\{u(t)\} \\ \{y(t)\} &= [C_c]\{x(t)\} + [D_c]\{u(t)\}\end{aligned} \tag{2.43}$$

Dynamic response measurements of a physical structure basically provide data in a discrete signal rather than a continuous time series. The discrete time data of state space model is analyzed by using time integration schemes. The signal is assumed to have a constant value between the discrete instant $k\Delta t$ and $(k+1)\Delta t$. The solution of the state equation in (2.43) for a given initial value $\{x(t_0)\}$ at an instant time $t = t_0$ can be written as:

$$\{x(t)\} = e^{[A_c](t-t_0)}\{x(t_0)\} + \int_{t_0}^{t} e^{[A_c](t-\tau)}[B_c]\{u(\tau)\}d\tau. \tag{2.44}$$

The sampling interval Δt of measured signals is usually constant. For $t = (k+1)\Delta t$ and $t_0 = k\Delta t$, Equation (2.44) becomes:

$$\{x((k+1)\Delta t)\} = e^{[A_c]\Delta t}\{x(k\Delta t)\} + \int_{k\Delta t}^{(k+1)\Delta t} e^{[A_c]((k+1)\Delta t-\tau)}[B_c]\{u(\tau)\}d\tau. \tag{2.45}$$

By assuming that the excitation is constant between two sampling instances $\{u(\tau)\} = \{u(k\Delta t)\}$ and replace τ with $\tau' = (k+1)\Delta t - \tau$, Equation (2.45) can be written as the following:

$$\underbrace{\{x((k+1)\Delta t)\}}_{\{x_{k+1}\}} = \underbrace{e^{[A_c]\Delta t}}_{[A]}\underbrace{\{x(k\Delta t)\}}_{\{x_k\}} + \underbrace{\int_{t_0}^{\Delta t} e^{[A_c]\tau'}d\tau'[B_c]}_{[B]}\underbrace{\{u(k\Delta t)\}}_{\{u_k\}}. \tag{2.46}$$

The stochastic state-space model for discrete time analysis yields

$$\begin{aligned}\{x_{k+1}\} &= [A]\{x_k\} + [B]\{u_k\} \\ \{y_k\} &= [C]\{x_k\} + [D]\{u_k\}.\end{aligned} \tag{2.47}$$

The process noise $\{w_k\}$ should be included in state equation (2.47) to take random disturbances and modeling inaccuracies into account. A similar idea is applied in the observation equation to introduce measurement noise $\{v_k\}$. The deterministic discrete time state-space model becomes:

$$\begin{aligned} \{x_{k+1}\} &= [A]\{x_k\} + [B]\{u_k\} + \{w_k\} \\ \{y_k\} &= [C]\{x_k\} + [D]\{u_k\} + \{v_k\}. \end{aligned} \tag{2.48}$$

Both random processes are assumed to have zero mean and constant spectrum (white noise). The covariance matrices for two arbitrary instants p and q are

$$E\left[\begin{Bmatrix} \{w_p\} \\ \{w_p\} \end{Bmatrix} \begin{bmatrix} \{v_q\}^T & \{v_q^T\} \end{bmatrix}\right] = \begin{bmatrix} [Q] & [S] \\ [S]^T & [R] \end{bmatrix} \delta_{pq}, \tag{2.49}$$

where E is the expected value and δ_{pq} is the Kronecker delta,

$$\delta_{pq} = \begin{cases} 1 & p = q \\ 0 & p \neq q \end{cases} . \tag{2.50}$$

In the stochastic system identification using ambient excitation, only output data or system responses are measured, while input data is not measured. This means that the stochastic excitation $\{u_k\}$ cannot be distinguished from the noise signal $\{w_k\}$ and $\{v_k\}$ in Equation (2.48). Hence, the stochastic excitation is merged into noise components. The discrete-time stochastic state-space model becomes:

$$\begin{aligned} \{x_{k+1}\} &= [A]\{x_k\} + \{w_k\} \\ \{y_k\} &= [C]\{x_k\} + \{v_k\} \end{aligned} \tag{2.51}$$

The state-space model in Equation (2.51) can be converted into the so-called forward innovation model by applying the Kalman filter.

$$\begin{aligned} \{\hat{x}_{k+1}\} &= [A]\{\hat{x}\}_k + [K_a]\{e\}_k \\ \{y_k\} &= [C]\{\hat{x}\}_k + \{e\}_k, \end{aligned} \tag{2.52}$$

where $\{\hat{x}_{k+1}\}$ is the estimate of the state $\{x_{k+1}\}$ and $\{e\}_k$ is the error between estimated and measured process at instant step k. $\{e\}_k$ also called the innovation vector. The matrix $[K_a]$ is called the steady state Kalman gain matrix.

2.4.2 SSI Damage Indicator

One of the most applied output-only methods for the identification of modal parameters of mechanical structures is the reference based covariance-driven stochastic subspace identification (SSI) method. One of the major steps in this algorithm is the formulation of the Hankel matrix $[H_{i-1}]$ of the output signals:

$$[H_{i-1}] = \begin{bmatrix} [R_i] & [R_{i+1}] & \dots & [R_{i+\beta-1}] \\ [R_{i+1}] & [R_{i+2}] & \dots & [R_{i+\beta}] \\ \vdots & \vdots & \ddots & \vdots \\ [R_{i+\alpha-1}] & [R_{i+\alpha}] & \dots & [R_{i+\alpha+\beta-2}] \end{bmatrix}, \tag{2.53}$$

where α and β define the size of Hankel block matrix, which is actually the number of time steps included in the analysis. The Hankel matrix block in Equation (2.53) can be decomposed into the extended observability matrix $[O_i]$ and the extended controllability matrix $[\Gamma i]$:

$$\begin{aligned} [H_{i-1}] &= \begin{bmatrix} [C] \\ [C]\,[A] \\ [C]\,[A]^2 \\ \vdots \\ [C]\,[A]^{\alpha-1} \end{bmatrix} [A]^{i-1} \underbrace{\begin{bmatrix} [G] & [A][G] & [A]^2[G] & \dots & [A]^{\beta-1}[G] \end{bmatrix}}_{[\Gamma i]} \\ &= [O_i][A]^{i-1}[\Gamma i]. \end{aligned} \tag{2.54}$$

The matrices $[A]$ and $[C]$ in Equation (2.54) contain all modal information of the system. These matrices are the system matrices of the state space model in Equation (2.51).

Basically, the concept of damage identification in structures is comparing modal characteristics in two different conditions, damaged and undamaged states. The damage indicator describes the change of modal properties of the system due to structural damage. In the context of state space model, a vector $\{\theta\}$ that contains the modal parameter of the system is defined:

$$\{\theta\} = \begin{Bmatrix} \{\Lambda_d\} \\ \{vec\,[\Psi]\} \end{Bmatrix}. \tag{2.55}$$

The vector $\{\Lambda_d\}$ holds the eigenvalues of matrix $[A]$. The application of the *vec* operator to the modal matrix $[\Psi]$ forms a vector by appending the eigenvectors. Based on $\{\theta\}$, a particular representation of the observability matrix can be formulated, [Basseville *et al.*, 2000].

$$[O_i(\theta)] = \begin{bmatrix} [\Psi] \\ [\Psi]\,[\Lambda_d] \\ [\Psi]\,[\Lambda_d]^2 \\ \vdots \\ [\Psi]\,[\Lambda_d]^{i-1} \end{bmatrix}. \tag{2.56}$$

$$[O_i] = [O_i(\theta)][T], \tag{2.57}$$

where [T] is a transformation matrix. The nominal parameter set $\{\theta_0\}$ agrees with an initial output covariance sequence R_i, which is characterized by the property that $[O_1(\theta_0)]$ and the initial output covariance block Hankel matrix $[H(1)]$ have the same left kernel space:

$$[S(\theta_0)]^T[O_1(\theta_0)] = [0] \tag{2.58}$$

$$[S(\theta_0)]^T[H(1)] = [0]. \tag{2.59}$$

This means that the left kernel space of the matrices $[O_1(\theta_0)]$ and $[H(1)]$ is spanned by the columns of a reference matrix $[S(\theta_0)]$. Applying the *vec* operator to Equation (2.59) gives

$$vec\left([S(\theta_0)]^T[H(1)]\right) = \{0\}. \tag{2.60}$$

[Mengelkamp, 2003] suggests

$$\{\zeta_n(\theta_0)\} = vec\left([S(\theta_0)]^T[H(1)]\right). \tag{2.61}$$

From equation (2.60),

$$\mathrm{E}\{\{\zeta_n(\theta_0)\}\} = 0, \quad \text{if} \quad \{\theta\} = \{\theta_0\}. \tag{2.62}$$

The mean value of vector $\{\zeta_n(\theta_0)\}$ should be zero, if the set of parameters $\{\theta\}$ has not changed. If this mean value is not zero one can assume that the system has changed, for instance, as a result of damage to structure. Hence, the vector $\{\zeta_n(\theta_0)\}$ can be considered

as residual vector. In [Mengelkamp, 2003], the change of system properties as described in Equation (2.63), acts as a damage indicator.

$$\chi^2 = \{\zeta_n(\theta_0)\}^T \left[\sum(\theta_0)\right]^{-1} \{\zeta_n(\theta_0)\}, \tag{2.63}$$

where $[\sum(\theta_0]$ is the covariance matrix of residual vectors that can be computed as follows:

$$[\Sigma(\theta_0] = \frac{1}{k-2} \sum_{n=2}^{k} \{\zeta_n\}\{\zeta_n\}^T. \tag{2.64}$$

The reference condition is developed by performing several observations in undamaged conditions. The damage identification of structures is done by comparing the actual condition to the undamaged state or reference. The procedure of damage identification through stochastic subspace damage indicator is summarized in the following steps [Mengelkamp, 2003]:

1. Performs the first measurement in the undamaged states of the structures. The output response is used to form the first Hankel matrix $[H_1]$.

2. The matrix $[S(\theta_0)]$ is extracted from $[H_1]$ by applying singular value decomposition as show in the following equations:

$$\begin{aligned} [H_1] &= [U]\ [S]\ [V]^T \\ &= [[U_1][U_2]] \begin{bmatrix} [S_1] & [0] \\ [0] & [0] \end{bmatrix} \begin{bmatrix} [V_1]^T \\ [V_2]^T \end{bmatrix} \end{aligned} \tag{2.65}$$

$$[S(\theta_0)]^T = [U_2]. \tag{2.66}$$

3. Perform the next measurements at the undamaged states to obtain the the residuals value in undamaged situation $\{\zeta_n(\theta_0)\}$. The residuals value should be close to zero, as the system has not change.

4. The covariance matrix for reference state $[\Sigma(\theta_0]$ of the subsequent measurements is calculated using Equation (2.64).

5. The damage indicator value in the reference state χ^2_{ref} is calculated using Equation (2.63).

6. The damage indicator value in the detection or monitoring phase χ_j^2 is calculated similar to the step 1 and 3.

During the monitoring phase, the dynamic response signal at certain time is used to recalculate the Hankel matrix $[H_j]$, residuals $\{\zeta_n\}$ and χ^2. The damage condition can be normalized by the damage indicator value in the reference state to obtain the damage index D_j [Mengelkamp, 2003].

$$D_j = \frac{\chi_j^2}{\chi_{ref}^2}. \tag{2.67}$$

Figure 2.5 summarizes the procedures of the covariance-driven stochastic subspace identification method for damage identification in a mechanical structure.

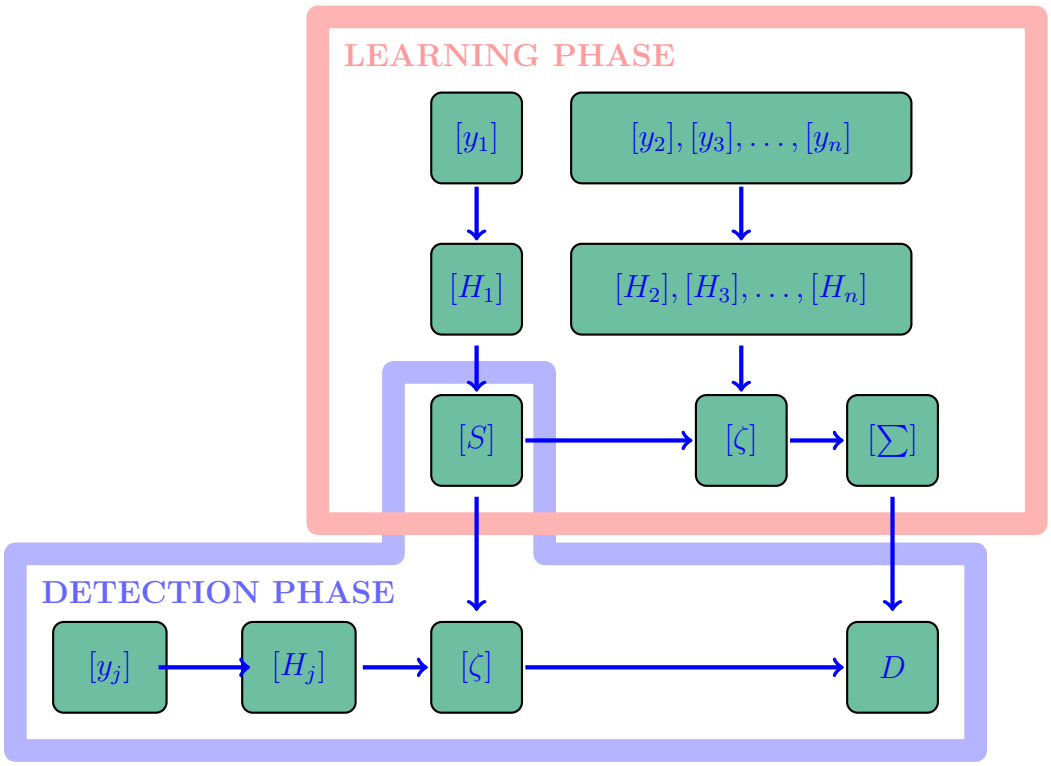

Figure 2.5: Procedure to calculate stochastic subspace identification (SSI) damage indicator according to [Mengelkamp, 2003]. y_1 is the response from the first measurement in the learning phase. y_j is a response during damage detection phase.

Chapter 3

Experimental Structural Dynamics

3.1 Introduction

One of the major activities in the application of vibration-based damage detection of a physical structure is data extraction and processing. It includes the process of acquiring and converting analogue data to digital electrical signals. Several important aspects should be considered in order to obtain optimum information and prevent significant data loss during the measurement process. Some of these aspects are presented in the following subsections.

3.2 Sampling Frequency

Sampling frequency f_s which is also known as sampling rate can be defined as the number of samples per second representing a continuous signal with a discrete form. If the sampling rate is too low, the existence of very high frequency components in the original signal may be misinterpreted. Meanwhile, too high sampling frequency requires higher cost for signal storage and processing.

According to the Nyquist-Shannon sampling theorem, the sampling frequency should be greater than twice of the highest frequency of the signal to allow a good reconstruction of the signal. Mathematically it can be written as

$$f_s = \frac{1}{\Delta t} = 2f_{Nyq}, \tag{3.1}$$

where f_s is sampling frequency and Δt is time step. Here, f_{Nyq} denotes the Nyquist frequency, which is the highest frequency that can be included in the spectrum. The frequency components above the f_{Nyq} tends to be reflected in the frequency range below f_{Nyq}. This phenomenon is known as aliasing, and it can produce significant error in signal interpretation and analysis. An appropriate sampling frequency prevents dynamic experimental tests from significant information losses with a reasonable computer memory.

3.3 Optimal Sensor Position

Sensor placement is an important issue in the implementation of an efficient structural health monitoring system. In many cases, the number of available sensors is restricted. Even though advances in sensing technology allow the use of a large number of sensors, the higher cost for data acquisition system and signal processing is still a concern. Hence, it becomes necessary to find the best sensor position to obtain optimum results. Therefore, an appropriate design of sensor placement will lead to an effective system identification; the capability to capture relevant information is optimized while the cost of equipment, data storage, and signal processing is minimized.

In many cases, the sensor positions for modal parameter identification are determined only based on visual inspection and 'engineering instinct'. However, the 'engineering instinct' approach is applicable only for simple structures, where their mode shape can be 'guessed'. Positions of the large amplitude of mode shapes of complex structures are difficult to predict. Therefore, many preliminary tests have to be performed in a trial-error scheme before the real measurement is conducted. This often requires much more cost and effort since not all components of the structure can be easily accessed.

Advances in Finite Element modeling and computer simulation allow engineers to have a good approximation of the mode shapes of large and complex structures, so that the numerical mode shape becomes the basis of sensor placement method. Many approaches have been proposed in literatures e.g. [Kammer, 1991], [Yao *et al.*, 1993], [Udwadia, 1994], [Reynier & Abou-Kandil, 1999], [Schwarz *et al.*, 2002], and [Li *et al.*, 2007]. The main criterion of sensor placement method is to find locations that are far from the nodal points of mode shapes of interest. Some common sensor placement methods are described in the following subsections.

3.3.1 Shape Product

The shape product is probably the simplest and most straightforward method in identifying the best reference sensor position. The analytical or numerical mode shapes are multiplied component by component, [Schwarz *et al.*, 2002]. The result of the multiplication is a vector such kind of a mode shape. The sensor should then be placed in the highest amplitude of the shape product vector. A similar concept is applied by the mode shape summation plot method where the mode shapes are summed instead of multiplied, [De Clerk & Avitable, 1998].

Consider $[\Phi]_{m,n}$ is the eigenvectors matrix of a structure with m degree of freedom and n extracted modes. If $\{\phi_1\}$ and $\{\phi_n\}$ are the first and last eigen modes respectively, the shape product vector SP and mode shape summation plot vector $MSSP$ can be expressed as

$$SP = \{\phi_1\} \otimes \{\phi_2\} \otimes \cdots \otimes \{\phi_n\} \tag{3.2}$$

and

$$MSSP = \sum_{i=1}^{n} |\{\phi_i\}|, \tag{3.3}$$

where $\otimes$ is the element wise multiplication symbol. The shape product and mode shape summation can be visualized like a mode shape to indicate the nodal points of target modes. Figure 3.1 illustrates the application of the shape product method to predict the best position of reference sensors for experimental modal analysis of a plate structure. The three lowest eigen modes are considered.

3.3.2 Modal Kinetic Energy

The modal kinetic energy method is widely used for sensor placement strategy. It was proposed by [Kammer, 1991] and further investigated by [Papadopoulos & Garcia, 1998] and [Li *et al.*, 2007]. The core of the modal kinetic energy method is the assumption that higher response amplitudes correspond to higher modal kinetic energy. Hence, the sensor location candidates are sorted according to the value of the modal kinetic energy. The modal kinetic energy method can be written as

$$MKE_{ij} = \Phi_{ij} \sum_{s=1} M_{is} \Phi_{sj}, \tag{3.4}$$

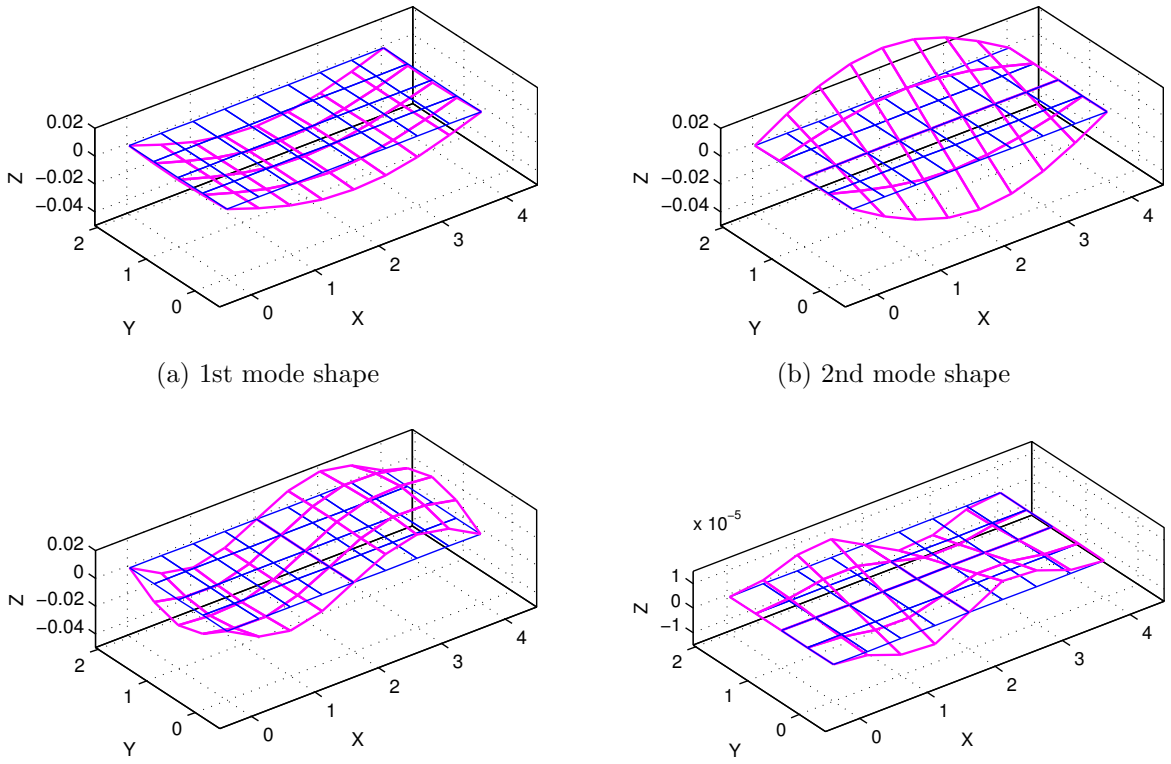

(a) 1st mode shape

(b) 2nd mode shape

(c) 3rd mode shape

(d) Shape product

Figure 3.1: The prediction of the reference sensor position using shape product method. A good position is indicated by high amplitude of the shape product.

where MKE_{ij} is the modal kinetic energy associated with the i-th degree of freedom in the j-th target mode, Φ_{ij} is the i-th coefficient in the corresponding mode, M_{is} is the term in the i-th row and s-th column of the mass matrix, and Φ_{sj} is the s-th coefficient in the j-th target mode [Kammer, 1991].

3.3.3 Effective Independence Method

The effective independence (EI) method was proposed by [Kammer, 1991]. The candidates of sensor locations are ranked based on their contribution to the linear independence of the numerical target modes. The sensor output at any instant time of a measurement can be expressed as,

$$y = H(q) + N, \tag{3.5}$$

where y is the sensor response vector, H is the symbol for process measurement, and q is the vector of target modal coordinate. N is the stationary Gaussian measurement white noise, and Ψ_0^2 is the variance of N. If $\hat{q}$ is the estimated value of q, the covariance matrix of the estimate error is given by

$$E\left[(q-\hat{q})(q-\hat{q})^T\right] = \left[\left(\frac{\delta H}{\delta q}\right)^T \left[\Psi_0^2\right]^{-1} \left(\frac{\delta H}{\delta q}\right)\right]^{-1} = \left[\frac{1}{\Psi_0^2}\Phi^T\Phi\right]^{-1} = Q^{-1}, \tag{3.6}$$

in which E denotes the expected value and Q is the Fisher information matrix. Maximizing functional on Q leads to a minimized value of the covariance matrix, meaning the best estimate of $\hat{q}$. The method is started by solving the eigenvalue problem in Equation (3.7).

$$\left[\Phi^T\Phi - \lambda I\right]\psi = 0 \tag{3.7}$$

where ψ is the orthogonal eigenvector. The EI coefficients of the candidate sensors are then calculated by the following equation,

$$EI = [\Phi\psi] \otimes [\Phi\psi]\ \lambda^{-1} \tag{3.8}$$

where $\otimes$ represents a term-by-term matrix multiplication. The number of candidate sensor is reduced by eliminating locations which do not contribute significantly to the independent information contained within the target mode. Figure 3.2 illustrates the application of the effective independence method to predict the best positions of reference sensors for experimental modal analysis of a plate structure.

3.4 Modal Pairing

Modal pairing is one of the most important steps in modal parameters identification of structures. Generally modal pairing refers to the investigation of correlation between measured (experimental) and predicted (numerical) mode shapes. The modes matching might be very difficult in experimental modal analysis, especially for structures that contain many closely spaced frequencies.

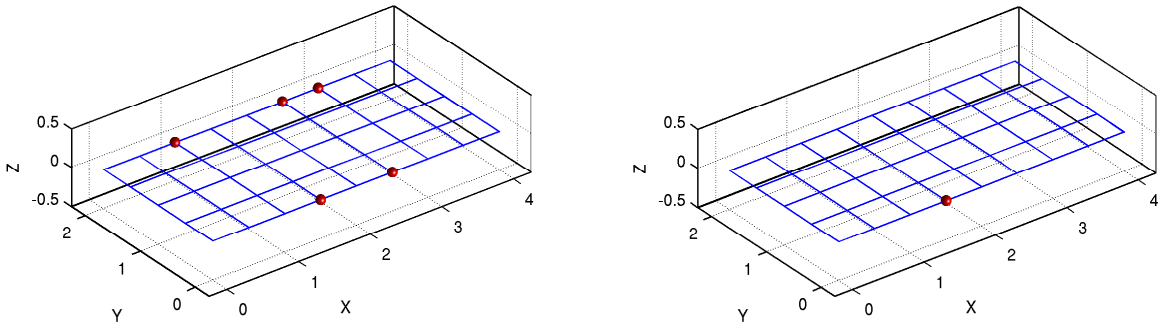

(a) Five sensors (b) One sensor

Figure 3.2: The best reference sensor position as predicted using the effective independence method

The modal pairing concept is not only useful in comparing experimental versus analytical mode shapes. Basically, it can be used for all sorts of comparison. In the frequency-based damage identification, damages might not only change the eigen frequency values but also the eigen frequency order. Hence, the modal pairing method is required to select the correct frequency pairs. In another case, modal pairing can be used to compare a pair of vectors obtained from two conditions, such as damaged and undamaged conditions.

Several modal pairing methods have been proposed by many researchers and well documented in standard text-books, e.g. [Ewins, 2000], [Maia & Silva, 1997] and [Allemang, 2003]. Some of these methods are shortly described in the following subsection.

3.4.1 Modal Scale Factor

A simple formula that can present a comparison between the modal parameter of an experimentally measured and a numerical model is called modal scale factor (MSF), [Allemang & Brown, 1982]. The MSF represents the slope of the best straight line through the points as is shown Figure 3.3. The modal scale factor is calculated as

$$MSF_{X,A} = \frac{\sum_{i=1}^{nr} \phi_{Xi}\phi_{Ai}}{\sum_{i=1}^{nr} \phi_{Ai}\phi_{Ai}} = \frac{\left(\{\phi_X^T\}\{\phi_A\}\right)}{\left(\{\phi_A^T\}\{\phi_A\}\right)}, \tag{3.9}$$

where ϕ_X and ϕ_A are the eigenvectors of experimental and numerical models, respectively. Here, nr is the number of elements for both data sets.

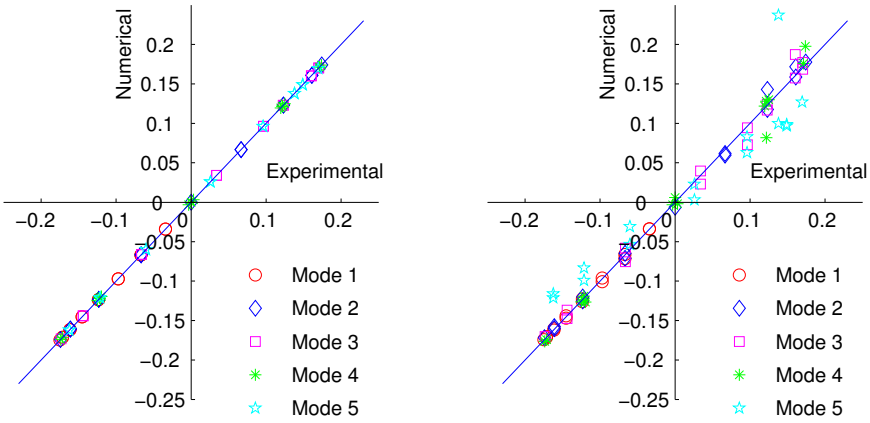

(a) Perfect match

(b) Systematic error

Figure 3.3: Comparison of two mode shapes obtained from experimental and numerical models. Figure 3.3a shows a perfect match where all points lie in a line. A systematic error is shown in Figure 3.3b

. .

3.4.2 Modal Assurance Criteria

The modal assurance criteria (MAC), also known as the mode shape correlation coefficient (MSCC), proposed by [Allemang & Brown, 1982] is one of the most popular tools for mode matching. MAC can be defined as a scalar constant relating the degree of consistency between one modal and another reference modal vector. MAC can be written as

$$MAC_{X,A} = \frac{\left(\{\phi_X^T\}\{\phi_A\}\right)^2}{\left(\{\phi_X^T\}\{\phi_X\}\right)\left(\{\phi_A^T\}\{\phi_A\}\right)}, \tag{3.10}$$

where ϕ_X and ϕ_A are the eigenvectors from the experimental and analytical solutions, respectively. The MAC value ranges between 0 and 1, where low values show poor resemblance and value of 1 means perfect correlation. However, MAC values greater than 0.9 already indicate a good correlation [Ewins, 2000]. Figure 3.4 shows MAC values that are obtained by comparing experimental mode shapes to numerical mode shapes. Strong correlations of all compared mode shapes are indicated by higher MAC values in all of the diagonal elements as is shown in Figure 3.4a, whereas, lower MAC values indicate no correlation between the two compared modes, for instance mode 4 in Figure 3.4b.

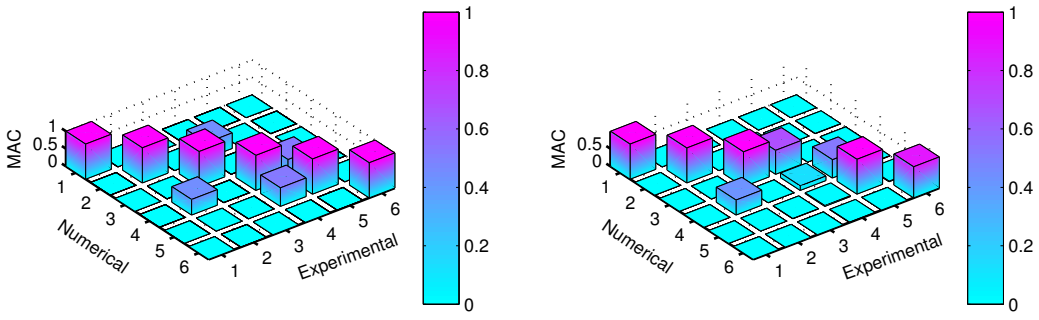

(a) Full matched (b) Partially matched

Figure 3.4: Comparison of MAC values of two mode shapes

3.4.3 Normalized Mode Difference

The normalized mode difference (NMD) was proposed by [Waters, 1995] and [Maia & Silva, 1997] for modes matching indicator. The normalized mode difference between the experimental $\{\phi_X\}$ and the numerical mode shape $\{\phi_A\}$ is defined as

$$NMD_{X,A} = \frac{\| \{\phi_X\} - MSF\{\phi_A\} \|_2}{\| MSF\{\phi_A\} \|_2}. \tag{3.11}$$

The NMD is closely related to MAC and can be written as the following equation

$$NMD = \sqrt{\frac{1 - MAC}{MAC}}. \tag{3.12}$$

NMD is not bounded and may yield to infinity. A good correlation between the two modes will be characterized by a small value of NMD. NMD is much more sensitive to mode shape differences compared to MAC, [Ewins, 2000].

Chapter 4

Response Surface Methodology

4.1 Introduction

Response Surface Methodology (RSM) can be defined as a collection of statistical and mathematical techniques useful for developing, improving, and optimizing processes [Myers *et al.*, 2007]. The processes are optimized through a surrogate model by employing statistical tools such as design of experiments (DoE), regression analysis, and analysis of variance. The surrogate model is developed from empirical data and is further used to explore the relationship between several independent variables and their contribution to the response variables. Together with sensitivity and uncertainty analysis, RSM has become a powerful tool for many engineering applications.

The RSM emerged in 1951 when G. E. P. Box and K. B. Wilson proposed an empirical model to study the relationship between some variables in a chemical experimental study [Box & Wilson, 1951]. The RSM was used to find the optimum composition of the chemical process. Three decades later, following advancements in computer and Finite Element analysis, the RSM approach has also been applied for numerical or computer experiments. For instance, RSM was used to diminish the computational cost of the function evaluation in structural optimization [Roux *et al.*, 1998]. RSM has been applied to optimize the high-speed mass transport, [Knill *et al.*, 1998]. In [Most, 2008] and [Bucher, 1990], the RSM approach was used for reliability analysis.

In this thesis, the response surface methodology is employed to develop so-called reference surface-based system identification method. The reference surface-based system identification combines the response surface methodology and vibration-based damage detection.

It can be used to handle the environmental and operational variables that often obscure the results of the ambient vibration-based damage detection of structures. The concept of the reference surface-based system identification will be presented in Chapter 5.

There are three crucial issues that should be well handled in order to obtain a good meta-model. The first issue is data sampling or often called the design of experiments. It refers to methods used to generate input data sets that represent the domain of interest. The second issue is the approximation methods that can be used to build a good model from scattered data. The last issue is the model evaluation and model selection. It refers to methods used to select the best model. A short overview of these issues is presented in the following subsections.

4.2 Design of Experiments

The procedure to select training or support points in a variable space is called the design of experiments (DoE). Basically, the common goal of the design of experiments method is to extract as much information as possible from a minimum number of laboratory or computer experiments [Giunta *et al.*, 2003]. Numerical model evaluations or physical experimental testing may be very expensive and time consuming. Therefore, it makes sense to have a sampling plan with fewer points but has a good representation of the domain. This means that sampling points should be distributed uniformly in the design space.

There are two basic strategies that can be employed to select training points in a design domain. The first strategy is to select training points according to a regular grid pattern superimposed on the experimental region. This strategy is also known as stratification. Another strategy includes using an algorithm to generate random numbers. Following this, the random numbers are mapped onto the experimental region. Most of the commonly-used sampling methods are developed from one of these approaches or a combination of both. The following subsection briefly describes some of the sampling methods.

4.2.1 Full Factorial Design

The full factorial design is the most straightforward method in sampling design. It is performed by dividing the design variable space into some uniform grids. The method can be easily expanded for multivariate systems. The objective function is evaluated for

every possible combination of design variable values. Therefore, a full factorial design is known to be a simple but conservative way in space filling.

Figure 4.1a shows an application example of the full factorial design for two variables (X_1, X_2). The number of experiments for n grid intervals and k variables is n^k. The number of experiments grows dramatically if the number of grid spaces or variables increase. This approach becomes ineffective if the data is very expensive to collect, for example if the experimental or computational cost to evaluate support points is very high.

4.2.2 Monte Carlo Method

According to [Giunta *et al.*, 2003], the application of the Monte Carlo sampling method for computer experiments was first introduced by [Metropolis & Ulam, 1949]. The basic idea of the Monte Carlo techniques is to use random numbers to mimic the random natural process. This means that the "heart" of the Monte Carlo sampling procedure is the numerical algorithm to generate random numbers. The major disadvantage of the Monte Carlo sampling method is that the results may not be space filling, since large areas of the design space may be left unexplored while others are densely sampled [Keane & Nair, 2005]. The drawback is more obvious for a small number of samples. Figure 4.1b provides an application example of the Monte Carlo sampling method.

The stratified Monte Carlo sampling is proposed to overcome this deficiency. The stratified Monte Carlo attempts to provide a more uniform sampling by splitting the design space into some intervals. The random number is generated for every sub-interval. As such, the stratified Monte Carlo provides better coverage of the design domain.

4.2.3 Latin Hypercube Sampling

Latin hypercube sampling (LHS) is perhaps the most popular method for data sampling in computer experiments. The LHS method was originally proposed by [McKay *et al.*, 1979] as an alternative to the Monte Carlo method. Basically, the LHS is a stratified sampling technique that ensures each of the input variables have all portions of its range represented [Sacks *et al.*, 1989]. The range of each parameter is divided into n bins of equal probability to obtain n samples. For p design parameter, the partitioning will lead to a total of n^p bins in the parameter space. The samples are randomly selected in the parameter space. Each sample is randomly placed inside a bin. There will be only one

sample in each bin of one-dimensional orthogonal projection. Figure 4.1c provides an application example of the Monte Carlo sampling method.

The random number generation that is used in the original LHS algorithm might provide a sampling plan that has different performance with regard to uniformity. In an extreme case, it might lead to poor design coverage, for instance many design points may lie along the diagonal of a 2D sampling design. Some extensions of the basic LHS algorithm were proposed to produce more uniform coverage of the design space. [Johnson *et al.*, 1990] and [Owen, 1994] suggest that the LHS may be improved by observing the minimum distance or correlation of sample points. [Johnson *et al.*, 1990] propose the use of the maximin metric to assess the uniformity of sampling plan.

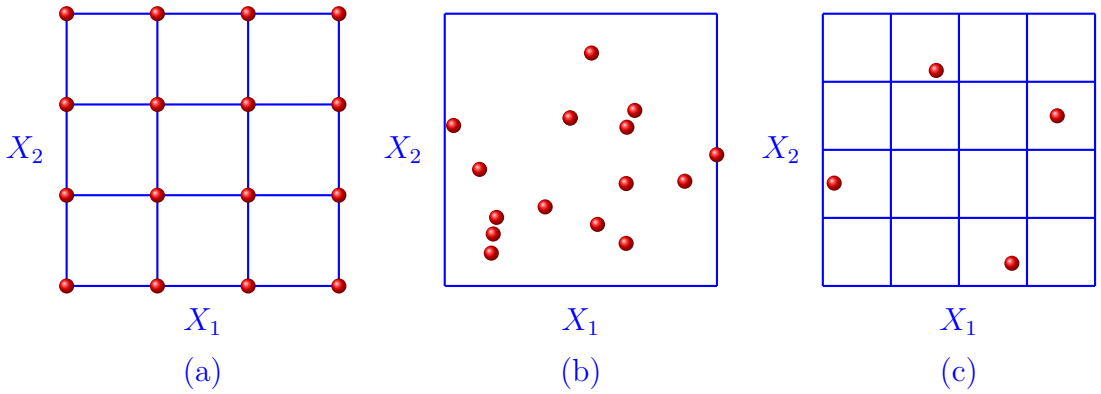

Figure 4.1: Design of Experiments: Full factorial design (a), Monte Carlo (b), and Latin hypercube sampling (c).

4.3 Scattered Data Approximation

The response surface methodology employs a meta-model to predict the response for a given input in the design space. The meta-model is trained using input-output data sets obtained from physical or numerical experiments. Several methods can be used to build a meta-model from scattered data. Polynomial regression, radial basis function, moving least squares, and artificial neural network approximation methods are used in this study. A short overview about these approximation methods is described in the following subsections.

4.3.1 Polynomial Regression

Polynomial regression is possibly the most widely used method to build a meta-model from scattered data obtained from physical or computer experiments. Basically, the polynomial model approximation of a function is similar to a Taylor series expansion of function f after $m+1$ terms [Box & Draper, 1987]. The polynomial model approximation of a function $y = f(x)$ of order m can be written as

$$\hat{y} = \beta_0 + \beta_1 x + \beta_2 x^2 + \cdots + \beta_m x^m, \tag{4.1}$$

where $\{\beta_0, \beta_1, \ldots, \beta_m\}$ are the regression coefficients. The approximate error $\varepsilon = y - \hat{y}$ is assumed to be statistically independent with mean value equal to zero. Considering that the function $f(x)$ is observed according to a sampling plan $x = \{x_1, x_2, \ldots x_n\}^{\mathrm{T}}$, leads to responses $y = \{y_1, y_2, \ldots y_n\}^T$. In a matrix form, the observation and approximation values can be expressed as

$$\begin{Bmatrix} y_0 \\ y_1 \\ y_2 \\ \vdots \\ y_n \end{Bmatrix} = \begin{bmatrix} 1 & x_1 & x_1^2 & \ldots & x_1^m \\ 1 & x_2 & x_2^2 & \ldots & x_2^m \\ 1 & x_3 & x_3^2 & \ldots & x_3^m \\ \vdots & \vdots & \vdots & \ddots & \vdots \\ 1 & x_n & x_n^2 & \ldots & x_n^m \end{bmatrix} \begin{Bmatrix} \beta_0 \\ \beta_1 \\ \beta_2 \\ \vdots \\ \beta_n \end{Bmatrix} + \begin{Bmatrix} \varepsilon_0 \\ \varepsilon_1 \\ \varepsilon_2 \\ \vdots \\ \varepsilon_n \end{Bmatrix}, \tag{4.2}$$

or as

$$y = X\beta + \varepsilon, \tag{4.3}$$

where X is the Vandermonde matrix. The estimation variables β are solved through a least square solution of Equation (4.3), which gives $\beta = X^+ y$. Here, $X^+ = (X^{\mathrm{T}}X)^{-1}X^{\mathrm{T}}$ is the Moore-Penrose pseudo-inverse. A greater value of the polynomial order m usually leads to a more accurate approximation because the model becomes more flexible. However, higher flexibility also means higher risk of overfitting if the data contains noise. An appropriate polynomial order m can be selected using model selection methods, for example cross validation.

For example, the polynomial regression model is used to approximate function $y = 2x + 0.5cos(5x) + sin(2x)$, for $0 \leq x \leq 5$. The results are shown in Figure 4.2. A higher order polynomial model yields to more accurate approximation. The best model is obviously indicated by the highest coefficient correlation value R^2 that can be calculated using Equation (4.20).

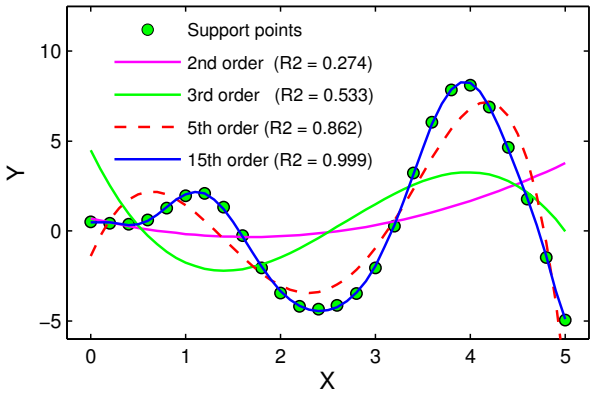

Figure 4.2: Polynomial regression of data without noise

However, a higher polynomial order or R^2 does not always indicate a better model if the observation data is contaminated by noise, as is illustrated in Figure 4.3. The target function is $y = 0.1x + (6x - 3)^2 + sin(6x - 4)$ for $0.1 \leq x \leq 0.8$. A good approximation model was already obtained by using 4th order polynomial and no significant improvement can be gained by using more than 5th order. The overfitting can be obviously seen in the 20th polynomial order. Generally, R^2 always increases when a higher order term is added to the model. In many cases, the adjusted coefficient correlation R^2_{adj} is more appropriate since it does not always increase when new higher order terms are included. R^2_{adj} can be calculated using Equation (4.23).

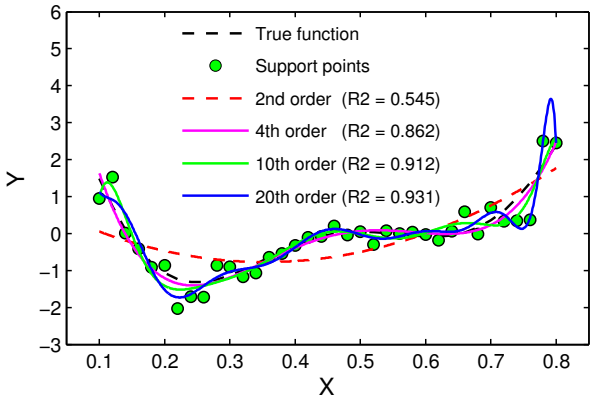

Figure 4.3: Polynomial regression of noise data

Generally, the output (or response) variable of a physical phenomenon is affected by many variables. Hence, the uni-variate polynomial model should be extended in order to cover multiple variables. The formulation of the polynomial regression model for multiple variables can be done by expanding the Equation (4.1). For example, a second order

polynomial regression model with k input variables may take form

$$\begin{aligned}\hat{y} = \beta_0 + \beta_1 x_1 + \beta_2 x_2 + \cdots + \beta_k x_k + \beta_{11} x_1^2 + \cdots + \beta_{kk} x_k^2 \\ + \beta_{12} x_1 x_2 + \beta_{13} x_1 x_3 + \cdots + \beta_{k-1,k} x_{k-1} x_k,\end{aligned} \tag{4.4}$$

or can be written as

$$\hat{y} = \beta_0 + \sum_{i=1}^{k} \beta_i x_i + \sum_{i=1}^{k} \beta_{ii} x_i^2 + \sum \sum_{i<j=2}^{k} \beta_{ij} x_i x_j. \tag{4.5}$$

The number of the polynomial order can be increased to obtain more flexibility of the model. However, a combination of a high polynomial order and a high number of variables leads to a huge number of terms in the equation. Various models can be formed by taking out different single or multiple terms. This means that extra effort is required to select the best model from overwhelming options. Furthermore, a greater number of terms also means more computational efforts to solve a larger system of equations.

The polynomial regression model can be classified as global approximation approach, whereby all training points are considered in calculating the regression coefficients β. All training points have the same contribution when a testing point (approximated point) is calculated, no matter how close the testing point is to all of the training points. Due to this lack of local influence, the polynomial regression model cannot well approximate a function with wavy characteristics.

4.3.2 Radial Basis Function Approximation

The concept of radial basis function (RBF) is basically driven by a motivation to have approximation models that accommodate local characteristics of support points. It is reasonable to consider higher influences from closer neighbors when a testing point is calculated in order to obtain a better prediction. The RBF takes into account this idea by adjusting the shape parameter in the weighting function. The RBF interpolation was initiated by [Hardy, 1971] and further developments of this method are well documented in [Buhmann, 2004], [Wendland, 2005], and [Fasshauer, 2007].

The general equation of the radial basis function approximation in space dimension S can be written as

$$F(x) = \sum_{i=1}^{N} c_i \varphi(\| x - x_i \|_2), \quad x \in \mathbb{R}^s, \tag{4.6}$$

where c_i is the interpolation coefficients and φ is the basis function. ($\| x - x_i \|_2$) is the Euclidean distance between a testing point and the training points. The Euclidean distance of two points, $x_1 = (x_{11}, x_{12}, \dots x_{1s})$ and $x_2 = (x_{21}, x_{22}, \dots x_{2s})$ in S space can be expressed as

$$\| x_1 - x_2 \|_2 \quad = \sqrt{(x_{11} - x_{21})^2 + (x_{12} - x_{22})^2 + \cdots + (x_{1s} - x_{2s})^2}. \tag{4.7}$$

The Equation (4.6) can be written as

$$\begin{bmatrix} \varphi(\| x_1 - x_1 \|_2) & \varphi(\| x_1 - x_2 \|_2) & \dots & \varphi(\| x_1 - x_n \|_2) \\ \varphi(\| x_2 - x_1 \|_2) & \varphi(\| x_2 - x_2 \|_2) & \dots & \varphi(\| x_2 - x_n \|_2) \\ \vdots & \vdots & \ddots & \vdots \\ \varphi(\| x_n - x_1 \|_2) & \varphi(\| x_n - x_2 \|_2) & \dots & \varphi(\| x_n - x_n \|_2) \end{bmatrix} \begin{Bmatrix} c_1 \\ c_2 \\ \vdots \\ c_n \end{Bmatrix} = \begin{Bmatrix} f(x_1) \\ f(x_2) \\ \vdots \\ f(x_n) \end{Bmatrix}, \tag{4.8}$$

or as

$$\Psi\, c = F(x), \tag{4.9}$$

where c and $F(x)$ are the interpolation coefficients and training points, respectively. Ψ is a matrix of Euclidean distance weighting functions, often called Gram matrix. The "heart" of the RBF approximation procedure is the computation of approximation coefficients c, by solving the Equation (4.9). The results of the approximation depend on the chosen basis function. The solution is unique if the Gram matrix is non-singular.

The non-singularity property of the Gram matrix can be ensured by choosing certain basis functions. The Multiquadric function is an example of a basis function that always produces non-singular Gram matrix, [Buhmann, 2004]. However, there is no method available to characterize the class of all basis functions φ that generate a non-singular matrix for any set of x of distinct data sites, [Fasshauer, 2007]. Therefore, a positive definite matrix is considered as an alternative way to ensure the Gram matrix is invertible. A positive definite matrix has a positive determinant and is therefore always non-singular. A symmetric positive definite Gram matrix is also applicable for the Cholesky factorization which is more efficient compared to the LU decomposition. Several basis functions that can be used in RBF approximation are shown in Table 4.1. In this context, r is the distance from the approximated point to the center (support point) and α is the shape parameter.

Gaussian	Multiquadric	Truncated Power
$\varphi(r) = e^{-(\alpha r)^2}$	$\varphi(r) = \sqrt{1 + (\alpha r)^2}$	$\varphi_l(r) = (1 - r)^l$
Inverse quadratic	Inverse multiquadric	Cubic
$\varphi(r) = \frac{1}{1 + (\alpha r)^2}$	$\varphi(r) = \frac{1}{\sqrt{1 + (\alpha r)^2}}$	$\varphi(r) = (r + \alpha)^3$

Table 4.1: Basis function for RBF approximation.

The Gaussian basis function is probably the most commonly-used basis function in the RBF approximation. This basis function will also be applied in this study. The shape parameter α has a significant effect on how flat or peaked the approximation results would be. The terms flat and peaked refer to how strong is the influence of the nearer support points. Figure 4.4 illustrates that the shape parameter α has a profound influence on the Gaussian radial basis function approximation in a two dimensional case. Generally, it also affects the accuracy and numerical stability of the approximate model.

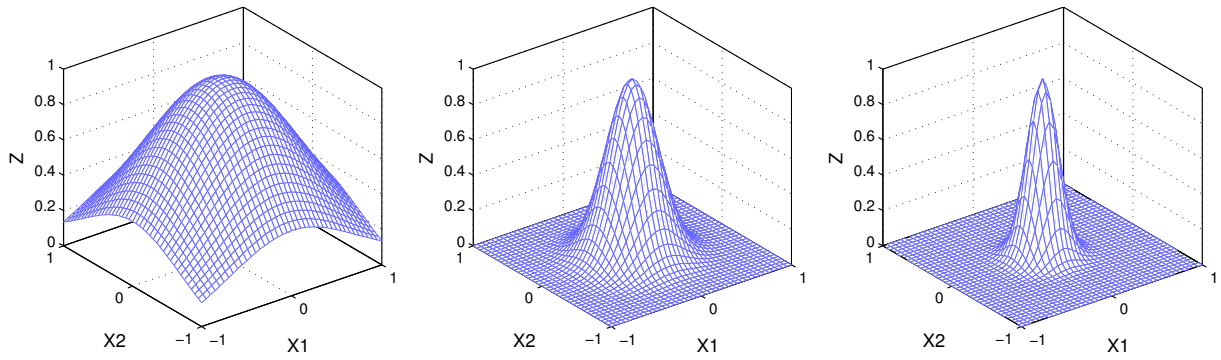

(a) $\alpha = 1$ (b) $\alpha = 3$ (c) $\alpha = 5$

Figure 4.4: Gaussian basis function with different shape parameters α

The influence of the shape parameter α on the radial basis function approximation results are illustrated in Figure 4.5. The surface shown in the figure is the response of a function that is widely known as the PEAKS function. The PEAKS function is obtained by translating and scaling the Gaussian function with two variables. The PEAKS function can be written as

$$f(x, y) = 3(1 - x)^2 e^{-x^2-(y+1)^2} - 10(\frac{x}{5} - x^3 - y^5)e^{-x^2-y^2} - \frac{1}{3}e^{-(x+1)^2-y^2}. \tag{4.10}$$

Figure 4.5a shows the output surface of the exact function in Equation (4.10). The sampling data with noise is shown in Figure 4.5b. The full factorial design with 18 grids in every direction was used. A larger shape parameter value leads to a higher local effect on the approximation results as is shown in Figure 4.5c. A lower local effect is shown in Figure 4.5d.

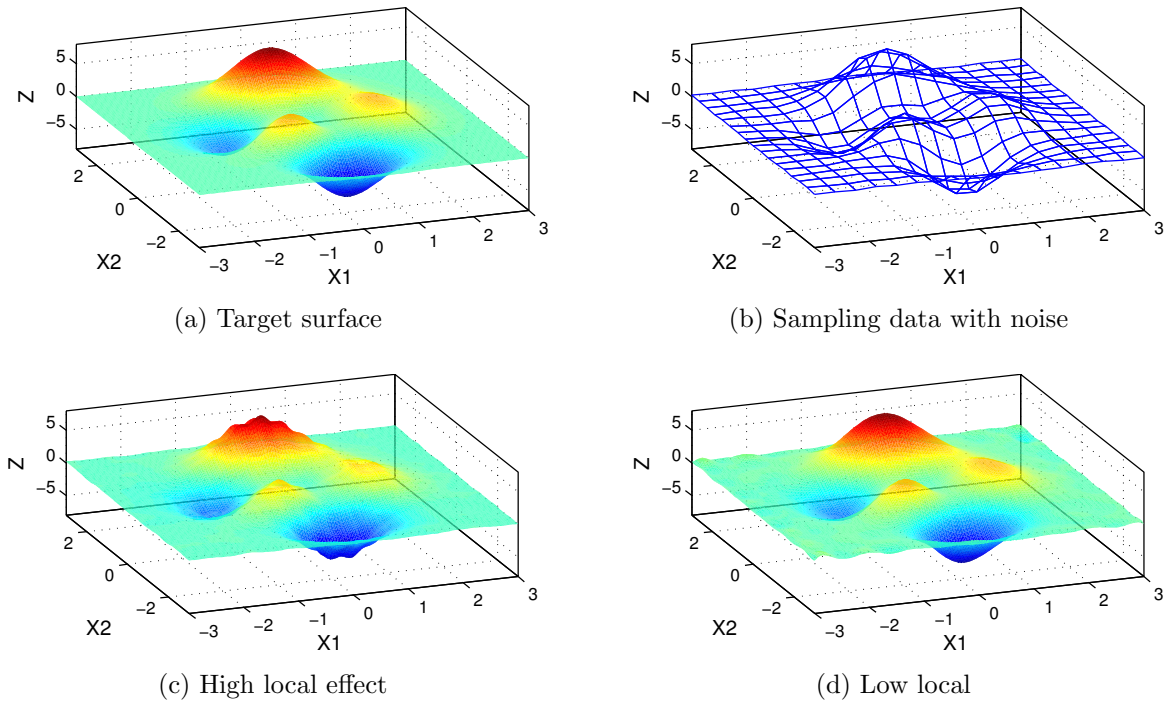

(a) Target surface

(b) Sampling data with noise

(c) High local effect

(d) Low local

Figure 4.5: The effect of chosen shape parameter on the RBF approximation results.

Figure 4.5 illustrates that a larger shape parameter α leads to a more flexible model. Hence, the radial basis approximation approximation may yield overfitting if the training points are corrupted by noise. One strategy that can be used to reduce the risk of overfitting is by reducing the number of basis entries. Another strategy that can be employed is by adding the regularization parameter λ to the main diagonal of Gram matrix, [Poggio & Girosi, 1990]. The coefficient c is calculated as

$$c = (\Psi + \lambda I)^{-1} F(x), \quad \lambda > 0, \tag{4.11}$$

where Ψ is the Gram matrix. $F(x)$ is the training point vector and I is identity matrix.

4.3.3 Moving Least Squares

The moving least squares (MLS) approximation method was first proposed by [Lancaster & Salkauskas, 1981] and is also documented in [Lancaster & Salkauskas, 1986]. It has been widely used for many applications, for instance in function approximation and surface construction. Another important application is in meshfree methods. The power of this method in interpolating, smoothing and derivative's approximation was described by many researchers, e.g. [Levin, 1998 and Breitkopf *et al.*, 2005].

The benefit of the MLS application for scattered data approximation is its ability to accommodate the local character of the input data. The local character influence is adjusted by modifying the shape parameter α and the radius of influence D. The smaller the radius of influence applied, the stronger local influence will be. The formulation of the moving least squares approximation is shortly presented in the following.

Assume $x_i = \{x_1, x_2, \ldots, x_s\}$ is a set of distinct data points in $\mathbb{R}^s$ and y_i is the output value of respective data points. If $P(x_i)$ is the approximation value of y_i, the weighted square error can be expressed as

$$L = \sum_{i=1}^{n} (P(x_i) - y_i)^2 w(\| x - x_i \|_2), \tag{4.12}$$

where w is a weighting function and $(\| x - x_i \|_2)$ is the Euclidean distance in $\mathbb{R}^s$. The number of training points is denoted by n. Equation (4.12) can be rewritten as

$$L = \sum_{i=1}^{n} \epsilon_i^2 w_i(x) = \varepsilon^T W(x) \varepsilon, \tag{4.13}$$

where $W(x) = diag(w_i)$. The best approximation can be obtained by minimizing the Equation (4.13). If the approximate function $P(x_i)$ is defined as $X\beta$ where X is polynomial function and β is the coefficient, the moving least squares approximation finally can be written as

$$\hat{y}_{MLS}(x) = P^T \left[X^T W(x) X \right]^{-1} X^T W(x) y. \tag{4.14}$$

There are several weighting functions that can be found used for MLS approximation. The most common type is the Gaussian weighting function as given in Table 4.1, where

$$r = \frac{\| x - x_i \|_2}{D}. \tag{4.15}$$

The application of moving least squares to approximate function $f(x) = 0.5x + (6x - 2)^2 sin(12x - 4)$ is shown in Figure 4.6. A smaller influence radius D leads to better approximation results. However, if the training points are contaminated with noise, a smaller influence radius does not always provide better results as is shown in Figure 4.7.

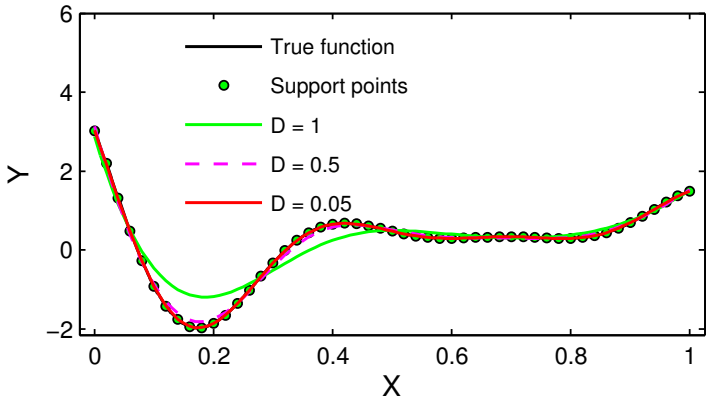

Figure 4.6: The effect of the influence radius D on the moving least squares approximation for data without noise. Smaller D lead to more accurate results

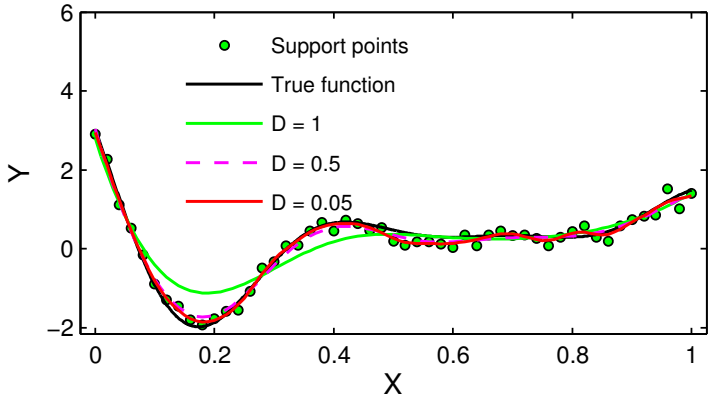

Figure 4.7: The effect of the influence radius on the moving least squares approximation for data contaminated with noise

4.3.4 Artificial Neural Networks

Artificial neural networks (ANN) have been applied in many engineering fields. Most intensive applications are found in image processing or pattern recognition, [Egmont-Petersen *et al.*, 2002]. Many applications are also found in optimization design. In civil engineering, the artificial neural networks have been used to study the reliability of

structures, e.g. [Papadrakakis *et al.*, 1996], [Hurtado & Alvarez, 2001], and [Schueremans & Van Gemert, 2005].

In this study, the artificial neural networks is used to build response surfaces from input output relation of the observation data. The network that is commonly used for surface approximation is called multilayer perceptron (or feed forward back propagation network). The network may consist of several layers that can be classified as input layer, hidden layer, and output layer. A layer may consist of single or multiple neurons. The configuration of the layer, neurons, and how they are connected to each other is called network architecture.

The flexibility of the network approximation model depends on the number of neurons, the number of layers, and the transfer function. The number of neurons (or nodes) in the input and output layers is equal to the number of external variables. However, the number of neurons in the hidden layer may vary. More neurons in hidden layers means that the networks will be more flexible. A two-layer network, with a sigmoid transfer function in the hidden layer and linear transfer function in the output layer, can approximate virtually any function of interest to a certain degree of accuracy, [Hagan *et al.*, 1996]. The network that will be used in this study is shown in Figure 4.8.

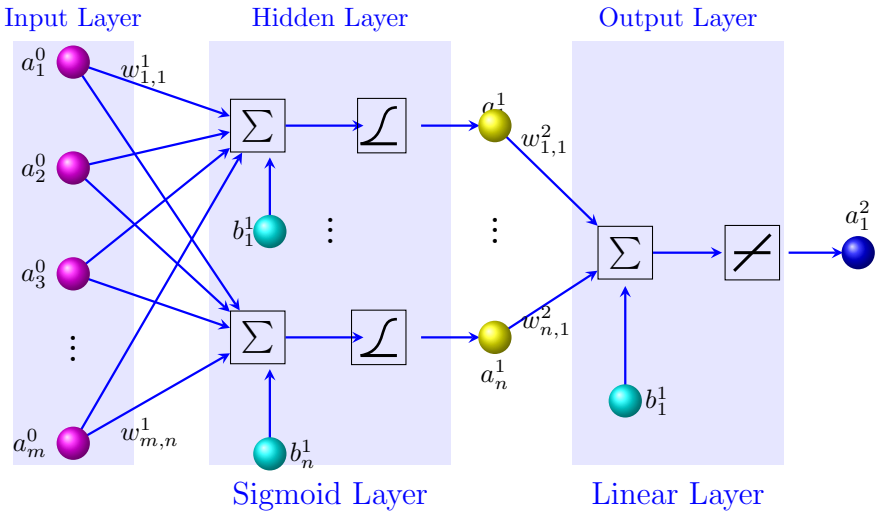

Figure 4.8: Multi layer networks

The information that is held by a neuron in a layer is fed to the neurons in the subsequent layer. The recipient neurons collect information, process it and send the result to the neurons in the subsequent layer. The output of a neuron is the result of a weighted sum operation that can be described as

$$a^{q+1} = f^{q+1}\left(W^{q+1}a^q + b^{q+1}\right) \quad \text{for} \quad q = 0, 1, \ldots, Q-1, \tag{4.16}$$

where a and b are output and bias values, respectively. The upper subscript is the layer number where $q = 0$ is the input layer and Q is the output layer. W is the weighting matrix and f is the transfer function (or activation function). A combination of sigmoid and linear transfer function is commonly used for the response surface approximation. Figure 4.9 shows some commonly used transfer functions.

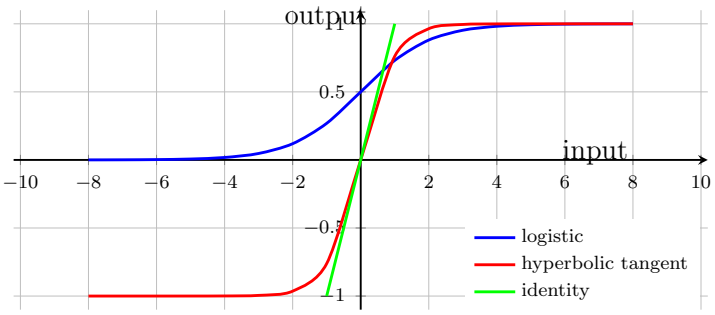

Figure 4.9: Activation function

The value of the network output from the first forward operation (iteration) generally does not fit the target. Therefore, the weight and bias are modified (or updated) by using equations

$$W^q(k+1) = W^q(k) - \alpha_r \, s_r{}^q \, (a^{q-1})^T \tag{4.17}$$

and

$$b^q(k+1) = b^q(k) - \alpha_r \, s_r^q, \tag{4.18}$$

where the index k indicates the current iteration and $k+1$ indicates the next iteration. Here, s_r and α_r are the sensitivity and learning rate, respectively. The same procedure is repeated until the target of performance is reached. The iteration can be terminated if the iteration does not improve the result (no convergence). The number of iterations or training loop is often called epoch.

4.4 Model Selection and Evaluation

Basically, a response surface model is an approximation of the relationship between input and output variables. Some differences (or approximate error) between the observation

and the prediction output are always exist. Different models may produce different quantities of error despite they use the same data. Hence, the response surface method requires a method to assess the adequacy of the meta-model. This section presents some common parameters that can be used for model selection and performance estimation.

The coefficient determination R^2 is probably the most famous parameter to check the quality of an approximate model. It is basically a statistical feature presenting the correlation between the observation data y and the approximation $\hat{y}$. The coefficient determination can be computed as

$$R^2 = \frac{cov^2(y, \hat{y})}{var(y)var(\hat{y})}. \tag{4.19}$$

A perfect model yields a value of R^2 equal to 1. However, $R^2 > 0.8$ indicates a surrogate with good predictive capabilities [Forrester *et al.*, 2008]. The coefficient determination is also often expressed as

$$R^2 = 1 - \frac{SS_E}{SS_T} = \frac{SS_T - SS_E}{SS_T}, \qquad 0 \leq R^2 \leq 1, \tag{4.20}$$

where SS_E and SS_E are the residual and the total sum of squares of the data, respectively.

$$SS_E = \sum_{i=1}^{n} (y_i - \hat{y}_i)^2 \tag{4.21}$$

$$SS_T = \sum_{i=1}^{n} (y_i)^2 \tag{4.22}$$

In the polynomial model, R^2 always increases when new terms are added to the model. In this case, this means that often a higher value of R^2 does not guarantee the data is well approximated. Alternatively, the adjusted coefficient determination R^2_{adj} can be used. The R^2_{adj} defined in Equation (4.23) does not always increase when new terms are included.

$$R^2_{adj} = 1 - \frac{SS_E/(n-p)}{SS_T/(n-1)} = 1 - \frac{n-1}{n-p}(1 - R^2), \tag{4.23}$$

where p is the number of parameters in the regression model.

Another way to assess the quality of the approximation model is called mean squared error (MSE). It can be calculated Equation (4.24). A model with the lowest value of MSE

is considered the best model. Root mean square error (RMSE) is also often used, which is obtained by taking the square root MSE.

$$MSE = \frac{1}{n}\sum_{i=1}^{n}(y_i - \hat{y}_i)^2. \tag{4.24}$$

Generally, it is also useful to have a visual understanding of the target and the predicted value. However, this can only be performed for models with one or two variables.

Chapter 5

Reference Surface-Based System Identification

5.1 Introduction

New advances in the system identification of mechanical structures allow the vibration-based damage detection method utilizing ambient excitations. The possibility to use natural excitations through the output only data identification concept gives a great advantage for the modal identification of a large structure where the use of artificial excitations is often unpractical and expensive. However, the examined structure might be sensitive to environmental and operational conditions, which may vary with time. It has been widely acknowledged that the surrounding condition of a structure has a significant influence on its vibration response. Many literatures reported that ambient temperature has a significant effect on the results of the modal frequency measurement of structures e.g. in [Cornwell *et al.*, 1999b], [Sohn *et al.*, 1999], and [Peeters & De Roeck, 2001]. Other environmental variables such as waves, wind, humidity and moisture content could also contribute to an alteration of the dynamics response. Moreover, the operational or loading condition such as vehicle speed and weight on a bridge, for instance, can introduce different excitation frequencies and amplitudes, respectively. These environmental and operational factors are called non-damaged parameters in the damage identification problem. In general, a damage indicator that is sensitive to damaged parameters is often also sensitive to non-damaged parameters, [Farrar *et al.*, 1994]. The vibration-based damage identification procedures may lead to poor result in situations where non-damaged parameters are not well handled. The structural health monitoring systems will not be

accepted in practical applications, unless robust techniques are developed to explicitly account for environmental and operational conditions, [Sohn, 2008].

Several different strategies have been proposed in order to eliminate certain environmental effects on the vibration-based damage identification. [Sohn *et al.*, 2002] proposed a so-called statistical classification where a combination of time series analysis, neural networks, and statistical inference techniques was applied to explicitly take into account the effect of changing environment and operational conditions. The proposed method was demonstrated through a numerical and experimental model of an eight-degree-of-freedom spring-mass system. The extension of subspace-based algorithm has been proposed by [Balmès *et al.*, 2008] to remove the temperature effect from a numerical bridge deck model. [Daraemaeker *et al.*, 2008] performed the system identification in two parts. In the first part, eigen properties of the structure are extracted using an automated stochastic subspace identification procedure. In the second part, the environmental effect model is built using factor analysis, based on long term monitoring of the undamaged structure. The post processing is applied to the damage indicator to remove the effects of the environment. This approach has been implemented to the Finite Element model of a three-span bridge.

Basically, the ambient vibrations of many structures such as long span bridges, buildings, oil platforms, and wind mills are affected by many non-damaged variables. The above proposed approaches seem to be be very complex if the dynamic responses of the structures are affected by many non-damaged variables.

This thesis proposes a simpler approach to handle multiple non-damaged variables in the vibration-based damage identification. The proposed method is called reference surface-based system identification, which combines response surface methodology with vibration analysis. In this proposed method, a meta-model is utilized to take into account the influence of non-damaged variables to the vibration response of a structure in undamaged condition; hence, the meta-model is called reference surface model. The basic concept, advantages, limitations, and other important aspects of the reference surface-based system identification are elaborated in the following subsections.

5.2 Reference Surface

In the context of damage identification, a reference surface can be defined as a mathematical model which describes the response (damage indicator value) of an undamaged

structure for given operational and environmental conditions. The reference surface models are developed based on the response surface methodology concept.

Consider y_i is the value of a vibration-based damage indicator (e.g., natural frequency, mode shape, modal curvature, maximum displacement, total energy, etc.) of an undamaged mechanical system, that is measured in s environmental and operational conditions $(x_{1i}, x_{2i}, \ldots, x_{si})$. If $g(x)$ is the exact function describing their relationship, the damage indicator value at a given input set of environmental or operational condition can be calculated as

$$y = g(x_1, x_2, \ldots, x_s). \tag{5.1}$$

In most applications of damage identification, $g(x)$ is unknown. However, an approximation function $h(x)$ can be used in the above expression to predict the value of y. Since the approximation function $h(x)$ is not exactly the same as $g(x)$, prediction error ε will be introduced into the equation. The Equation (5.1) can be written as

$$y = h(a_1 a_2 \ldots a_n; x_1 x_2 \ldots x_s) + \varepsilon. \tag{5.2}$$

The damage indicator value (output) that is described by the approximate function $h(a_1 a_2 \ldots a_n; x_1 x_2 \ldots x_s)$ is called the reference surface model. The input values $(x_1, x_2, \ldots x_s)$ refer to operational and environmental variables (e.g., temperature, moisture content, wind velocity, etc). The parameters $(a_1 a_2 \ldots a_n)$ can be estimated by using input-output relationship of the observation data, in such a way that,

$$h = E[y], \tag{5.3}$$

where E is the expectation operator. Several methods can be used to build the reference surface models from scattered observation data. Some of the most commonly used approaches have been described in Chapter 4.

The application of the proposed method for damage identification of a structure in time variant environment has some advantages. Many non-damaged variables can be easily included or excluded in the model. The damage detection can be performed any time if the ambient vibrations are used. The reference surface model can be built from vibration signals of a single sensor. However the usage of multiple sensors increases the probability to detect damages, as sensitivity of damage indicator also depends on the distance to the damage. Furthermore, multiple reference surface models based on different damage indicators can be used to improve the reliability of damage detection results.

In many numerical examples, certain damage indicator such as eigen frequency is not able to detect small damages, [Ahmad *et al.*, 2011]. However, the capability of the frequency damage indicator to discriminate damaged and undamaged condition increases monotonically with respect to damage severity. For comparison, wavelet energy damage indicator is more sensitive to small damage compared to the eigen frequency, but it does not present a monotonic trend if the damage becomes much more severe.

The proposed reference surface-based system identification method can be split into two phases; learning (or training) phase and detection (or monitoring) phase. These phases are briefly elaborated in the following subsections.

5.3 Learning Phase

The learning phase can be considered as the most critical part of the reference surface-based system identification. In this phase, data regarding all important environmental and operational variables of structures are collected. The vibration response signals are processed and converted into a feature called damage indicator. Some of these damage indicators and how they are calculated are briefly described in Section 2.2, 2.3, and 2.4. In the reference surface-based system identification method, the environmental and operational variables are called input variables while the damage indicator is called output or response variable.

The input and response variable data sets that are obtained during the learning phase will be used to train the reference surface models. Hence, the learning phase can also be called the training phase. Many reference surface models can be built based on the input variables that are considered. For instance, several uni-variate reference surface models can be built by taking into account only one of many available environmental and operational variables (e.g. temperature, wind speed, moisture content, etc.). Multivariate reference surface models can be built by considering two or more environmental or operational variables. Furthermore, various reference surface models can be built depending on the response variable that is used. As an example, the first eigen frequency reference surface model refers to a meta-model which uses the first eigen frequency as the response variable.

Basically, vibration responses of structures that are located in the open space are affected by many variables. Some of these variables might have a significant influence to the vibration response of the structure while others not. Theoretically, it is possible to build

a reference surface model that covers all of these variables. However, according to Occam's razor (parsimony) principle, less complex models are often preferable, since unimportant input variables increase the complexity of the model while the approximation quality is not significantly improved. These insignificant input variables can be eliminated from the meta-model by considering how important an input variable is to the variation of the output. This approach is known as sensitivity analysis. These input variables can then be ordered with respect to the sensitivity indexes, where a higher value indicates a higher importance. It should be noted that the sensitivity index order might not be the same in all design space (input variables range). For example, consider a reference surface model for damage identification of a short span bridge built from three environmental and operational variables: train speed, temperature, and humidity. A long series train at constant speed generates a periodic loading when it passes through the bridge. Hence, the bridge's responses during this time are highly affected by the train speed. At certain speed, the frequency of the periodic loading might be close to one of the natural frequencies of the bridge, thereby highly amplifying the responses. In this situation, the train speed might be a more important variable compared to the other two. Also, the temperature has a nonlinear relation with the shear or Young modulus of some materials; hence, the order of importance might change depending on the combination values of these variables. In extreme cases, the rank of an input variable might vary from high to low importance. In cases such as above, partial reference surface models that cover only certain range and input variables might be more appropriate than a single reference surface model that covers all input variables and ranges.

5.3.1 Time Interval of The Learning Phase

The learning phase is commenced based on a very important assumption; there is no damage present in the structure. This fundamental assumption is not an important issue in a numerical simulation study. It is also less important in a laboratory testing where the experimenter has full control of the experimental model. However, this assumption is very crucial in a real physical structure because there is no guarantee on the absence of damage.

Based on that reason, the learning phase of the reference surface-based system identification is ideally applied to new structures where the risk of existing damages is low. The learning phase should start soon after the construction work is finished. However, it should be kept in mind that an early damage might take place during the learning phase

due to unpredictable situations such as material imperfection, over loading or inappropriate assumption during design and construction process. A regular local inspection can be integrated into the learning phase to ensure the absence damage in the structure.

In essence, the time interval for the training phase should be long enough to cover all possible environmental and operational conditions. This can vary depending on the relevant environmental or operational variable. For instance, one year is approximately required to complete the learning phase if temperature effect is a concern. Figure 5.1 illustrates the variation of some environmental and operational variables. The data was obtained from the long term monitoring system of Saaletalbrücke bridge located near Naumburg, Germany. Three variables are presented in the figure: temperature, axle load, and train speed variation. The temperature reached below -10 Celsius degree during winter seasons and increased to more than 30 Celsius degree during summer seasons (Figure 5.1a). The maximum speed was limited to 90 km/h due to the track layout condition (Figure 5.1c). The variation of axle load of two different types of train is shown in Figure 5.1b.

In a numerical or laboratory experiment, the design of experiment (DoE) is used to choose the combination of variable input values (sampling plan). Several methods can be employed to deal with this issue as described in Section 4.2. However, it is difficult in the field application to obtain the same combination of variable input value as the DoE result. The value of operational or environmental variable varies arbitrarily and cannot be adjusted such as in the laboratory test. Hence, the collected data might be densely scattered in certain regions of the design space.

5.3.2 Computer Versus Physical Experiments

The fundamental issue considering a physical and a computational experiment is that random error exists in the laboratory experiments, but it does not exist in the computational simulation. A computational experiment is deterministic in that repeated observations with the same set of inputs yield an identical response. Repetition is apparently not necessary in the computational experiments. A single observation is sufficient to present the relation between input and output variables. Therefore, the results of the design of experiment should contain only the distinct points.

On the other hand, the same setup of numerous physical experiments could lead to a variation of responses due to imperfection in experimental settings and measurement equipments. For instance, the dynamic responses of a simple beam excited with a shaker (in a laboratory) vary since the force generator cannot generate the same force in every

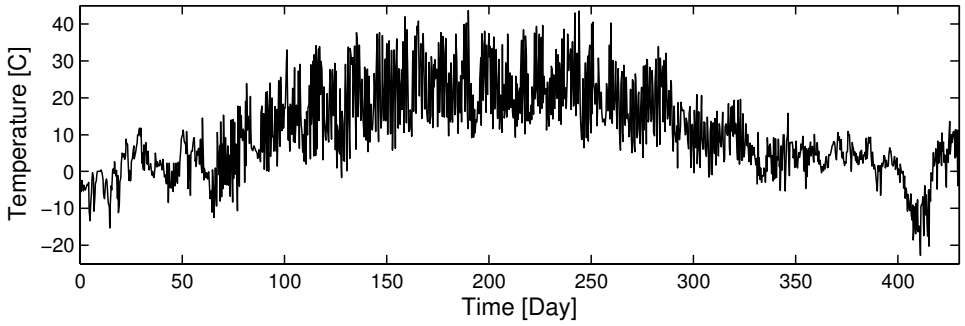

(a) The temperature variation over a year period

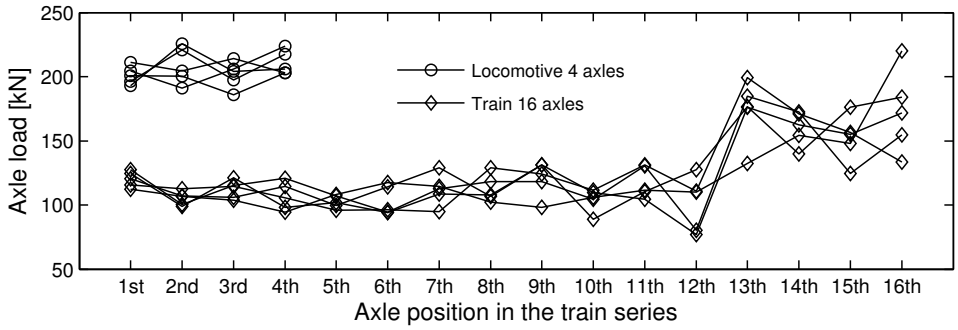

(b) The axle load variation of two different train types

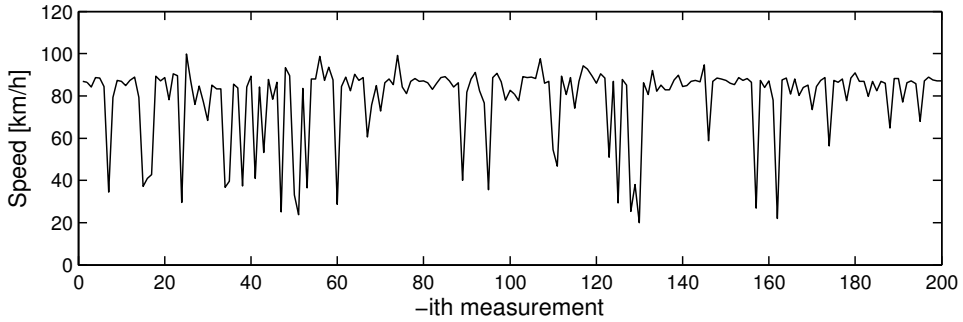

(c) The variation of train speed

Figure 5.1: The environmental and operational conditions of the Saaletalbrüke bridge, Naumburg-Germany.

single test. Furthermore, the surrounding condition such as temperature or external noise, may cause undesirable effect on the responses. Repeated observation of the same set of input may result in a variation of responses. The existence of random errors in physical experiments creates complexity in data analysis and reference surface model building.

Replication of the test is often suggested to reduce and control the magnitude of error in a physical experiment. The sample means of replicated responses have smaller variances than the individual responses. In the application of reference surface-based system iden-

tification method with noisy data, test replication can be useful to avoid overfitting in searching for the best meta-model. The reference surface model can be built by using the mean value of the replication tests as training points.

Some basic statistical properties of the observation data during the learning phase are required in order to conclude whether a new measurement belongs to the damaged or undamaged system. Some of the basic probabilistic distribution theories are described in the following:

The probability density function is the derivative of probability distribution function $F(x)$ and can be written as

$$f(x) = \frac{d}{dx}F(x), \tag{5.4}$$

where

$$\int_{-\infty}^{\infty} f(x)dx = 1. \tag{5.5}$$

The expected value (or expectation, mean) of a random variable X can be described in term of the probability density function as

$$\bar{X} = E[X] = \int_{-\infty}^{\infty} xf(x)dx. \tag{5.6}$$

A measure of how far a data from a random variable is spread out from its mean value is called variance (σ^2 or V(X)). The variance can be written as

$$V(X) = E[(X - \bar{X})^2] = \int_{-\infty}^{\infty} (X - \bar{X})^2 f(x)dx. \tag{5.7}$$

The positive square root of the variance is called the standard deviation σ_x and can be written as

$$\sigma_x = \sqrt{E[(X - \bar{X})^2]}. \tag{5.8}$$

The covariance of two random variable x and y can be described as

$$\begin{aligned} \sigma_{x,y} &= E[(X - \bar{X})(Y - \bar{Y})] \\ &= E[XY] - E[X]E[Y]. \end{aligned} \tag{5.9}$$

The above formulations are from the continuous probability theory and can be applied to the discrete probability theory by calculating these equations using finite sums instead of integrations. Assume n replications are done to obtain information of a support point of a

reference surface model candidate and each value has the same probability. The variance of these replication tests can be computed as

$$V(X) = \frac{1}{n}\sum_{i=1}^{n}\left[x_i - \bar{X}\right]^2 \tag{5.10}$$

and the standard deviation can be written as

$$\sigma_x = \sqrt{\frac{1}{n}\sum_{i=1}^{n}\left[x_i - \bar{X}\right]^2}, \tag{5.11}$$

where $\bar{X}$ is the expected value of x and n is the number of data.

The most commonly used distribution of random variable is probably the normal (or Gaussian) distribution where its probability density function can be described as

$$f_X(x)\frac{1}{\sigma_x\sqrt{2\pi}}exp\left[-\frac{(x-\bar{X})^2}{2\sigma_x^2}\right], \qquad -\infty < x < \infty, \tag{5.12}$$

The distribution is called the standard normal distribution if $\bar{X} = 0$ and $\sigma_x = 1$.

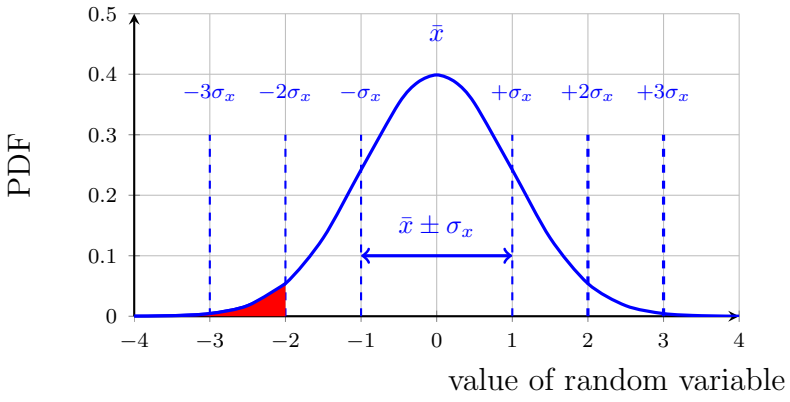

Figure 5.2: Normal probability density function

The probability of an event to occur is calculated by integrating the probability density function, that is calculating the area under the curve as shown in Figure 5.2.

$$F(z) = \frac{1}{\sqrt{2\pi}}\int_{-\infty}^{z} exp\left(-\frac{1}{2}w^2\right)dw, \tag{5.13}$$

where

$$w = \frac{x - \bar{X}}{\sigma_x}. \tag{5.14}$$

A closed form solution of the integral in Equation (5.13) does not exist. However, the integral can be approximated by using numerical analysis and the result has been written in table. Generally, the table consists of the normal probability of the standard normal distribution. There exists a so-called empirical rule (or three-sigma rule) which states that for a normal distribution, nearly all values lie within 3 standard deviations of the mean as is shown in Figure 5.2, [Upton & Cook, 2008]. About 68.27% of values lie within 1 standard deviation of the mean. Similarly, roughly 95.45% and 99.73% of values lie within 2 and 3 standard deviations of the mean, respectively.

The probabilistic features that have been described above are used to define the threshold of the reference surface models. The predefined threshold is an upper and lower shift of the response variable values that account for variation of the observation points used to build the reference surface models. Points that lie between the thresholds are considered to be derived from the same system used to collect the training points.

5.3.3 Notes on Reference Surface

The product of the learning phase is a reference surface model which can be defined as a benchmark of responses of a healthy structure in various environmental and operational conditions. A significant deviation from the reference surface model can be suspected as a response of a different mechanical system such as damaged structures. Several reference surface models of a monitored structure can be built depending on the relevant input variables (environmental and operational conditions) and response variable (damage indicator). For example, a frequency reference surface model refers to a meta-model that uses eigen frequency as the response variable. The same analogy can be applied to wavelet energy reference surface model, wavelet entropy reference surface model, stochastic subspace identification (SSI) reference surface model etc. Figure 5.3 illustrates the learning phase of a structural response with a single environmental variable.

Since a reference surface model is a representation of a healthy structure, the model should be able to approximate the training points precisely or with very small prediction error. The quality of the approximate model has a direct consequence on the reliability of the reference surface model to detect damages in a structure.

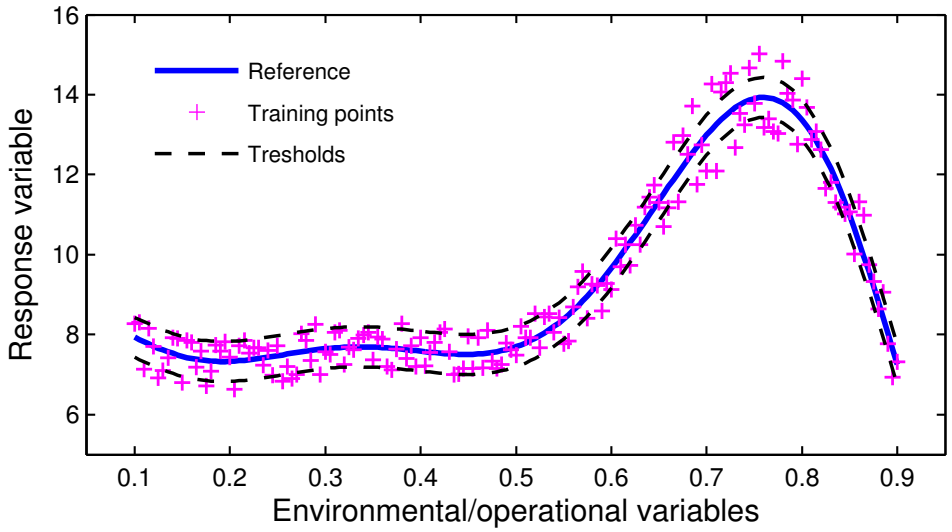

Figure 5.3: Training phase: the reference surface model is built from observation points using scattered data approximation methods

In general, the capability of a reference surface model to approximate the scattered observation points is affected by:

- the chosen damage indicator.
  The characteristic of a damage indicator has a significant effect on the ability of a scattered data approximation method to produce a good reference surface model. For instance, eigen frequency damage indicator always presents a monotonically trend with a slight slope. Therefore, almost all of the approximation methods can easily produce a good meta-model with very small error. Other damage indicator, such as wavelet energy or wavelet entropy, does not always have a monotonic trend, especially if a large change exists in the mechanical system. The surface will have many peaks and troughs, making it very difficult for a global approximation method, such as polynomial regression with lower order, to approximate, particularly when applied to a multivariate data set.

- data sampling.
  The data sampling should have a good representation of the entire design space. Some common methods for space filling and model validation are described in Chapter 3. It is difficult to predict the minimum number of data required without a prior knowledge of how the reference surface looks like. It depends on how dynamic the target surface is with respect to gradient changes. A data set should also be allocated for validation purpose because most of the approximation models produce

more accurate predictions in the vicinity of sampled points. Therefore, it is important to test the model out of the training points.

A threshold is introduced to a reference surface model to take into account the variation of the observation data. It may be included into the reference surface model in the following way:

1. by directly constructing two reference surface models. The first reference surface is called the upper bound reference surface, where it is built from the top limit of response variable values. The second reference surface is called the lower bound reference surface, where it is built from the bottom limit of response variable values. The top limit and the bottom limit of the response variable values are determined based on the standard deviation of the respective training points.
2. by shifting the reference surface. The reference surface is duplicated and shifted to the top and the bottom to form the upper and lower bound reference surfaces, respectively. The standard deviation is assumed similar for all of the training points.

5.3.4 Observation Data Selection

It has been shown in Subsection 4.3.2 and 4.3.3 that the shape parameter α and the influence radius D have profound effects on the result of local approximation methods such as radial basis function and moving least squares. The chosen shape parameter or influence radius might not suit all region of the design space if the training points are distributed irregularly. A regular (uniform grids) support point has a positive impact on the quality of the model since the chosen radius suits well in all region of the design space. However, it is almost impossible to obtain observation points that lie in regular grids from a long term structural health monitoring system. The environmental and operational variables vary arbitrarily with respect to time. The training points might be concentrated in certain regions distinct from others, such as those near a boundary. In this situation, instead of using an adaptive algorithm that can adjust the shape parameter or the influence radius, the following two strategies are proposed.

1. Preselected strategy
   The preselected strategy can be applied to reduce the irregularity of the training points. This means that not all observation data will be selected and used to train the reference surface model. The unselected observation points can later be used

to validate the model. The design space is divided into n bins with similar sizes. Only one observation point per bin will be selected. If there are many observation points in a bin, the one closest to the bin center will be considered. Aside from improving the regularity of the training points, the preselected strategy also reduces the computational cost as the size of the linear equation system matrix becomes smaller.

2. Observation point reconstruction
   The observation point reconstruction strategy can also be applied to improve the regularity of training points by creating artificial observation points. The observation data is clustered into blocks, and by using an approximation method, artificial observation points are created in each block. Thereafter, the reference surface model is built using the artificial support points or combination of artificial and preselected support points. However, this procedure requires more computational effort since many local approximation models are built before the reference surface model is constructed. The approximate error is calculated based on the original support points to avoid error accumulation. The concept of the observation points reconstruction strategy is illustrated in Figure 5.4.

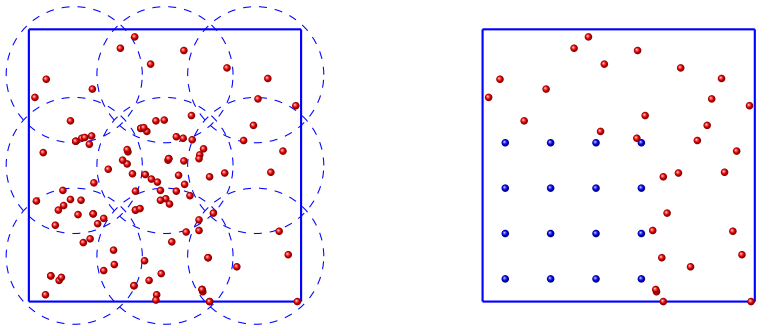

Figure 5.4: Support points reconstruction: (a). The original support points. (b). Reconstructed support points.

5.4 Detection Phase

The detection phase of the reference surface-based system identification method can be done after the thresholds are defined. The damage detection is a determination of whether a recent response is discordant or inconsistent compared to the undamaged condition

response of the structure. This phase is often called the monitoring phase because it is used to monitor the performance of the structure.

The damage detection can be easily performed as follows. Vibration responses and environmental or operational conditions are measured. The response signals are converted to damage indicators. The damage indicator value that is obtained is compared to the reference surface model. Those between the upper and lower bound reference surfaces are classified as normal (undamaged response). On the contrary, damage indicator values that lie outside of the thresholds are declared as anomalies, which may reflect damages in the structure.

Figure 5.5 illustrates the concept of the reference surface-based system identification method that proposed in this thesis. The solid line represents the benchmark response variable value of healthy structures. The scatter plots are responses during the monitoring phase. The dash lines illustrate the upper and lower bounds of the response variable values.

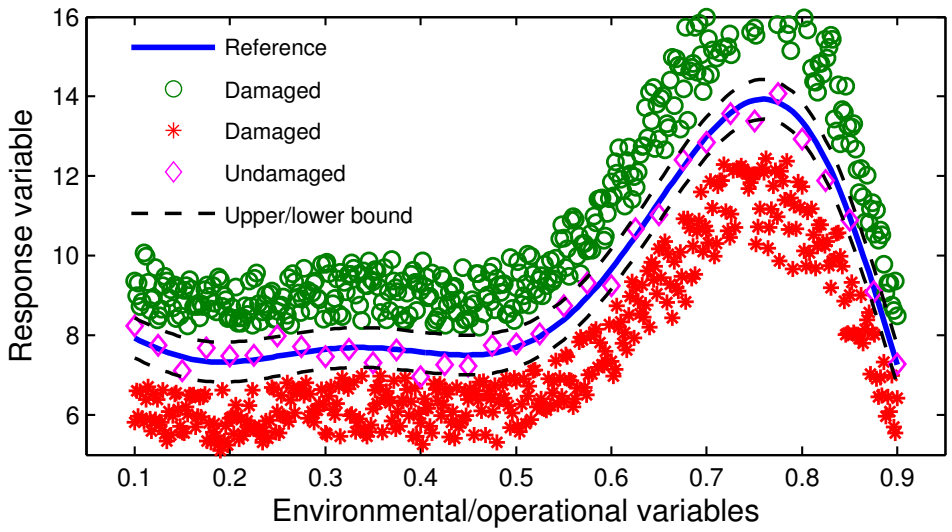

Figure 5.5: Illustration of the detection phase in the reference surface-based system identification method. Recent response variable values are compared to response variable values of the reference surface.

The structures can be declared undamaged if the following expression is fulfilled,

$$Ru \geq Ra \geq Rl, \tag{5.15}$$

where Ru and Rl are response variable values of upper and lower bound reference surface

models, respectively, and Ra is the response variable value of a recent measurement. Since the upper and lower bound reference surface models are built based on the standard deviation σ of the observation data, the Equation (5.15) can be written as

$$Rm + ct\,\sigma \geq Ra \geq Rm - cb\,\sigma, \tag{5.16}$$

where σ is the standard deviation. The coefficients ct and cb depend on the confidence interval and probability distribution of the observation data. Here, Rm denotes the response variable value of the reference surface model. If the observation data has a symmetric distribution, ct is equal to cb. Hence, the damaged or undamaged condition can be expressed as

$$DI = \frac{\mid Ra - Rm \mid}{c\,\sigma}, \tag{5.17}$$

where DI is the damage index and values ≥ 1 indicate damage. The value c is dependent upon the chosen confidence interval. As an example, the damage index DI with 95 % probability can be obtained by choosing $c \simeq 2$ if the training points has a normal (or Gaussian) distribution.

Ideally, multiple tests are performed before a structure is declared damaged or undamaged. The results of multiple damage detection tests can be expressed as

$$\overline{DI} = \frac{1}{k}\sum_{i=1}^{k} \frac{\mid Ra_i - Rm_i \mid}{c\,\sigma_i}, \tag{5.18}$$

where $\overline{DI}$ is the mean value of damage index and i is the damage detection point at given environmental and operational conditions. The number of damage detection test is k and σ_i the prediction of standard deviation at detection point i.

The results of the multiple damage detection test of a structure can also be expressed in a probability value. For instance, by using the Bayes' theorem, the probability of the structure to be in damaged condition can be expressed as

$$P(D|I) = \frac{P(I|D)P(D)}{P(I|D)P(D) + P(I|U)P(U)}, \tag{5.19}$$

where $P(D)$ is interpreted as prior probability of the structure to be in damaged condition. $P(D|I)$ is the posterior probability, after information from damage detection test is included. $P(I|D)$ and $P(I|U)$ are probabilities of the structure to be in damaged and undamaged conditions, respectively, according to the results of damage detection tests.

Many reference surface models that correspond to the chosen damage indicators can be built from the same observation data. In many cases, the capability of these reference surface models to discriminate the damaged and undamaged conditions is different from one to another. There may be cases where not all reference surface damage detection models yield the same results.

For instance, frequency reference surface models are less sensitive to the change in the structure compared to wavelet energy in some cases, [Ahmad *et al.*, 2011]. The word 'sensitive' in this context means the ratio of damage indicator changes between damaged and undamaged conditions. However, the sensitivity of the frequency reference surface model increases monotonically with respect to damage severity. On the contrary, the wavelet energy reference surface model does not have a monotonic trend of sensitivity with respect to damage severity. Figure 5.6 illustrates the behaviour comparison of these damage indicators with respect to damage severity. In this case, the disagreement can be encountered in two scenarios: very small or very large damage.

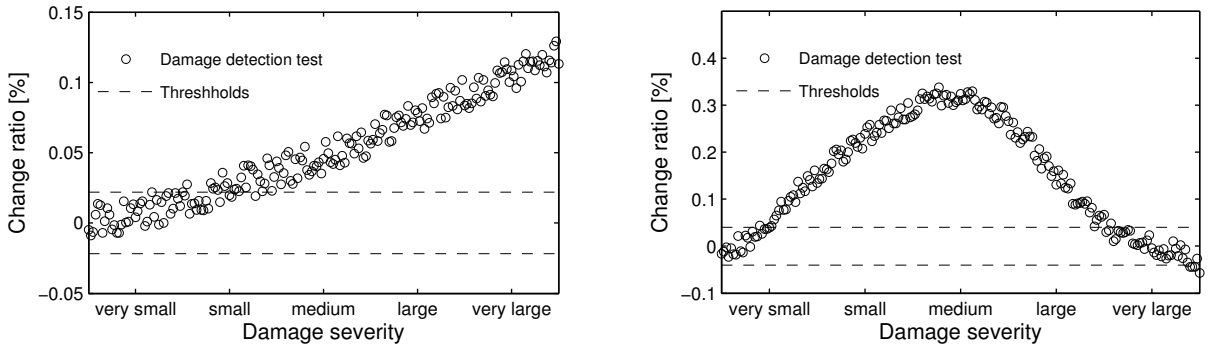

(a) Eigen frequency

(b) Wavelet energy

Figure 5.6: The comparison of frequency and wavelet energy

Since there has been no quantitative measure developed for this case, it might be reasonable to present the conclusion in a qualitative way. For instance, the term 'damaged' is distinguished into two terms, 'all-damaged' and 'semi-damaged'. All-damaged indicates the agreement of all results while semi-damaged means the discrepancy of some. In the very small damage scenario in Figure 5.6, the frequency and wavelet reference surface models give 'negative' and 'positive' results, respectively, which may be caused by subtle changes in the frequency are masked by noise. Due to this, the structure will be first declared 'semi-damaged'. It is a warning sign, so that a regular scheduled damage detection can be planned. The later measurements tend to show greater responses as damages

grow. The status can be changed to 'all-damaged' if a positive correlation coefficient is obtained from the regular schedule measurement data.

5.5 Summary

It has been widely acknowledged that the use of ambient vibrations for damage detection of structures might yield poor results, if effects of the surrounding conditions of the structures are not considered. The dynamic response change due to damages is influenced by the effects from non-damaged variables; hence, it is unknown whether the damage indicator change is a product of structural damages or environmental effects only.

The reference surface-based system identification method is proposed in this thesis to overcome this problem. A surrogate model is used to take into account the effects of environmental and operational conditions to the vibration response of the structure. The surrogate model is called the reference surface model, which is the benchmark response of healthy structures. The proposed method allows simple handle of multiple non-damaged variables, which seems to be very complex in other methods.

The reference surface models are trained by using input output relation of observation data. The inputs are the environmental and operational conditions while the output is the damage indicator. Once the reference surface model is obtained, the damage detection can be performed at any time using the current ambient vibration data. The capability to detect damage at any environmental and operational conditions is very important for structural health monitoring system.

At this moment, the proposed reference surface-based system identification method is focused on the first level of Rytter's damage identification terminology, [Rytter, 1993], which is to detect the presence of damages. It may be possible to extend the proposed damage identification method to be used for damage localization and quantification, such as by using a monotonic type damage indicator, Finite Element model, and model updating.

Chapter 6

Numerical Simulation Model

6.1 Introduction

In this chapter, the proposed reference surface-based system identification method is applied to a numerical simulation model. A train passing over a bridge model is considered since its dynamic response is obviously affected by many environmental variables (e.q., surrounding temperature, humidity etc.) and operational parameters (e.q., train speed, axle load, wagon configuration etc.). In this simulation, only temperature and train speed are considered.

The Erfttal-Brücke, a high-speed railway bridge on the line between Cologne and Brussels is chosen due to the following reasons. First, a long term measurement has been performed on this bridge, therefore some basic information such as support stiffness and modal damping ratio are already available in order to calibrate the model. This bridge has been discussed in several references such as in [Brehm *et al.*, 2009] and [Cantieni *et al.*, 2009]. The skewed bridge consists of two separated superstructures; each of these is subjected to support one track. In this simulation, only one track is loaded by a passing train. This does not account for the scenario whereby two trains going in the opposite direction pass the bridges at the same time. The layout and basic dimensions of the Erfttal-Brücke is shown in Figure 6.1. Further detailed information about the numerical simulation model is described in the following sections.

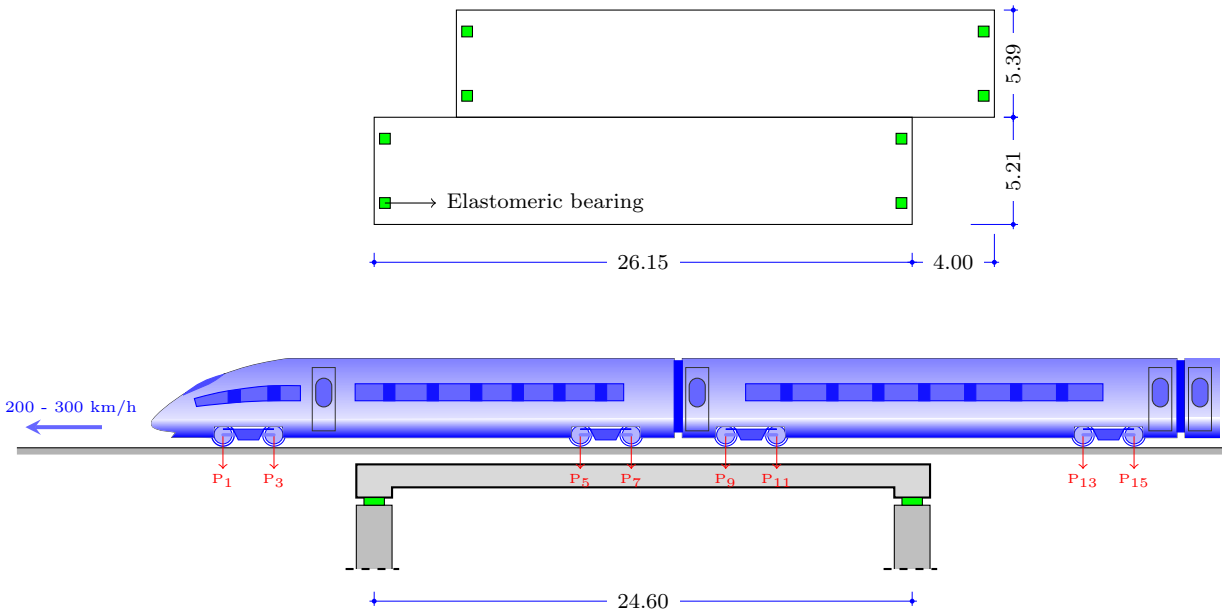

Figure 6.1: Layout and basic dimensions of the Erfttal-Brücke railway bridge

6.2 General Description of the FE Model

The Finite Element (FE) model of the bridge is developed using the software package SLang (Structural Language), [Dynardo GmbH & Bauhaus University Weimar, 2009]. The bridge type is known as a concrete filler beam structure where the main components of the structure are concrete deck slab and I shape steel main girders. The deck slab and the I shape steel main girders are modeled using shell and beam elements, respectively.

In this simulation, another important component of the FE model is the elastomeric bearings which directly support the superstructure. The temperature is assumed to affect only the elastomeric bearings. The changes of stiffness in the elastomeric bearings lead to a change of the eigen frequency and response of the superstructures. The three dimension (3D) spring elements are used to model the elastomeric bearings. The 3D spring elements also used to model the ballast. Five 3D spring elements are allocated to represent ballast under a sleeper. Beam elements are used to model the sleepers. The cross section of the FE model is illustrated in Figure 6.2.

The material properties of the numerical simulation model are summarized in Table 6.1. The values in this table are basically based on results of the experimental testing and model updating of the real bridge that has been reported in [Brehm, 2011].

The FE model of the Erfttal-Brücke railway bridge used in this study is shown in Figure

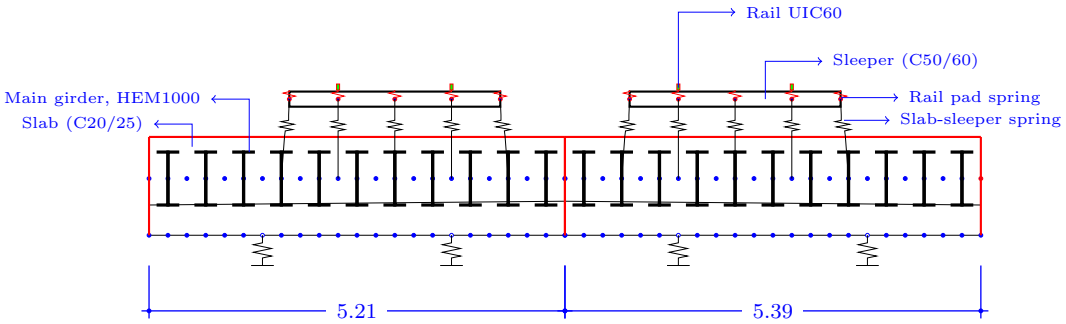

Figure 6.2: Cross section of the finite element model of the Erfttal-Brücke railway bridge

Table 6.1: Input parameters of the finite element model of the Erfttal-Brücke railway bridge

No.	Input Parameter	Input Value	Unit
1.	Young's modulus of I main girder	$2.00.10^{11}$	N/m^2
2.	Young's modulus of concrete slab	$2.70.10^{10}$	N/m^2
3.	Young's modulus of sleeper	$3.00.10^{10}$	N/m^2
3.	Density of I main Girder	$7.80.10^{3}$	Kg/m^3
4.	Density of concrete Slab	$3.00.10^{3}$	kg/m^3
5.	Density of concrete Sleeper	$2.10.10^{3}$	kg/m^3
6.	Poisson ratio I main girder	0.25	-
7.	Poisson ratio Concrete Slab	0.18	-
8.	Poisson ratio sleeper	0.20	-
9.	Shear modulus of elastomer 1	$3.00.10^{6}$	N/m^2
10.	Shear modulus of elastomer 2	$3.00.10^{6}$	N/m^2
11.	Stiffness of rail pad u_x	$1.00.10^{5}$	N/m^2
12.	Stiffness of slab-sleeper u_x	$5.00.10^{4}$	N/m^2

6.3. The six lowest natural frequencies of the numerical Finite Element model of the bridge are shown in Figure 6.4. In this figure, some mode shapes clearly show significant amplitudes in the elastomeric bearing elements; changing the stiffness of the elastomeric bearing elements may lead to significant changes in natural frequencies.

The dynamic simulation is carried out by adopting the moving load concept; neglecting the contribution of the train-bridge interaction to the response. A series of point loads is applied and shifted for each time step to excite the system. This collective load represents

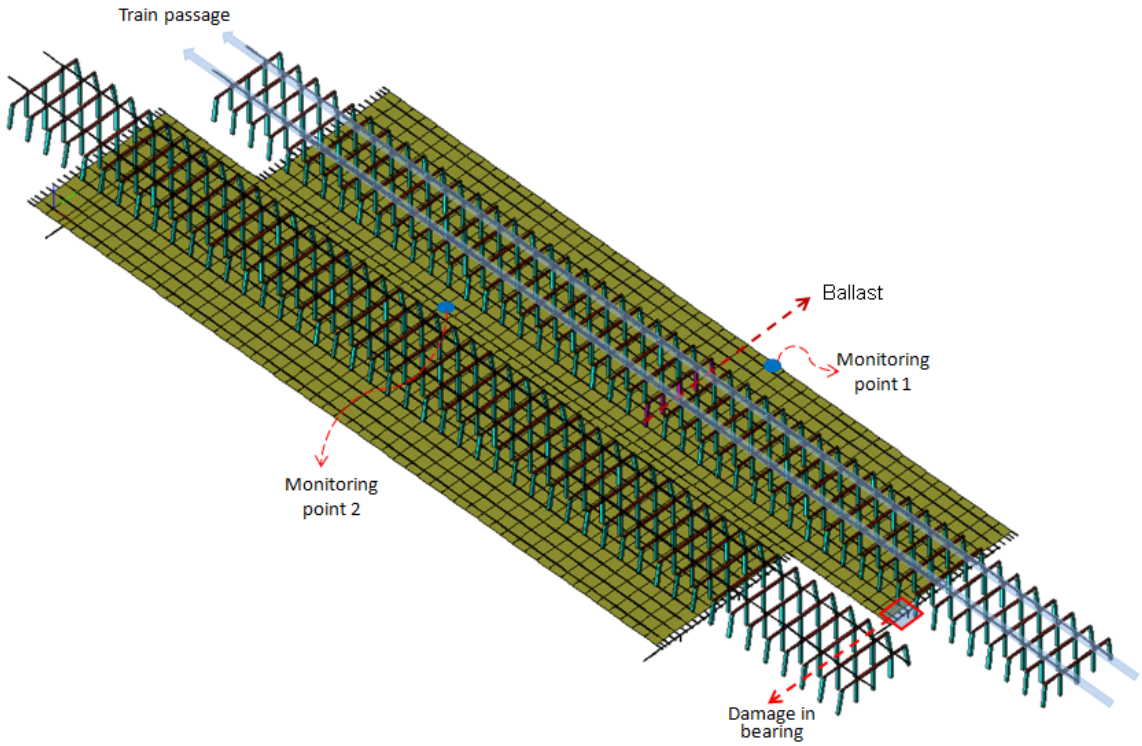

Figure 6.3: Finite Element model of the Erfttal-Brücke railway bridge

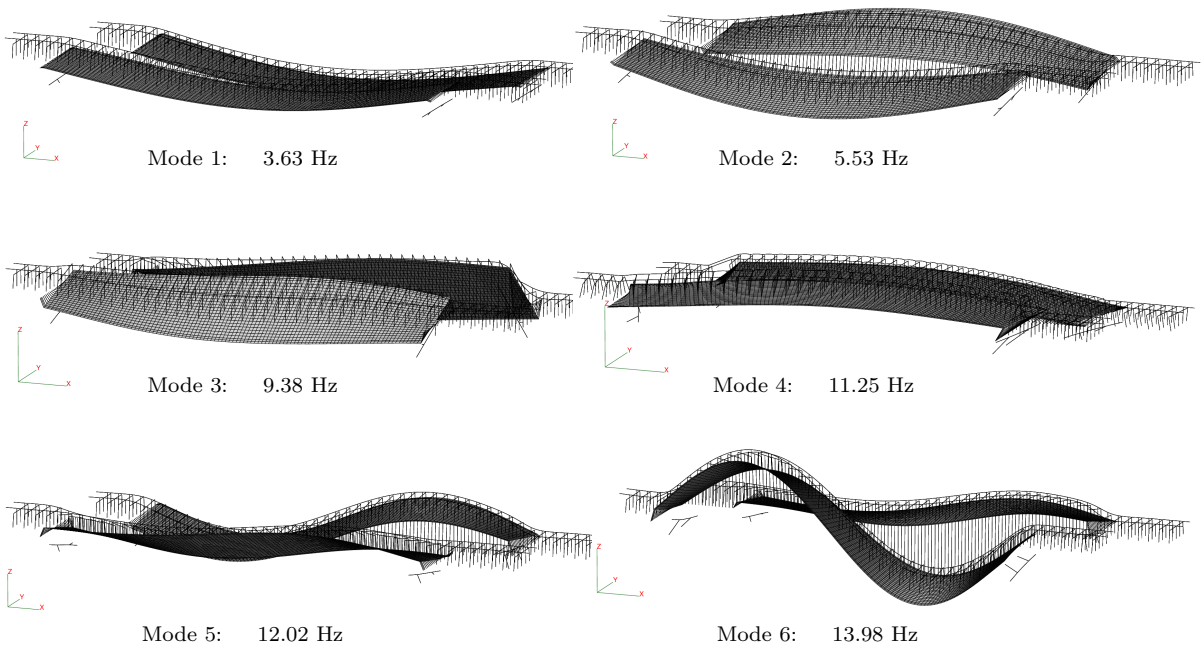

Figure 6.4: Eigen frequency and mode shape of the FE model of the Erfttal-Brücke railway bridge

an ICE-3 train series, one load for each wheel. This means that 64 vertical point loads were applied to the structure in every time step. The sampling rate is 500 Hz, which means that the load series is shifted and the response is measured every 0.002 second. Possible effects due to rail-roughness and wheel irregularities are neglected for simplification.

The dynamic acceleration is calculated using the Newmark method. The Rayleigh damping model is adopted to build the damping matrix. The damping matrix is constructed from two modal damping ratios obtained from the measurements. The damping model is shown in Figure 6.5.

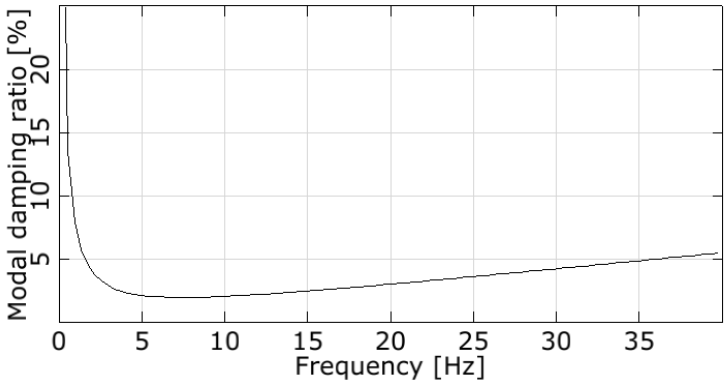

Figure 6.5: Rayleigh damping model for train passing simulation over the Erfttal-Brücke railway bridge

The dynamic response is computed up to 16 seconds. Typical acceleration responses in the time and frequency domain are shown in Figure 6.6. In this figure, the influence of the train speed to the dynamic response can be clearly seen. The acceleration amplitude increases significantly when the train speed is changed from 200 to 240 km/h.

6.3 Non-Damaged Variable

Basically, dynamic responses of a real structure located in an open space might be affected by many non-damaged variables, for instance temperature, wind, humidity, etc. However, only two non-damaged variables are considered in this numerical simulation study. The first non-damaged variable represents operational conditions while the second represents environmental effects.

The first non-damaged variable is train speed. It is widely acknowledged that excitations from a train series might have a similar effect such as harmonic excitations, particularly

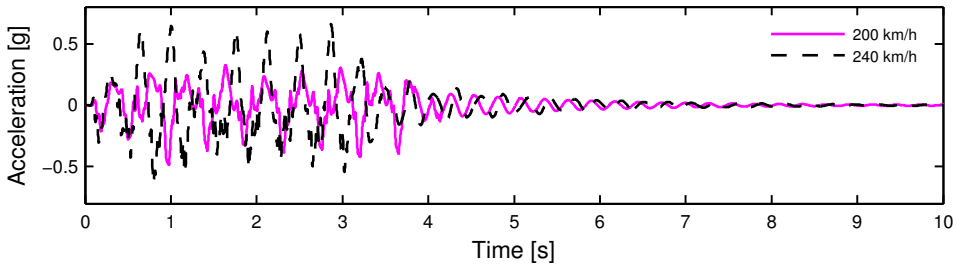

(a) The acceleration signal in time domain

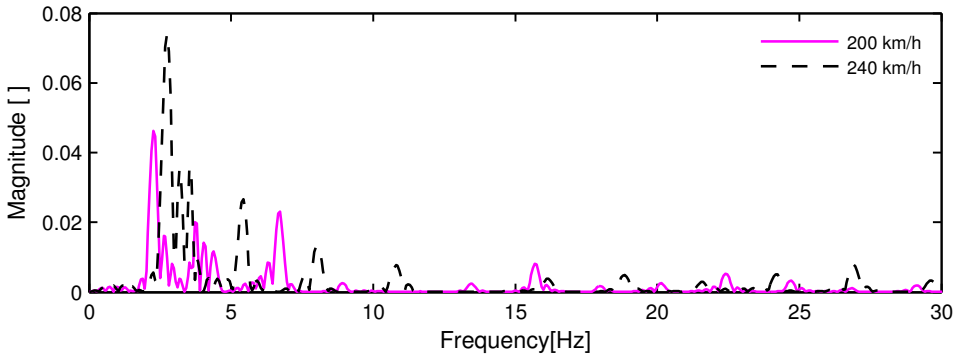

(b) The acceleration signal in frequency domain

Figure 6.6: Typical acceleration response signal

for a short span bridge. For certain train speed, the excitation frequency might be close to one of the natural frequencies of the bridge. It creates significant changes on the dynamic response of the bridge. The normal speed of the ICE train is approximately 240 km/h. Therefore, in this numerical study, the interval of the train speed is set between 200 and 300 km/h.

The second non-damaged variable is temperature. Most of civil engineering structures experience temperature variation. There is a significant fluctuation in temperature over the course of a year, for instance between summer and winter. Basically, the temperature affects the whole parts of the structure, more or less. However, for simplification, only elastomeric materials are affected by the temperature in this simulation. Hence, only the stiffness of the 3D spring elements in the bridge supports is modified with respect to temperature variation. The temperature is assigned by using a temperature-shear modulus curve in Figure 6.7, which is adopted from [Zabel *et al.*, 2010]. The curve was obtained from long-term monitoring data of a bridge that is similar to the simulation model. The temperature variation between -5° to 20° Celsius degree is considered in this numerical simulation study.

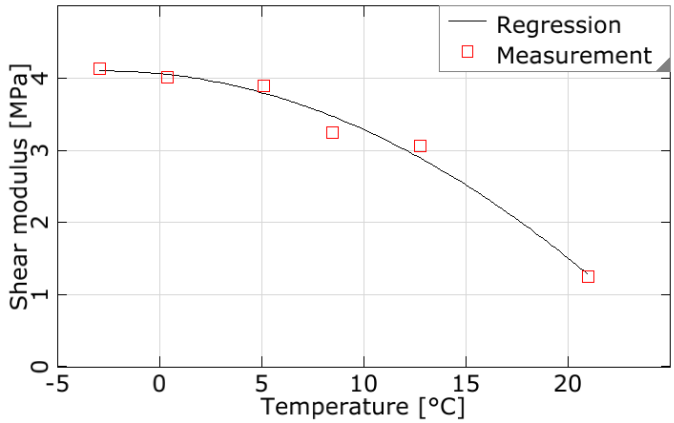

Figure 6.7: Shear modulus versus temperature.

Two methods are used for data sampling, full factorial design and Latin hypercube sampling design. Each of them is used to generated thirty-six training points. The motivation behind applying both methods is to observe the influence of regular and non-regular grid data to the approximation results. Each of the sampling methods is also used to generate twenty-five testing (validation) points, which will be used to validate the approximation models. The training and testing points are shown in Figure 6.8.

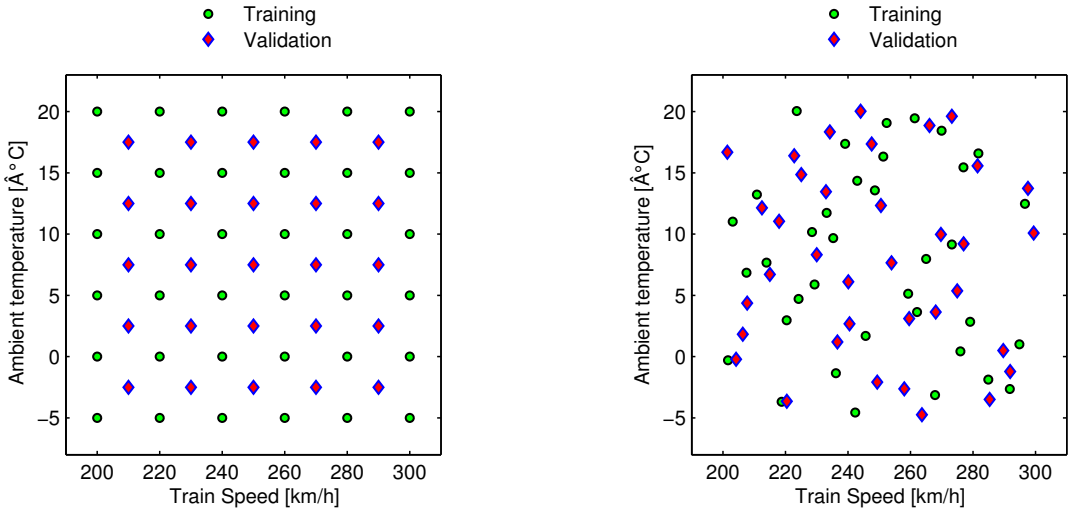

(a) Full factorial design

(b) Latin hypercube sampling

Figure 6.8: Design of experiment for the train passing simulation with variation of ambient temperature and train speed.

6.4 Training Phase

Training phase refers to some activities used to collect data and to train the reference surface model. In this numerical simulation study, this phase begins by calculating the dynamic response of the Finite Element model in all combinations of non-damaged variables that has been set using the space filling design, as is shown in Figure 6.8. The dynamic response signals are used to calculate damage indicators. The damaged indicators that are used in this study are briefly described in Sections 2.2, 2.3, and2.4. A pair of input (non-damaged variables) and output (damage indicator) is called the support or training point. The reference surface models are trained using these support points.

6.4.1 Reference Surface Models

Several methods can be applied to approximate the reference surface models from scattered observation data. In this simulation, four approaches are used for comparison. These methods include the radial basis function, polynomial regression, moving least squares, and artificial neural networks. All of these approximation methods have been described in Subsection 4.3.1 to 4.3.4. The neural network architecture that is used in this study is limited to three layers (one input layer, one hidden layer,and one output layer) as shown in Figure 4.8.

Based on the results of the train passage simulation model, three different reference surface models are built, namely the frequency reference surface, the wavelet energy reference surface, and the stochastic subspace identification (SSI) reference surface. The name of the reference surface model refers to the damage indicator used. These reference surface models are briefly described in the following sub-subsections.

6.4.1.1 Frequency Reference Surface

The frequency reference surface model is probably the simplest among the reference surface models considered in this study, as it can be extracted from the solution of the dynamic eigenvalue equation. It means, in this numerical study, only the temperature affects the result. Hence, the frequency reference surface model becomes a univariate approximation model. Several models can be built by using different approximation methods. The best model is considered as the model with a minimum approximate error.

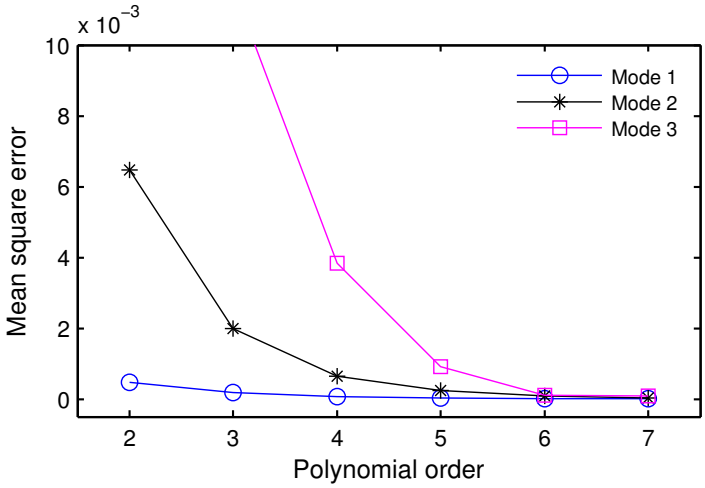

Figure 6.9: Mean square error (MSE) of different polynomial frequency reference surface models

Polynomial regression is probably the most common method for the approximation of a univariate model. Generally, a more flexible regression model can be obtained by increasing the polynomial order. In this case, many polynomial regression models have been built and the approximate errors have been calculated by using the Equation (4.24) in order to find the best model. Figure 6.9 shows the mean square error of the frequency reference surface model candidates that are built from different polynomial orders. The model with polynomial order six is considered the best polynomial frequency reference surface model.

The shape parameter α and influence radius D have significant effects on the result of the radial basis function (RBF), and the moving least square (MLS) reference surface models. A smaller influence radius leads to higher local effects, which means that the approximation model becomes more flexible. The optimal shape parameter and influence radius can be obtained by iterations. The chosen radius with the minimum mean square error is considered as the best RBF and MLS response surface models. Figure 6.10 shows the variation of the mean square error with respect to the shape parameter α of the frequency reference surface model candidates.

Generally, a better artificial neural network (ANN) approximation model might be obtained by conducting more training. However, too many iterations (epochs) may lead to overfitting. Two criteria can be assigned to the network in order to stop the training. The first criterion is the number of maximum epochs for which the training will stop after the maximum number of epoch is reached. The second criterion is the performance level

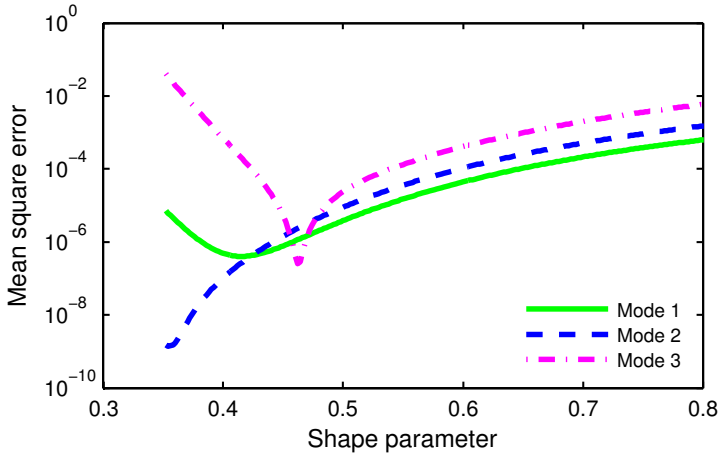

Figure 6.10: Iteration to find optimum frequency reference surface model by using radial basis function approximation method

for which the training will stop after the targeted performance level (e.g. mean square error) is reached. Figure 6.11 shows that a better approximation model is obtained as the number of training step increases.

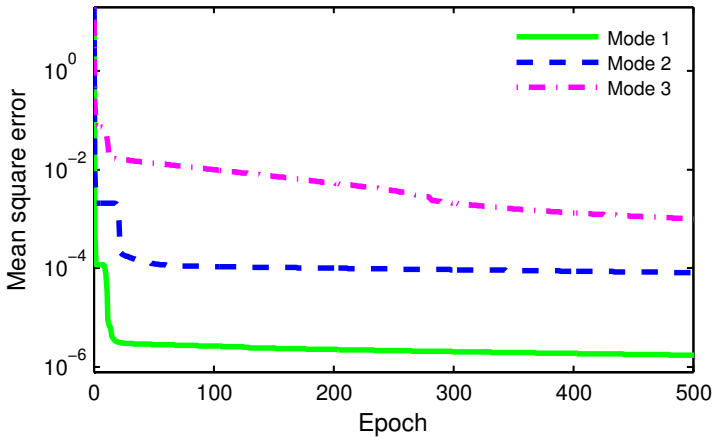

Figure 6.11: Iteration to find a better frequency reference surface model using artificial neural networks approximation method

In this simulation study, all chosen approximation methods (polynomial, RBF, MLS, and ANN) work well in presenting the relationship between the natural frequencies of the bridge model and the temperature changes. All of obtained frequency reference surface models have very good quality ($R^2 > 0.99$). The comparison of the mean square errors (MSE) of the frequency reference surface models are summarized in Table 6.2.

Table 6.2: Approximate errors in the frequency reference surface models that were generated from different approximation methods: polynomial regression, radial basis function (RBF), moving least squares (MLS), and artificial neural networks (ANN).

Eigen mode	MSE			
	Poly6	RBF	MLS	ANN
1st	$2.5.10^{-6}$	$3.8.10^{-7}$	$0.3.10^{-7}$	$1.2.10^{-6}$
2nd	$2.0.10^{-6}$	$0.6.10^{-7}$	$1.5.10^{-7}$	$1.7.10^{-5}$
3rd	$1.2.10^{-6}$	$3.7.10^{-7}$	$4.4.10^{-7}$	$6.9.10^{-5}$
4th	$0.7.10^{-5}$	$3.6.10^{-6}$	$2.5.10^{-6}$	$2.8.10^{-5}$
5th	$2.9.10^{-5}$	$3.8.10^{-6}$	$3.2.10^{-6}$	$4.9.10^{-5}$

The frequency reference surface models for the first and second eigen modes are shown in Figure 6.12. The eigen frequency of the first mode changes by approximately 2.95 %, if the temperature varies between -5° to 20° Celsius. A similar trend but higher amplitude (5.53 %) is shown by the eigen frequency of the second mode. Figure 6.12 strongly indicates that the temperature (which is one of environmental variables) has profound effects on the changes in the eigen frequencies. The damage detection that is performed by observing the eigen frequency changes may lead to poor results if the temperature effects are not considered. The proposed reference surface-based method is an efficient way to overcome this problem.

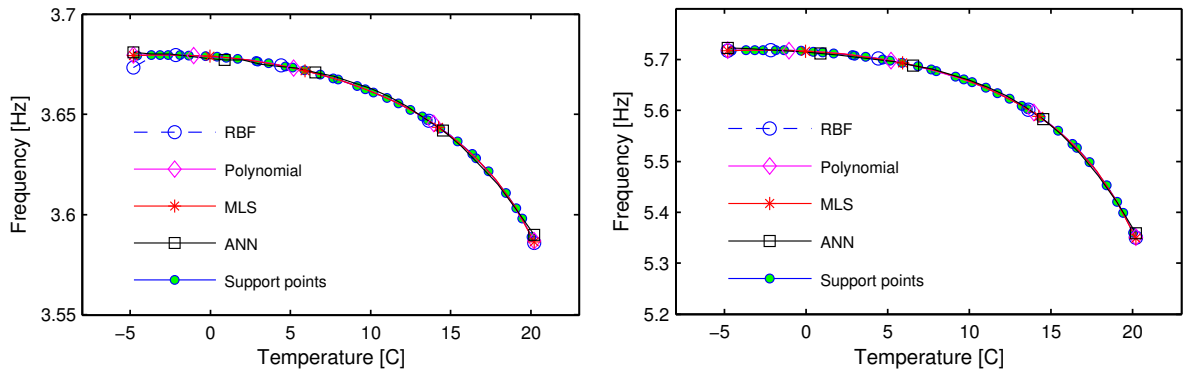

(a) Mode 1

(b) Mode 2

Figure 6.12: Frequency reference surface models for the finite element model of the Erfttal-Brücke railway bridge.

The main drawback of the frequency reference surface model is its sensitivity. Sensitivity in this context means ratio between the amount of frequency changes and damage severity.

In many cases, the frequency damage indicator is not powerful enough to be applied for small local damage identification, as small frequency changes might be masked by noise. However, the amount of changes grows with respect to damage severity.

6.4.1.2 Wavelet Energy Reference Surface

In some numerical studies, wavelet-based damage indicators are more sensitive to small damage compared to the eigen frequencies, [Ahmad *et al.*, 2011]. In addition to its good sensitivity, the wavelet-based damage indicators are also very simple and cheap to be acquired, considering measurement equipment and signal processing. For instance, data from a single accelerometer sensor is sufficient to build a wavelet-based reference surface model. However, multiple sensors have significant advantages, since damage can be present anywhere in the structure. The sensor closest to the damage location would be more sensitive to the structural response changes.

There are several types of the wavelet-based damage indicators, as Section 2.3 describes. However, this numerical study only uses the wavelet energy damage indicator. Basically, the wavelet energy damage indicator observes the amount of energy of the signal that moves from one to other frequency sub-bands. This means that the amount of energy the signal has in a sub-band can increase or decrease when the structure is changed.

First, the acceleration signal is decomposed into several levels using the wavelet decomposition algorithm. The algorithm is based on a multiresolution analysis that was originally proposed by [Mallat, 1989]. The algorithm has been implemented in the software packet SLang, [Dynardo GmbH & Bauhaus University Weimar, 2009] and was used in this study. The Daubechies wavelet of order 5 with 10 coefficients was chosen for all wavelet decompositions. Second, the energy of the decomposed signal is calculated using Equations (2.29), (2.30), and (2.31). Finally, the wavelet energy in each level is normalized to the total energy of the signal, to reduce the effect of different excitations.

Since the energy of the acceleration response signal is used, the wavelet energy reference surface model considers both the input variables (temperature and train speed). The input variable values are normalized and scaled because the radial basis function and moving least squares approximation methods use Euclidean distances in the weighting function. For multivariate models, the contribution of a variable to the result of the Euclidean distance might be to too high when compared to other variables, if the input value of that variable is much higher compared to the input value of other variables. Input variable scaling may avoid that problem, as all variables will have the same range

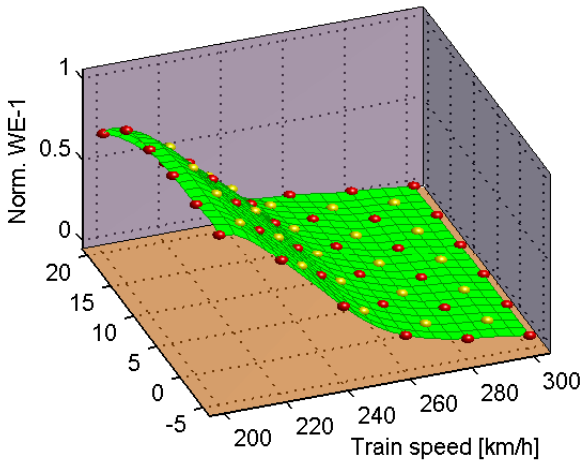

Figure 6.13: WE-1 reference surface model obtained by using the RBF approximation method. The red and yellow points are training and validation points, respectively. Similar reference surface models are also obtained by using the MLS, Polynomial regression, and the ANN approximation methods.

of input values. In this numerical simulation study, the temperature variation, which is originally between -5° to 20° Celsius, is scaled to between 0 and 1. Similarly, the train speed variation, which is originally between 200 to 300, km/h is also scaled to be in the range of 0 and 1.

All considered approximation methods can build good reference surface models for the first decomposition level wavelet energy (WE-1). All approximation methods yield a similar surface as is illustrated in Figure 6.13, where the mean square error (MSE) is less than 0.01 %. Similar performances are also shown by all of the considered approximation methods in building the WE-2 reference surface models.

The performance of the polynomial regression method to approximate the higher level wavelet energy reference surface models (WE-3 to WE-8) drops drastically, since the reference surface models become more complex with high gradient changes. The polynomial regression method is not able to generate reference surfaces with acceptable errors (MSE $\leq$ 0.01 %). For instance, in the wavelet energy reference surface model level 3 and 4 (WE-3 and WE-4), as Figure 6.14 illustrates, the reference surface that are generated using polynomial regression method has a significant error at many support points. In this case, the polynomial regression method is not suitable to approximate higher decomposition level wavelet energy reference surface models.

In this simulation study, the artificial neural network (ANN) approximation method also

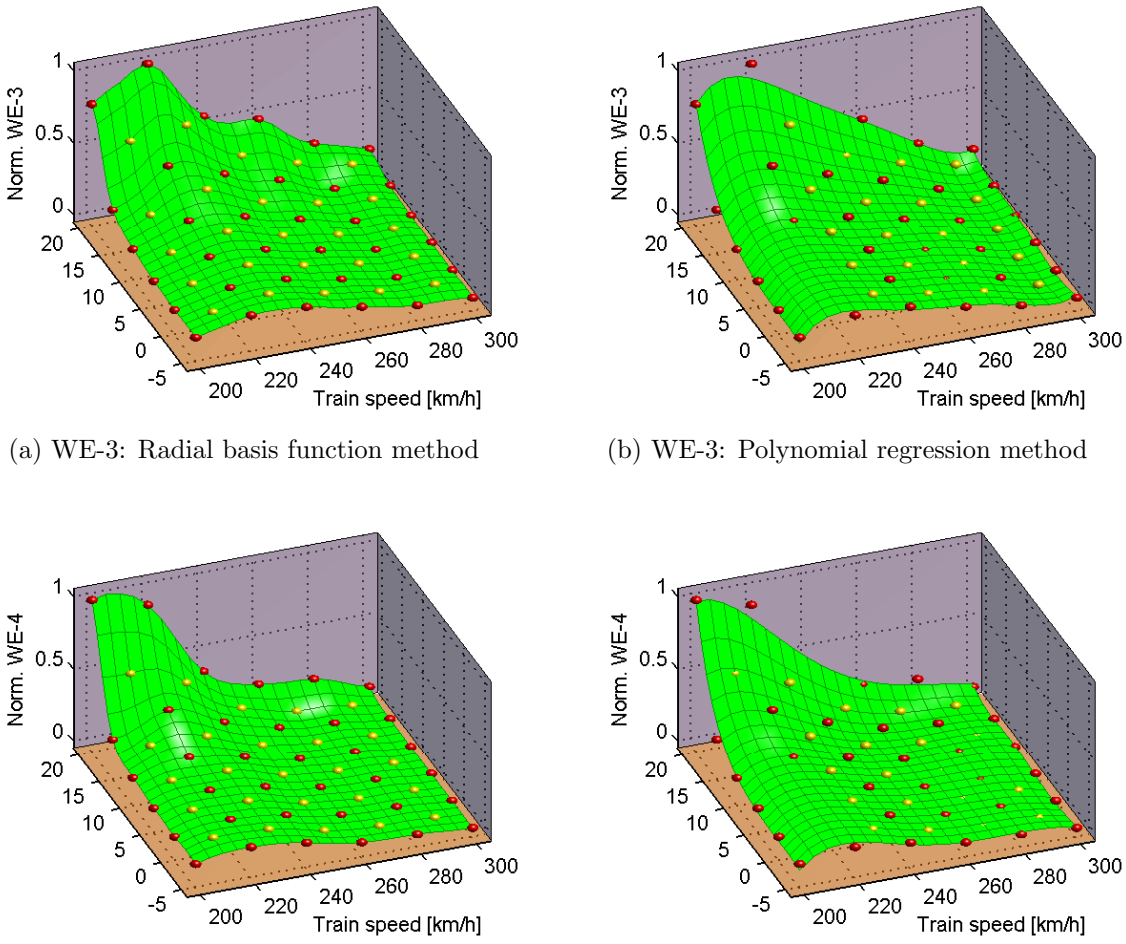

(a) WE-3: Radial basis function method

(b) WE-3: Polynomial regression method

(c) WE-4: Radial basis function method

(d) WE-4: Polynomial regression method

Figure 6.14: The comparison of WE-3 and WE-4 reference surface models that are obtained by using radial basis function and polynomial regression method

encounters difficulty to converge on the target points of the WE-3 reference surface model. An acceptable WE-3 reference surface model was obtained after more than 5000 epochs. The network still did not have a good approximation for the WE-4 reference surface model after 10,000 epochs. Most of the MSE value is contributed by the testing points near to the boundary.

The radial basis function (RBF) and moving least square (MLS) approximation methods seem to be the best options to create the wavelet energy reference surface models in this numerical simulation study. The shape parameter α and influence radius D can be adjusted to have suitable local effects in order to produce a smaller approximate error. The value of α and D might not be suitable for all regions of the input variable value of

the reference surface model, if the input data does not has uniform grids. The influence of uniform and non-uniform grid data on the results of the RBF approximation method is shown in Subsection 6.4.2.

6.4.1.3 SSI Reference Surface

Instead of frequency and wavelet energy damage indicators, the stochastic subspace identification (SSI) damage indicator was also used in this numerical study. The concept and formulation of the SSI damage indicator has been described in Section 2.4. In SSI reference surface models, a base training point has to be defined first before other training points can be calculated. The SSI reference surface model is built by the following steps.

Step 1 The first acceleration response signal of the healthy structure is calculated and considered as the base signal. In this simulation study, the acceleration response of the Finite Element model at a train speed of 260 km/h and a temperature of 10° Celsius is chosen as the base point. This point is approximately located near the center region of the design space.

Step 2 Other response signals in the same input conditions are required to compute the residuals value (Equation (2.64)). For this case, the first acceleration response signal is replicated to obtain five new response signals, and the random noise is added to the replicated signals.

Step 3 The data from Step 1 and Step 2 are used to calculate the output value of the base point by using Equation (2.63).

Step 4 The output value of other training points are calculated similar to Step 3, and the results are normalized to the output value of the base point.

The training points for the stochastic subspace identification (SSI) reference surface model are shown in Figure 6.15. Figure 6.15 indicates that the SSI damage indicator changes significantly with respect to a change in input variables, especially in the variation of train speed. The SSI reference surface model seems to be very sensitive to the change in the structure. However, a high sensitivity damage indicator may also raise difficulties in building a reference surface that covers all input variable ranges. The ratio of output variable values in a region is much higher or lower compared to output variable values in the neighboring regions. For instance, the output values at speed around 240 km/h are much lower compared to at an approximate speed of 300 km/h.

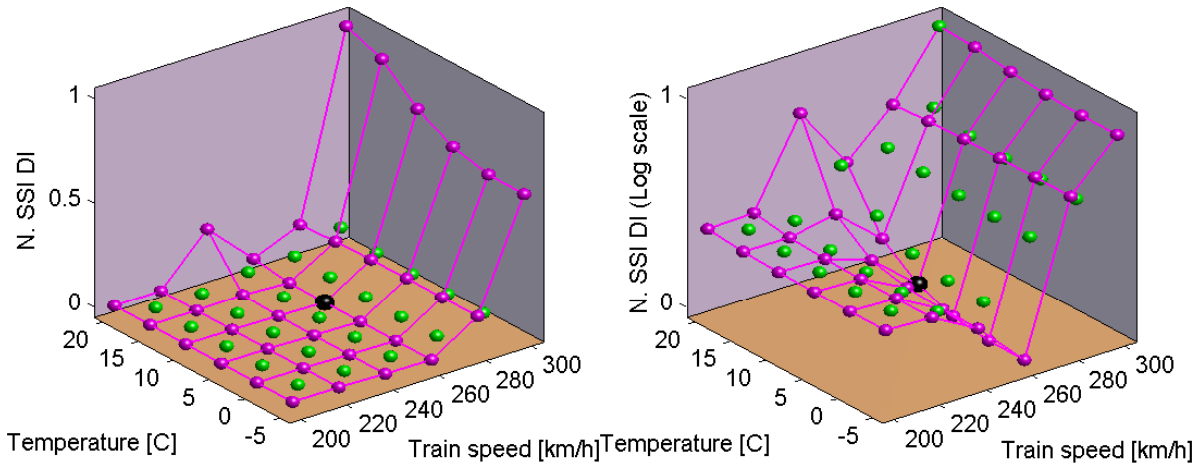

(a) (b)

Figure 6.15: Stochastic subspace damage indicator training points in normal scale (a) and logarithmic scale (b) according to the design of experiment in Figure 6.8a.

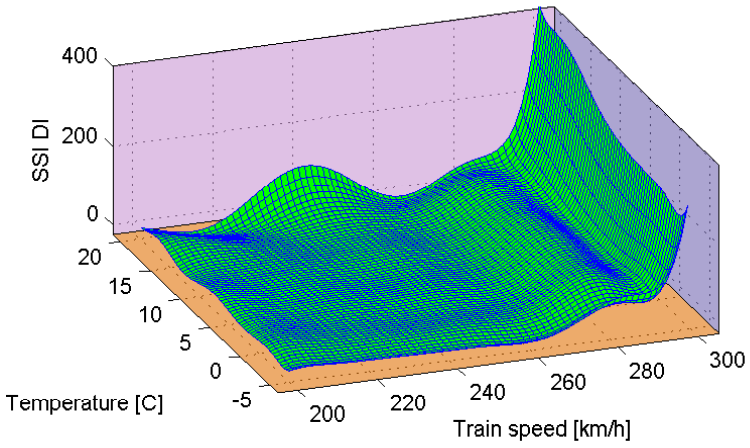

Figure 6.16: Stochastic subspace identification reference surface model

The SSI reference surface model created by using the RBF approximation method is shown in Figure 6.16. At a glance, the reference surface in Figure 6.16 looks acceptable, and the mean square error value is considerably small (≤ 0.01). However, it is important to consider that the mean square error (MSE), which is calculated by using Equation (4.24), is an average measure. In this case, the obtained MSE is very small for the output variable values of certain regions, while it is considerably high for the output variable values of other regions. If the minimum value of the SSI DI axis in Figure 6.16 is set

to zero, some negative response values can be clearly seen, as is shown in Figure 6.17. Basically, the values of the SSI training points always have a positive sign, since they are actually the ratio of considered support points and the base point. The reference surface model is not acceptable if the approximate error in individual training and validation points are still significant.

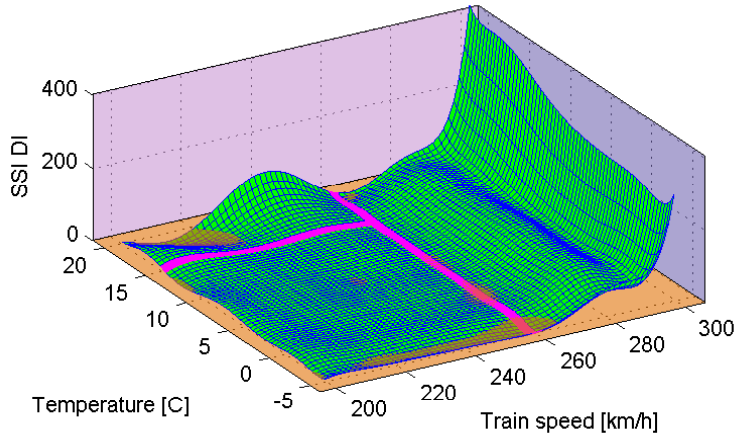

Figure 6.17: The original stochastic subspace identification reference surface model is clustered in three regions with respect to the gap of the output response values

Clustering might be a remedy for a reference surface with the characteristics described above. The entire design space is divided into some blocks according to the amplitude of the response surface values, for instance, into three blocks as is shown in Figure 6.17. In this case, the clustering is performed manually. However, it seems possible that an algorithm that could do it automatically could be developed. One of the clustered SSI reference surface models is shown in Figure 6.18. This reference surface model has a much lower approximate error when compared to the same region of the model in Figure 6.16.

6.4.2 Uniform and Non-Uniform Grid Data

In many cases, the input data is not arranged in uniform grids, where it is sparsely distributed in one region while densely distributed in another region of the design space. Regularity of the input data has significant effects on the result of some approximation methods, such as the radial basis function (RBF) and moving least square (MLS).

For instance, in the RBF approximation methods, the weighting function is based on the Euclidean distance of the training points. The shape parameter α is also included

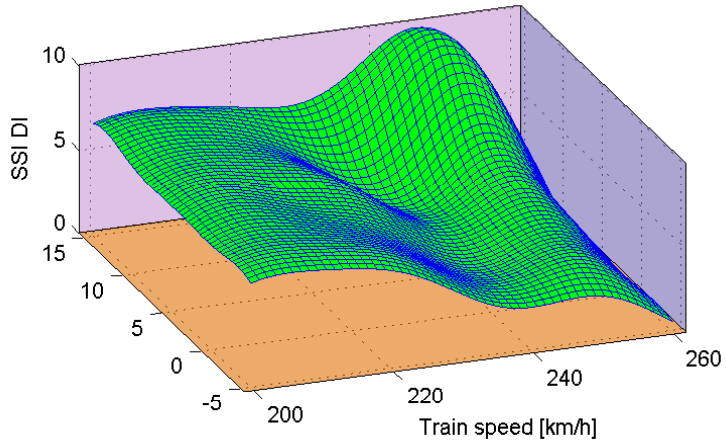

Figure 6.18: Partial stochastic subspace identification reference surface

in the weighting function to adjust local influences. The shape parameter α that leads to the minimum approximate error is considered as the optimum shape parameter. This approach may work very well if the distance between support points is nearly similar, such as the sampling plan with a uniform grid points.

However, the chosen shape parameter α might not be suitable for all regions of the design space, if the training points are spread irregularly. Figure 6.19 shows two examples of the effect of a chosen shape parameter α on the result of the reference surface model. In Figure 6.19a, the chosen shape parameter is suitable for all regions. The chosen shape parameter α is too localized for some support points, particularly near the boundary, Figure 6.19b.

The effect of non-uniform grid data can be alleviated by using an adaptive algorithm that is able to adjust the shape parameter with respect to the data distribution. However, if training points are plenty available, the data selection strategy that has been described in the Section 5.3.4 seems to be also a reasonable approach.

6.4.3 The Presence of Noise

Generally, the dynamic response signals of a physical structure always contain noise. In the damage detection application, noise causes a variation in the damage indicator value. As such, the noise affects the capability of a reference surface model to identify damage. The change of structural response due to damage might be masked by noise, particularly when the damage is very small.

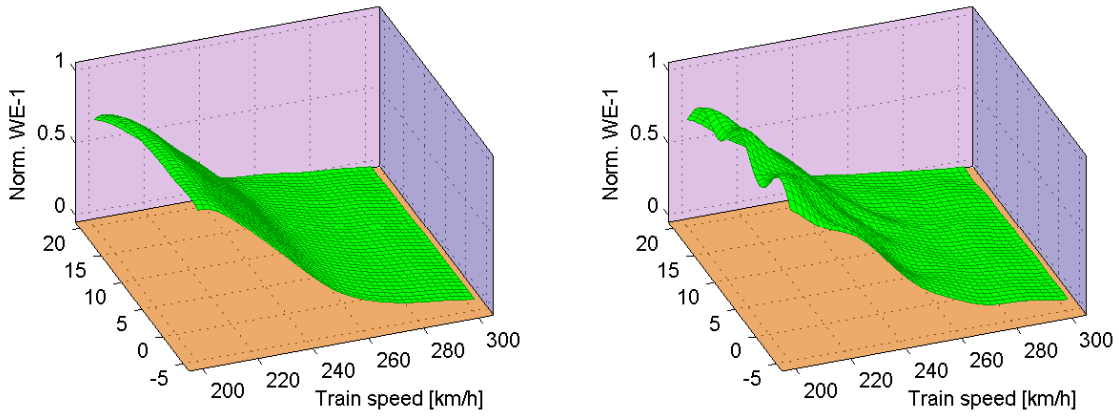

(a) Uniform data grids

(b) non-uniform data grids

Figure 6.19: The effect of uniform and non-uniform grid data to the results of the reference surface model.

In the reference surface-based system identification method, noise is taken into account by adjusting the thresholds. A higher level of noise leads to higher variance in the reference surface model's output variable value. It means that the distance between the upper bound and lower bound surfaces is expanded for higher noise levels. However, the noise effects may not be similar to all damage indicators. A similar signal may yield different variance for the different damage indicators.

In this simulation study, noisy acceleration signals are obtained by adding random noise to the acceleration signals that are obtained from the numerical simulation. It can be done as follows: the original acceleration signals are replicated to obtain ten new signals. Following which random noise with zero mean value is added to the replicated signals to obtained ten different signals. Figure 6.20 shows the effect of noise signals on the variation of wavelet energy damage indicator. The amplitude of the noise signals is calculated according to the acceleration signal at train speed equal to 200 km/h and a temperature of -5° Celsius.

The results of the numerical simulation study show that the standard deviation of the training points increases with respect to the noise level. The effect of low level noise ($\leq$ 0.5 %) seems to be higher in the lower level wavelet decomposition (WE-1 and WE-2). However, the trend changes at the higher level noise ($\geq$ 2%), where the standard deviation of most WE-1 and WE-2 become more constant. Standard deviation value less than 2 % is obtained in most cases when noise up to 5 % is added to the signals.

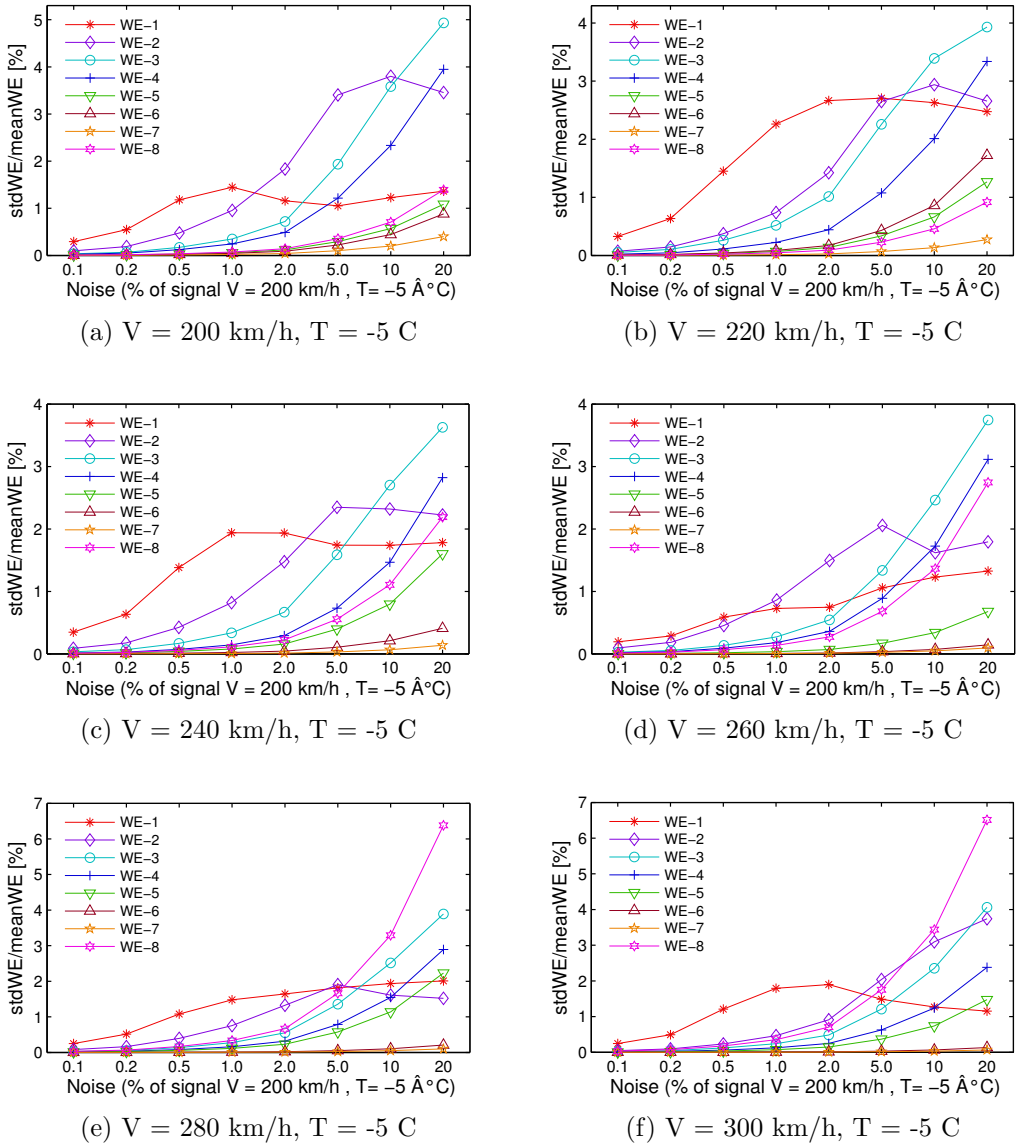

(a) V = 200 km/h, T = -5 C

(b) V = 220 km/h, T = -5 C

(c) V = 240 km/h, T = -5 C

(d) V = 260 km/h, T = -5 C

(e) V = 280 km/h, T = -5 C

(f) V = 300 km/h, T = -5 C

Figure 6.20: The change of standard deviation of wavelet energy due to noise

6.5 Detection Phase

In the reference surface-based system identification method, the damage detection phase can be performed after the learning phase. The damage detection is done by comparing the recent damage indicator values of the structures to the response of the reference surface models. The damage indicator values that lie between the upper and lower bound surfaces are classified as healthy responses. In contrast, damage indicator values that are greater than the upper bound or smaller than the lower bound are classified as damaged

structures.

To demonstrate the detection phase of the reference surface-based system identification method, the Finite Element model of the Erfttal-Brücke railway bridge is modified. The modification is done only for one 3D spring element (elastomeric bearing) to prescribe damage. The damage is assigned by reducing the stiffness of the elastomeric bearing element by 50 %. The damage location is indicated in Figure 6.3.

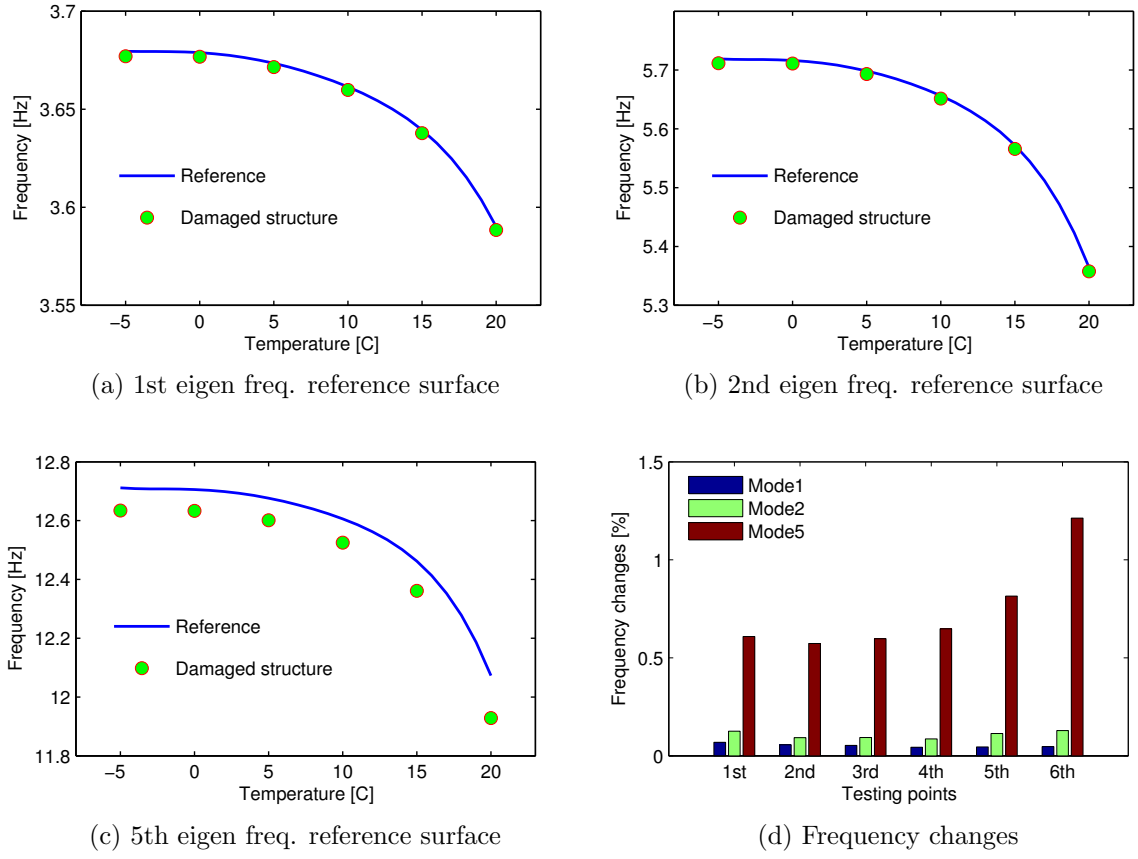

(a) 1st eigen freq. reference surface

(b) 2nd eigen freq. reference surface

(c) 5th eigen freq. reference surface

(d) Frequency changes

Figure 6.21: Detection phase using frequency reference surface model

The global stiffness and global mass matrices of the structure are rebuilt. The modal properties of the damaged structure are extracted by solving the eigenvalue problem. Furthermore, acceleration response signals of the modified structure are recalculated. The acceleration response signals are calculated in different input variables values according to sampling data in Figure 6.8a. The acceleration response signals are used to obtain damage indicators. Finally, the damage indicator values are plugged into the reference surface models, in order to assess the condition of the structures.

The damage detection phase using the frequency reference surface models is summarized in Figure 6.21. For instance, the damage detection using the first eigen frequency reference surface model is shown in Figure 6.21a. The difference between damaged and undamaged conditions is considerably small ($\approx 0.2\%$). A similar result is also obtained by using the second eigen frequency reference surface model, Figure 6.21b. This amount of change might be obscured by noise. For instance, if the confidence interval of the damage detection result is assumed to be 95% probability and the observation data has a normal distribution, the maximum standard deviation value of the observation data should be less than approximately 0.1%, otherwise the first and the second frequency reference surface models will not be able to detect the damage in the numerical model.

However, more promising results can be obtained by observing some other eigen frequency reference surface models. For instance, changes from 0.6 % to 1.2 % are obtained from the third and fifth eigen frequency reference surface models. The comparison of the damage detection using the first, the second, and the fifth frequency reference surface models is depicted in Figure 6.21d.

The frequency reference surface models do not show a strong performance to discriminate the damaged and undamaged scenarios in this numerical simulation study. Significant changes can be observed only for some particular eigen modes. The primary possible reason for this is the position of the damage. The stiffness change in the damaged element (one of the bearings) does not has a strong impact on the two lowest modes of the finite element model of the bridge.

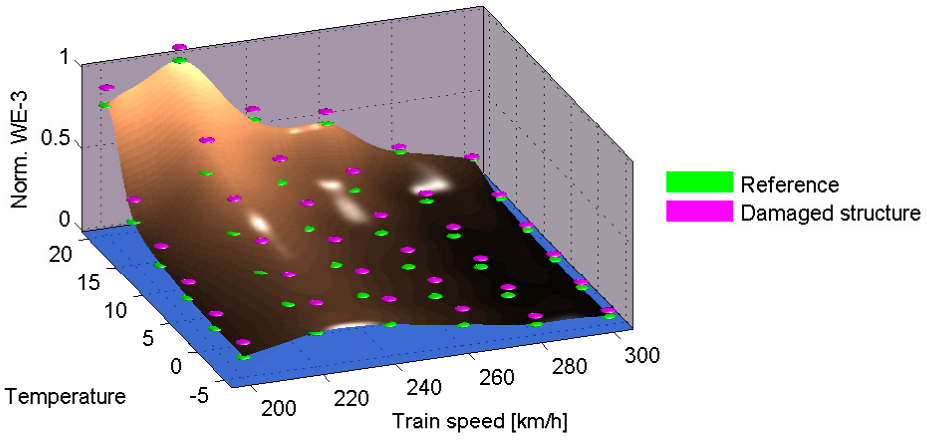

Figure 6.22: Detection phase using wavelet energy reference surface

The damage identification using one of the wavelet energy reference surface models (WE-3) is illustrated in Figure 6.22. The differences between the damaged and undamaged

conditions at all damage detection points are quite clear. A change of up to 40 % is obvious at some damage detection points. In this numerical simulation model, the minimum change in the WE-3 is more than 2 %. Another interesting result in this particular case is that the damage indicator value of the damaged structure is higher than the undamaged structure in all damage detection points. In general, the wavelet energy of a damaged structure may be greater or less than the wavelet energy of healthy structures (reference surface models).

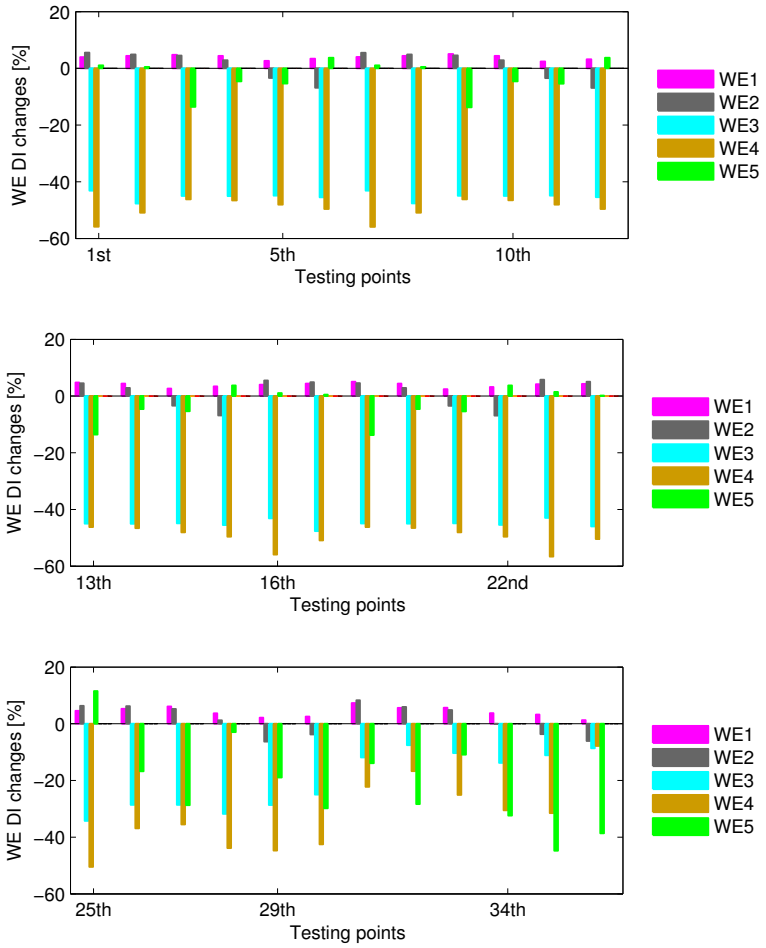

Figure 6.23: Wavelet energy changes of 36 testing points

Figure 6.23 illustrates damage identification using the first five level wavelet energy reference surface models. The wavelet energy of the damaged structure may be higher or lower than the wavelet energy reference surface, depending on the wavelet decomposition level and the input variables values. For instance, the change of wavelet energy level 5 (WE-5) has positive sign in some damage detection points, while at other damage detection points, it indicates negative signs, as Figure 6.23 depicts.

The wavelet energy damage indicator observes the energy composition at a certain wavelet decomposition level. The energy might move from one level to other levels when the dynamic properties or loading conditions of the structure are changed. At some wavelet levels, the energy increases, while it decreases on the other level. However, contrasting characteristics may be obtained for other conditions of loading and dynamic properties. If the damage becomes increasingly severe, wavelet energy changes might not exhibit monotonic trends.

The wavelet energy damage indicator changes in Figure 6.23 should be subtracted from the upper or lower bound values if the the signals contain noise. In this numerical study, the effect of noise on wavelet energy is shown in Figure 6.20. For instance, by adding 5% Gaussian noise to the acceleration signal, the standard deviation of WE-3 is obtained approximately 1.1% of the mean value (Figure 6.20e). The damaged condition can be identified if the WE-3 changes in Figure 6.23 are greater than 2.2% (95% probability).

In this numerical study, the damaged condition can be identified at all of the damage detection points if the noise is less than 5% by considering certain wavelet level, for instance WE-4 and WE-5. The wavelet energy changes at these levels are greater than 7% at all damage detection points. This value is greater than the threshold, as Figure 6.20 illustrates, which is approximately less than 3%.

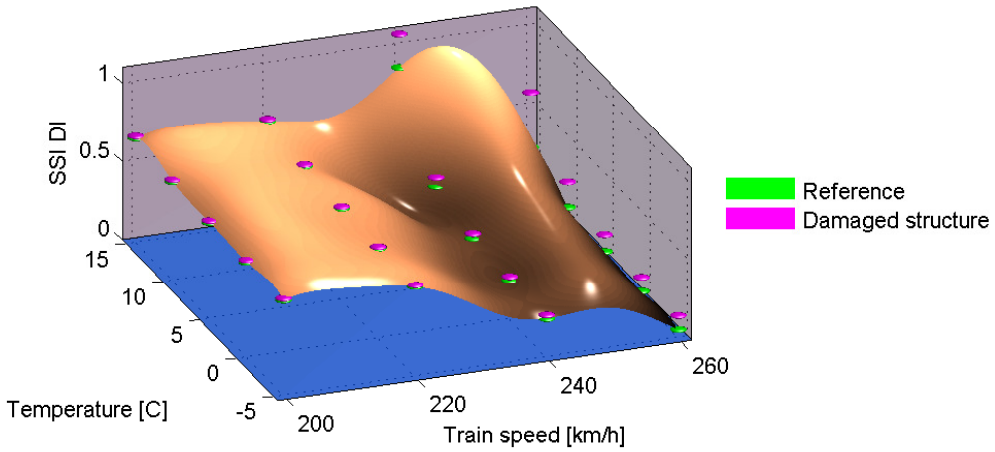

Figure 6.24: Detection phase using stochastic subspace identification reference surface.

The damage detection phase using stochastic subspace identification reference surface model is summarized in Figure 6.24. In this case, the response of the damaged structure is always greater than that of the healthy condition. The amount of change at certain damage detection points is very high when compared to some other damage detection

points. Changes above 3% are obtained for all twenty testing points, shown in Figure 6.25.

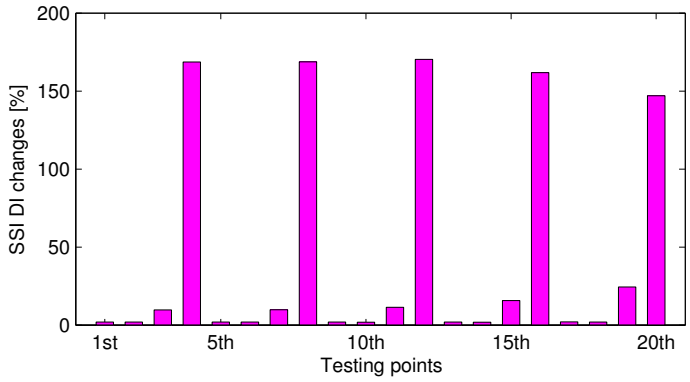

Figure 6.25: SSI damage indicator changes.

6.6 Summary

The proposed reference surface-based system identification method has been applied to a numerical model of the Erfttal-Brücke, a railway bridge near Cologne. The bridge was excited by moving loads of an ICE train model. Two non-damaged parameters were considered, temperatures and train speed. Damage was assigned by reducing the stiffness of one elastomeric bearing of the bridge.

Three types of reference surface models were introduced, frequency, wavelet energy, and stochastic subspace identification reference surface models. The reference surface models were built using four approximation methods, polynomial regression, radial basis function, moving least squares, and artificial neural networks. Full factorial design and Latin hypercube sampling method were used to choose the sampling data.

The results of this numerical study show that the reference surface-based system identification method is able to discriminate the damaged and undamaged conditions of the bridge model. Furthermore, Gaussian random noise was added to the acceleration signals to assess the impact of the noise on the damage detection results. The reference surface models are still able to distinguish damaged and undamaged scenarios when noise was added for up to 5% of the maximum amplitude of the acceleration signals.

Basically, multiple reference surface models can be built from the same observation data, based on the damage indicator that is used. The use of multiple reference surface models

may improve the capability of the proposed method to identify damage. However, it may also yield a situation where the damage detection results of a reference surface model are different from other reference surface models. As such, it would be necessary to develop a method to combine multiple reference surface models in the future.

Chapter 7

Experimental Model

7.1 Introduction

In Chapter 6, the reference surface-based system identification method was applied to the Finite Element model of the Erfttal-Brücke railway bridge. The frequency, wavelet energy, and stochastic subspace identification reference surface models are able to detect the changes in the structure due to damage, while two non-damaged variables vary. In this numerical simulation study, the non-damaged variables used are the temperature and train speed. The proposed reference surface-based system identification method was also able to discriminate the healthy and damaged conditions of the structure, when random noise with a zero mean value was added to the acceleration signals. The random noise was limited up to 2% of the maximum amplitude of the acceleration signal at a speed of 200 km/h and temperature of -5° Celsius.

The noise in the response signals of physical structure experiments might be different from the one that was assigned to the acceleration signals of the Finite Element model. Rather than measurement devices, the variation of the structural responses might be caused by other factors that are time or frequency dependent. This information is the motivation for observing the performance of the proposed reference surface-based system identification method, if it is applied to a real structure.

In this chapter, the proposed damage identification method is applied to a simple beam model. Detailed information about the experimental specimen, setup, encountered problems, and results are briefly presented in the following subsections.

7.2 Description of the Model

The main component of the experimental specimen is a 3300 mm length standard European profile IPE-80 steel beam. The profile is strengthened by adding 31 pieces of a 150 x 46 x 3 mm steel plate to its bottom flange. Four M6 standard bolts are used to join every plate to the beam. The modified section has 18 % higher in the cross sectional area compared to its original or 25 % higher in the moment of inertia in respect to the strong axis (X-X). The modified section is considered the structure's healthy condition. Damage is assigned by restoring the section to its original condition by removing the additional plate. Figure 7.1 depicts more detailed information about the specimen.

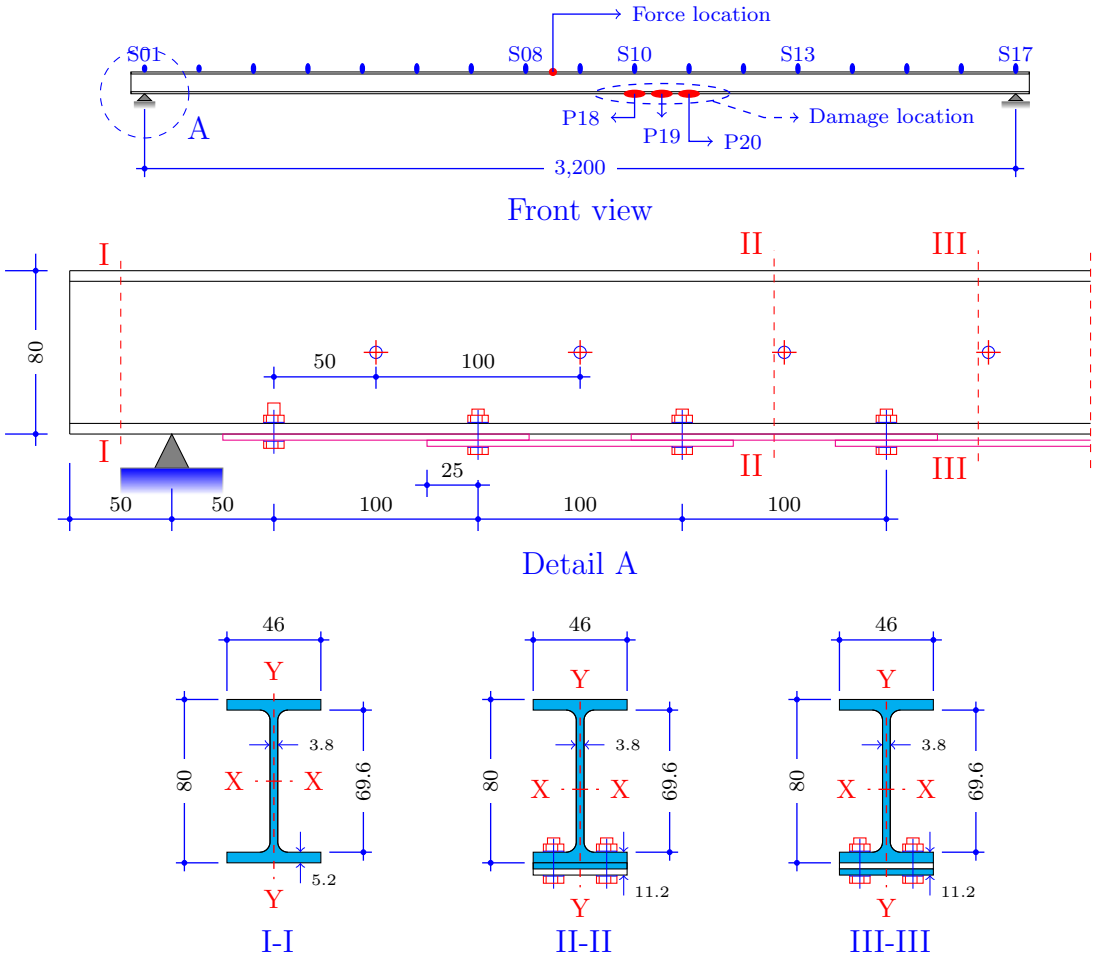

	G [kg/m]	h [mm]	A [mm^2]	I [mm^4]
Original section (I-I)	6.00	80.00	7.64x10^2	8.01x10^5
Modified section (II-II)	7.08	83.00	9.01x10^2	1.00x10^6

Figure 7.1: The modified IPE-80 steel beam.

7.3 Environmental and Operational Variables

Chapters 5 and 6 have discussed that one of the crucial issues in the vibration-based damage identification are the environmental and operational variables. These variables are called non-damaged variables in some literature. Ideally, the non-damaged variables considered in the numerical model (Chapter 6) are also used in this experimental work. However, it is difficult to assign temperature and moving load to the testing specimen in our laboratory. Finally, three non-damaged variables were assigned to the beam specimen, a variation in support stiffness, force amplitude, and additional concentrated mass. The motivation and more detailed information about these non-damaged variables are briefly described in the following subsections.

7.3.1 Variation of the Bearing Stiffness

The variation of the bearing stiffness is chosen as the first non-damaged variable. It is used to mimic the effect of temperature on the vibration responses. It has been widely accepted that temperature has a significant effect on the elastomeric bearing pad. Two scenarios have been considered to adjust the bearing stiffness of the beam (Figure 7.2). The first applies composed of rubber material and the stiffness is adjusted by modifying the dimension of the rubber block. The second uses a steel plate spring, whereby spring stiffness is modified by dragging the supports of the steel plate. Based on simplicity and material availability, the plate spring model is more convenient scenario for this experimental test. The elastic support of the experimental beam shown in Figure A.1.

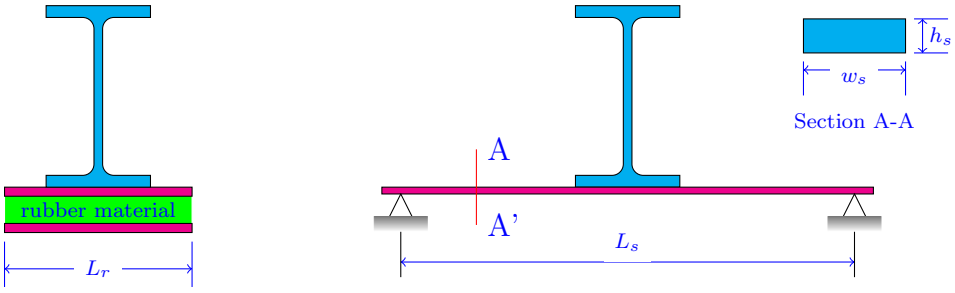

Figure 7.2: Spring model: rubber material (left) and plate spring (right).

7.3.2 Impulse Force

The second non-damaged variable is the excitation force, which is a single impulse. This force is only considered for wavelet energy and stochastic subspace identification reference surface models. The frequency reference surface models requires different kinds of excitation in order to extract as many modes as possible. The algorithm used to extract the modal properties treats the excitation signals as noise. As such, multiple impulse excitations are more suitable to obtain better results.

In the early proposal, single impulse forces will be generated using an impulse hammer similar to Figure 7.3a. The applied forces are clustered according to amplitude, as is shown in Figure 7.4. The baseline is defined and the impulse within the upper and lower bounds are selected. Impulses greater than the baseline are discarded. In fact, the number of discarded tests increases considerably if the baseline becomes narrower (smaller standard deviation value).

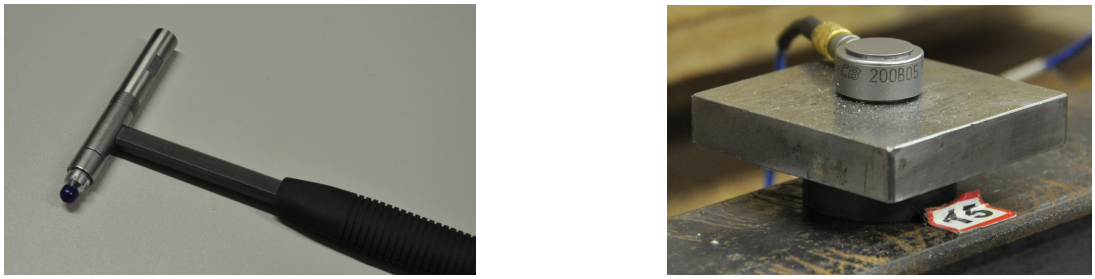

(a) (b)

Figure 7.3: Excitation force measurement options: Impulse hammer (left) and Force sensor (right).

This method works for factorial design space filling, where the number of clusters refers to the number of stratum. However, if the number of cluster and variable grows, this approach becomes inefficient as many tests will be discarded. Furthermore, the expected value is difficult to obtain if the random types of space filling design such as Monte Carlo, and Latin hypercube sampling are used.

In this study, a combination of a load cell (Figure 7.3b) and an elastic ball is proposed as an alternative procedure to overcome this problem. The ball is dropped vertically from a certain height and will hit the load cell as is shown in Figure 7.5. The load cell will measure the collision force. The target force can be obtained by adjusting the dropping height. This procedure is expected to significantly reduce the number of discarded data.

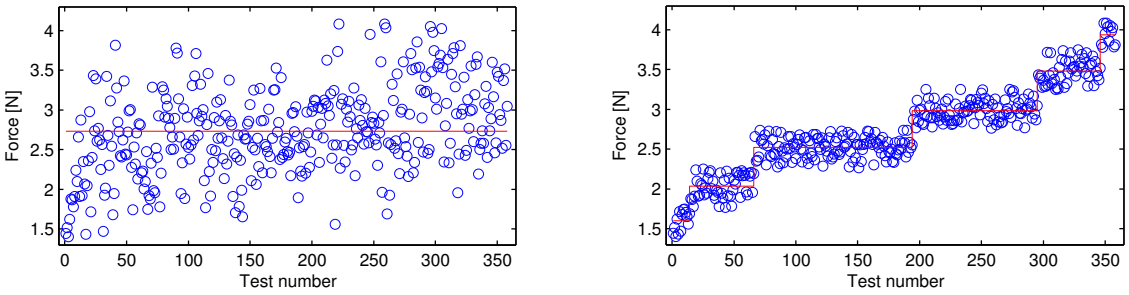

(a) Unclustered (b) Clustered

Figure 7.4: Random single impulse excitation using hammer

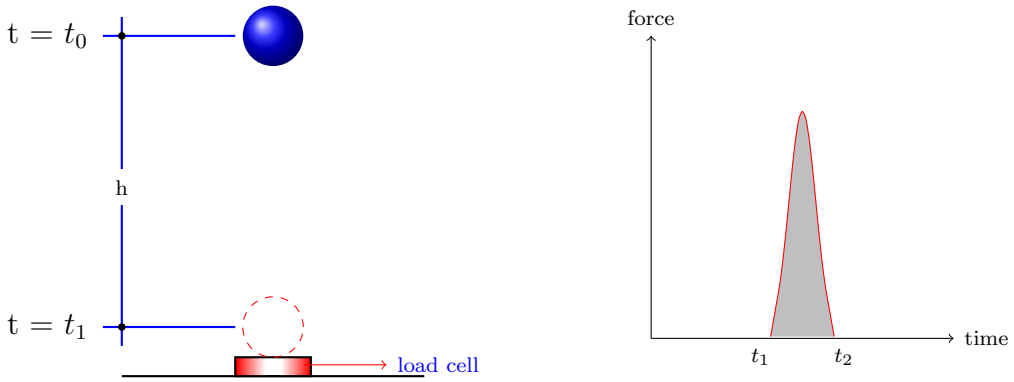

(a). Dropping ball (b). Impulse

Figure 7.5: Impulse force of an elastic dropping ball

The dropping time $(t_1 - t_0)$ primarily depends on the mass of the ball, acceleration, and height; the friction with the air is omitted. The energy of the ball is transferred to the force sensor during collision. The collision duration depends on the ball's material. Therefore, it is more appropriate to describe the ball excitation in terms of impulse rather than maximum force. The total energy of the ball in Figure 7.5 can be written as

$$\frac{1}{2}m.v^2 + m.g.h = 0, \tag{7.1}$$

where m, v, h, and g refer to mass, velocity, height, and the gravity value, respectively. The velocity of the ball when it touches the load sensor is

$$v_1 = \sqrt{2.g.h} \tag{7.2}$$

The change of momentum during contact with the load sensor is called impulse and can be described as

$$I = \Delta p = \int_{t_1}^{t_2} F dt, \tag{7.3}$$

where t_1 and t_2 are the time as the first and the last contact, respectively. The impulse described in Equation (7.3) is actually the area shown in Figure 7.5b. The expected force according to the design of experiment can be obtained by predicting the dropping height h. The proposed excitation method works well in the preliminary test. Some of the results are summarized in Figures 7.6 and 7.7.

Figures 7.6a and 7.6b show the variation of impulse and the expected forces. 10 replications are done for every setup (target force). In general, there is no notable difference regarding collision duration among these three different target force amplitudes. Figure 7.7a shows the comparison of acceleration signals. The variation of wavelet energy distribution over decomposition level is shown in Figure 7.7b. Based on these preliminary results, the drop ball method are much more suitable than the use of an impulse hammer for this experiment.

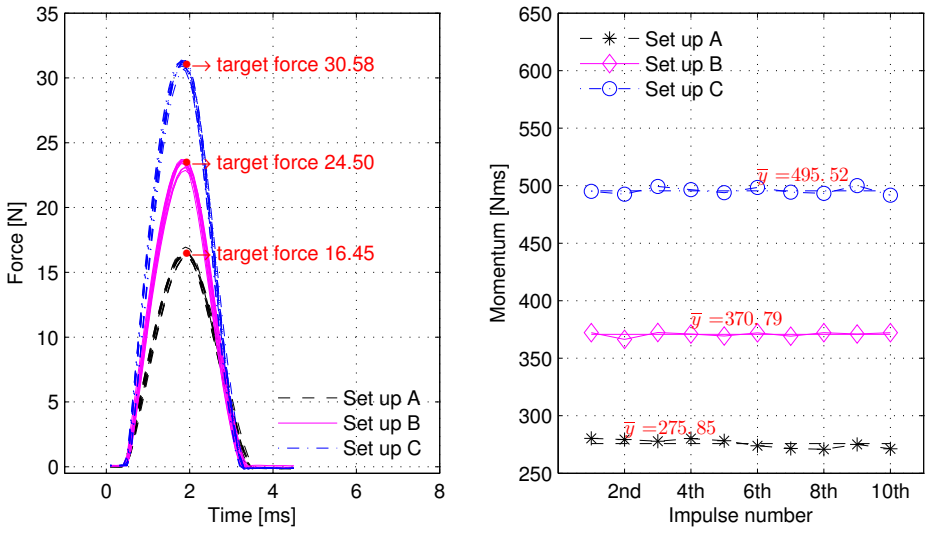

(a) Impulse shape

(b) Impulse

Figure 7.6: Forces and impulse variation obtained from dropping ball experiments with three different setups and 10 replications

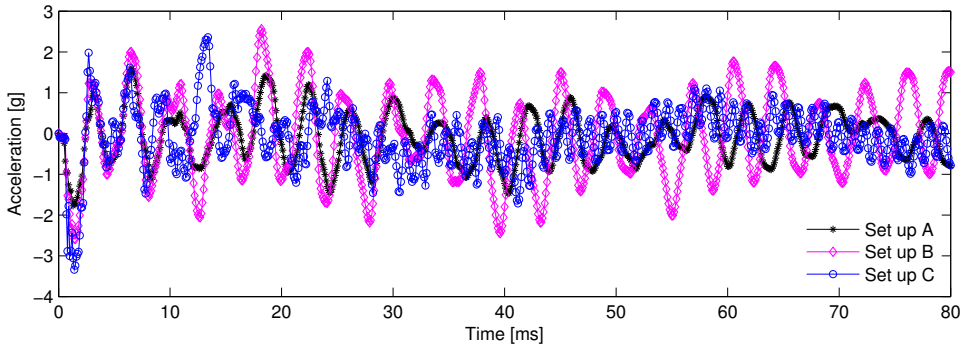

(a) Acceleration signals

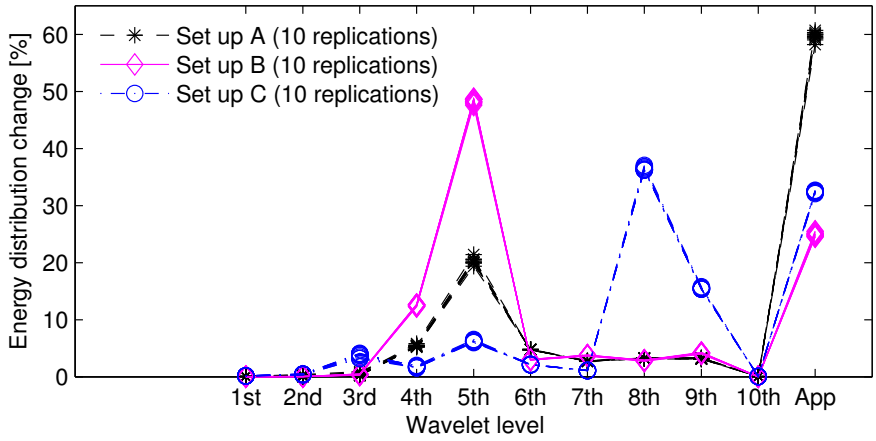

(b) Energy distribution

Figure 7.7: Acceleration signals and energy distribution over wavelet decomposition level of the signal obtained from dropping ball experiments with three different sets up and 10 replications

7.3.3 Additional Mass

The third non-damaged variable is the additional concentrated mass. Mass has significant effects on the modal properties and dynamic response of a structure. Generally, eigen frequency of the structure decreases with respect to the additional mass. The effect depends on the quantity and position of the mass. In this experiment, a steel cylinder is used as is shown in Figure 7.8. The cylinder's weight is 850 gr or approximately 3.5% of the specimen's total weight. The cylinder is mounted to the top flange of the beam using a magnet. However, in some particular tests it has to be moved to the lower flange, as its original location was too close or coincided with the accelerometer or force sensors.

(a). Front view (b). Top view

Figure 7.8: Additional mass

7.4 Damage Scenarios

Damaged scenario is carried out by removing a single or multiple additional steel plates of the modified IPE-80 beam. Many damage scenarios can be assigned regarding location and the number of removed plates. Only single damage locations are applied in this experiment, to reduce the complexity of data analysis. Three different damage scenarios are planned considering the number of removed plates as is shown in Figure 7.9. The damage position is shown in Figure 7.1.

In the first damage scenario, only a single steel plate is removed (P18). The plate P19 is also removed in the second damage scenario. In the third damage scenario, three plates are removed (P18, P19, and P20). In every damage scenario, the removed plates are remounted to the beam's web near its original location by using a single M6 bolt to preserve the mass. The change of the global stiffness of the structure is affected by the number and locations of the removed plates. Hence, the three damage scenarios can be interpreted as three damage levels, where higher number of the removed plates indicates more severe damage.

7.5 Preliminary Test

The preliminary tests were addressed to assess whether the system can supply reliable data. It was also important to ensure that the planned damage scenario is strong enough to be identified by the considered damage indicators.

In this test, the distance between the two spring's supports (L_s) were assigned 15 cm. The structure was subjected to multiple random impulses to obtain the eigen frequencies and respective mode shapes. The typical measured acceleration signal due to multiple impulse

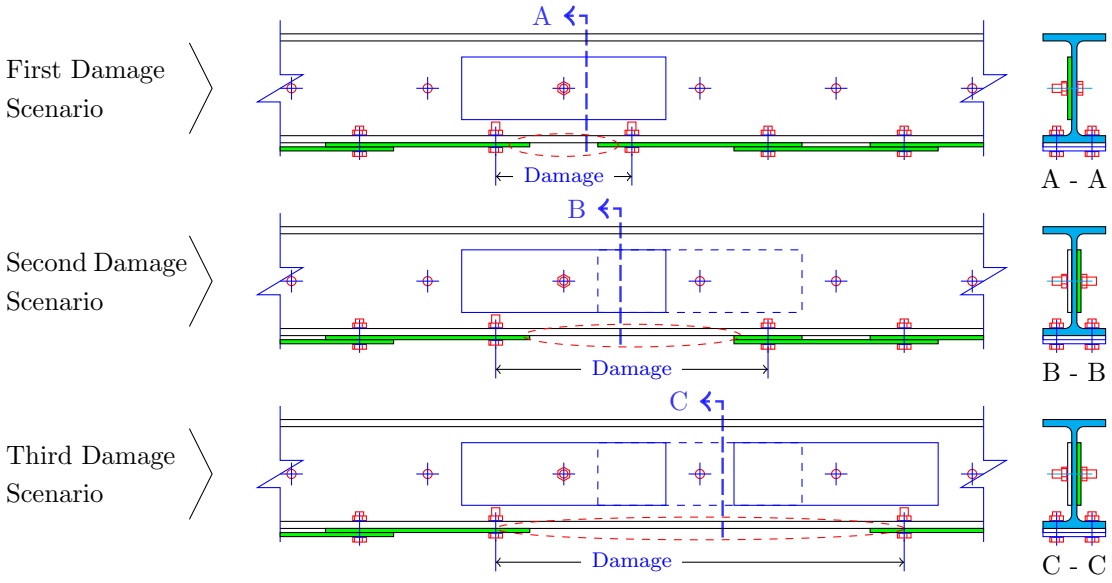

Figure 7.9: Three level of damage scenarios

excitations is shown in Figure 7.10a. The frequency response function of the acceleration signals obtained from two different sensor locations are shown in Figure 7.10b.

The modal properties were extracted by using the stochastic subspace identification algorithm, implemented in software package MACEC, [Reynders *et al.*, 2011]. The eigen frequencies and associated mode shapes are shown in Table 7.1 and Figure 7.11, respectively. The first mode shape clearly shows the vertical displacement of the spring. This mode seems to be a combination of the first individual mode shape of the simple supported beam and the springs. The second mode shape shows the vertical displacement of the two springs in the opposite direction. This mode might not be so useful for damage identification.

There are no dramatic changes in eigen frequencies due to the prescribed damage as shown in Figure 7.12. The five lowest eigen frequencies of the beam in the three damage scenarios change from 0.2% to 1.5% depending on the eigen mode that is considered. The amount of change increases with respect to damage severity. The lowest eigen frequency change is obtained from the second mode.

The wavelet energy distribution of the three different damage scenarios is presented in Figure 7.13. The wavelet energy shifts with respect to the damage scenarios are obvious. A large amount of the signal's energy in level 5 (WE-5) moves to level 7 (WE-7), and this moved energy is greater with respect to damage severity. Meanwhile, a different charac-

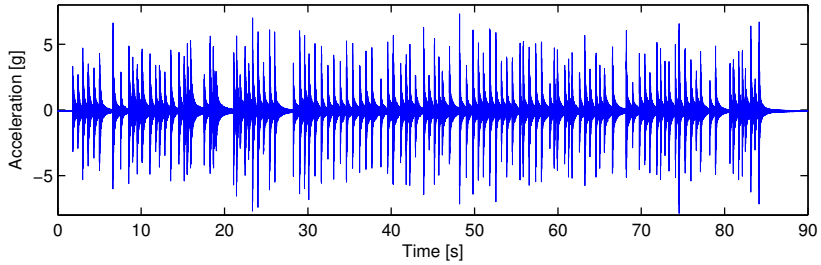

(a) The acceleration signal in time domain

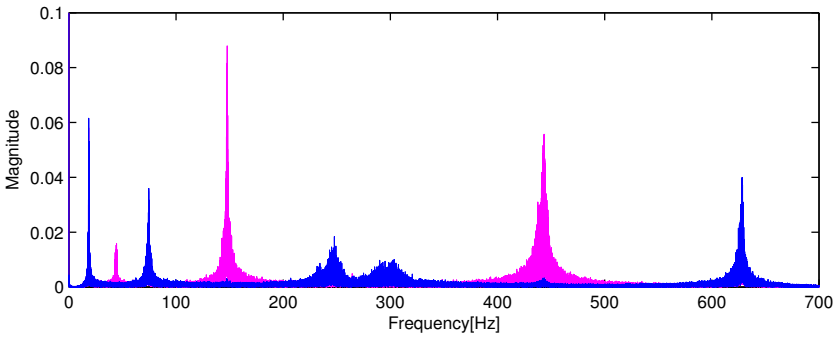

(b) The acceleration signal in frequency domain

Figure 7.10: Typical acceleration signals and its frequency response measured from two different sensor positions

Table 7.1: Eigen frequencies of the modified IPE80 beam with spring support (L_s = 15 cm)

Mode	Frequency [Hz]				
	Test 1	Test 2	Test 3	Mean value	STD
1st	18.631	18.635	18.685	18.650	0.0301
2nd	44.196	44.316	44.186	44.299	0.0961
3rd	74.428	74.564	74.579	74.524	0.0832
4th	147.745	147.965	147.817	147.842	0.1122
5th	272.333	274.626	273.784	273.581	1.1599
6th	443.484	443.197	443.410	443.697	0.4346

teristic is shown by the WE-6. Its energy remains approximately constant in all damage scenarios. However, it should be noted that these characteristics might not always be the same if the damage severity level is constantly increased until the structure collapses. A different setup (excitation amplitudes, damage location, etc.) might result in varying characteristics of the wavelet energy distribution and shifting.

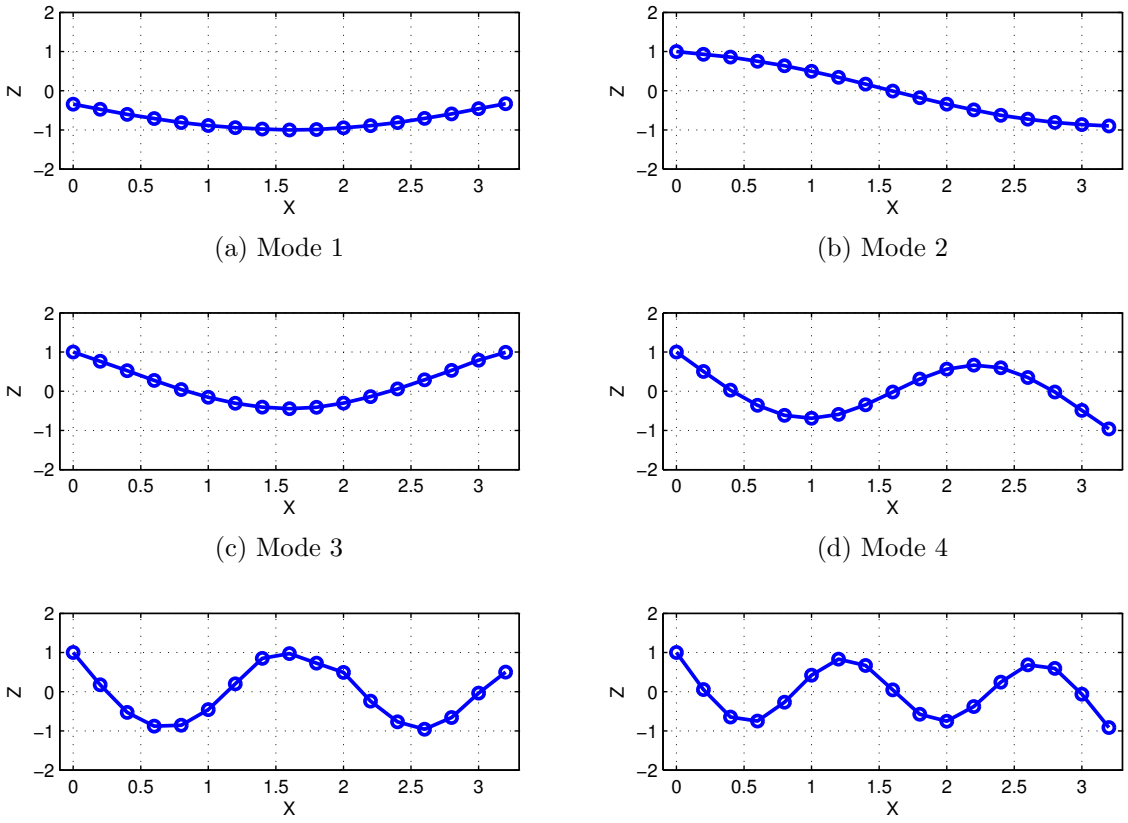

(a) Mode 1

(b) Mode 2

(c) Mode 3

(d) Mode 4

(e) Mode 5

(f) Mode 6

Figure 7.11: Typical 6 lowest mode shapes of the modified IPE-80 beam with spring support.

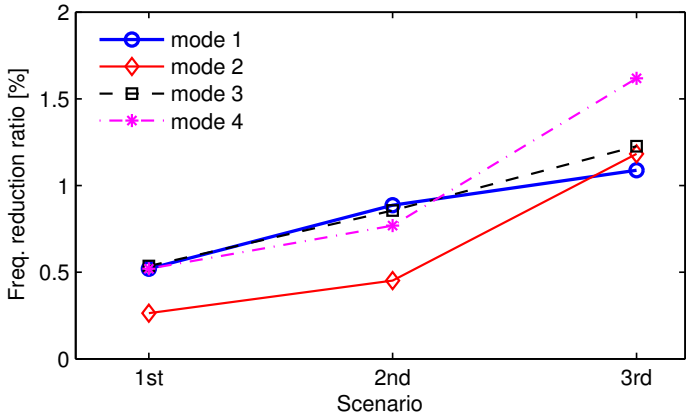

Figure 7.12: The frequencies of the three different damage scenarios when compared to the frequencies of the healthy structure.

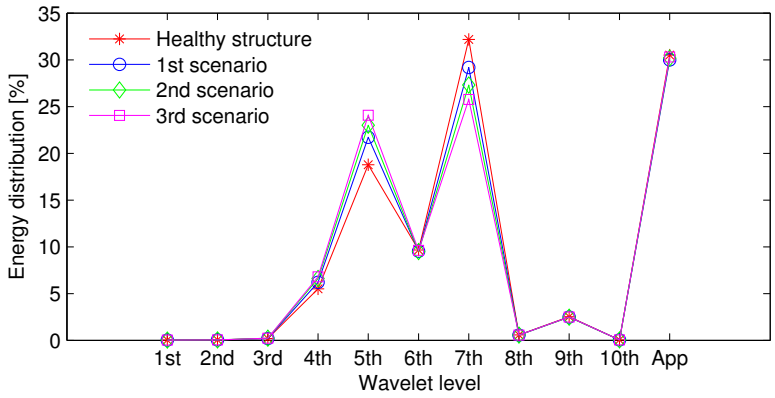

Figure 7.13: Energy distribution along the wavelet level with respect to the damage scenario.

In this preliminary test, the wavelet energy damage indicator gives a clearer picture about the structural change (damage scenarios) when compared to the frequency damage indicator. The amount of change varies depending on the considered wavelet level. Significant changes are obviously shown by the WE-4, WE-5, and WE-7, whereas no notable changes are found for WE-6, WE-8, and WE-9. The wavelet energy change ratio in the three damage scenarios are shown in Figure 7.14.

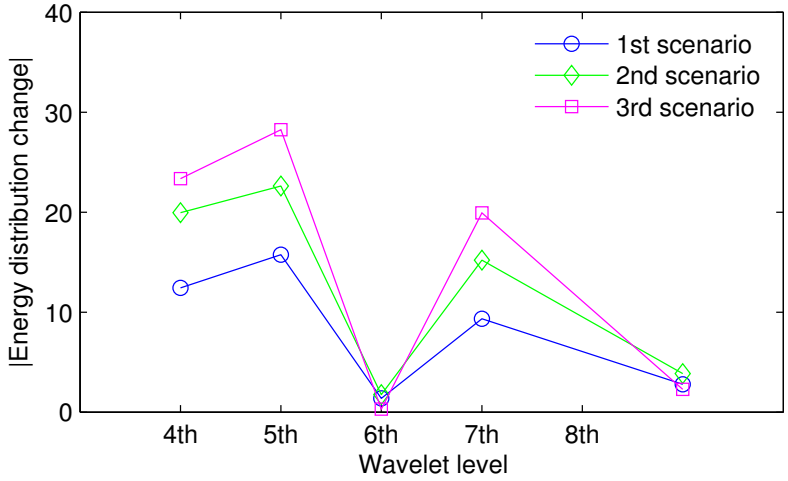

Figure 7.14: The wavelet energy change ratio with respect to the damage scenario.

7.6 Sampling Plan

One of the crucial issues in building a reference surface model is the sampling plan. A better quality reference surface model can be obtained through the use of a higher number of training points. However, in a situation where the experiment of training point is expensive or many input variables are considered, the sampling plan becomes problematic. There is a trade-off between the number of samples and the approximation quality. The simplest way to obtain a sampling plan is by using the full factorial design. However, this method was not used in this experimental study because it yields a high number of samples. For example, 1,250 tests are required if every non-damaged variables has 5 strata with 10 replications. In this situation, the Latin hypercube sampling seems more reasonable.

The Latin Hypercube Sampling was finally used to select twenty training points for the three non-damaged variables (mass position, spring supports distance, and impulse force). In this experimental study, the mass position can be placed across the whole span of the beam. However, the spring support distance can only be adjusted between 12 cm to 37 cm. The dropping height of the ball is planned from 40 cm to 100 cm and expected to generate forces between 15 and 40 N. The Latin hypercube sampling algorithm was also used to select 5 validation points. The result of the sampling plan is shown in Figure 7.15.

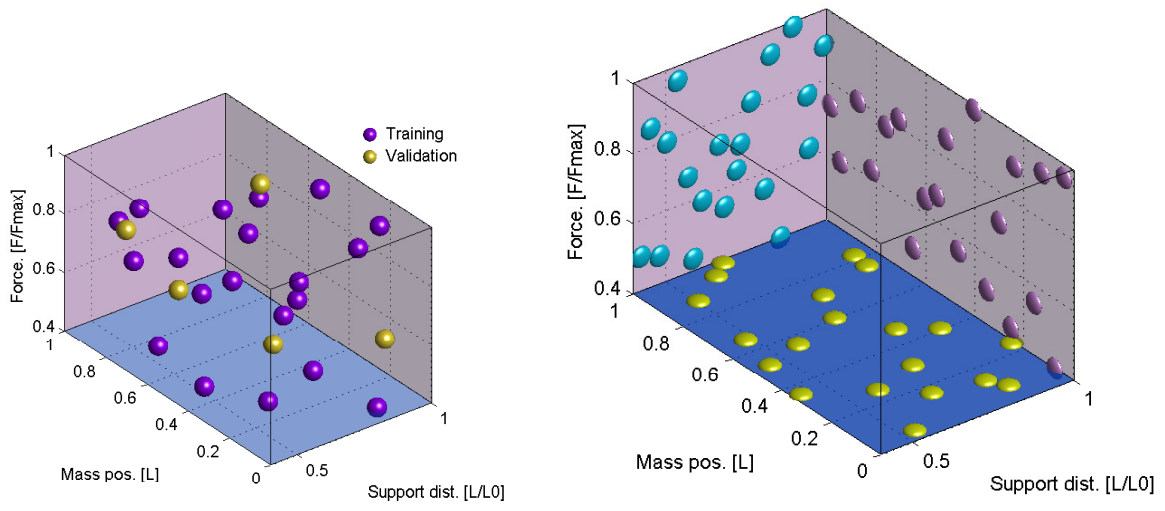

(a) Sampling points

(b) Orthogonal projection of the training points

Figure 7.15: Sampling plan of the experimental test.

7.7 Learning Phase

The main part of the reference surface-based system identification is called the learning or training phase, where the observation data is employed to develop the reference surface model. According to observation data that is available in this experimental study, three types of reference surface models will be built, frequency reference surface model, wavelet energy reference surface model, and stochastic subspace identification reference surface model.

7.7.1 Frequency Reference Surface

The eigen frequency is probably the most commonly used damage indicator in structural damage identification. In the numerical model presented Chapter 6, the eigen frequencies were calculated by solving the dynamic eigen value problem in Equation (2.2). In contrast, greater efforts are required to obtain the modal properties of a real structure. In a physical model, the eigen frequency and its respective mode shape can be identified using several methods. The most common method for modal identification is the stochastic subspace identification method. In this method, the excitation signal is handled as noise, and will thus not be measured.

By ignoring the excitation force, the frequency reference surface of the experimental model in this study becomes simpler. It contains only two non-damaged variables (the mass position and spring supports distance). This situation has a great advantage, since the frequency reference surface model can be visualized using three dimensional plots. Visualization is a good feature to assure the quality of the approximation model, instead of using the error quantification method, such as the sum squared error (SSE) and mean squared error (MSE).

The force that is required to extract modal properties of the structure is different from the one described in Section 7.3.2. Here, random multiple impulses are used. Three measurements are done for every setup. The modal properties are extracted using stochastic subspace algorithm implemented by software package MACEC, [Reynders *et al.*, 2011]. The Modal Assurance Criteria described in Subsection 3.4.2, is used to assure that similar mode shapes have been extracted from every setup.

The four scattered data approximation methods used in Chapter 6 are also applied for this subsection. In this case, the radial basis function, artificial neural network, and

moving least squares approximation methods provide better results when compared to the polynomial model approximation method. The best frequency reference surface models obtained using RBF are shown in Figure 7.16.

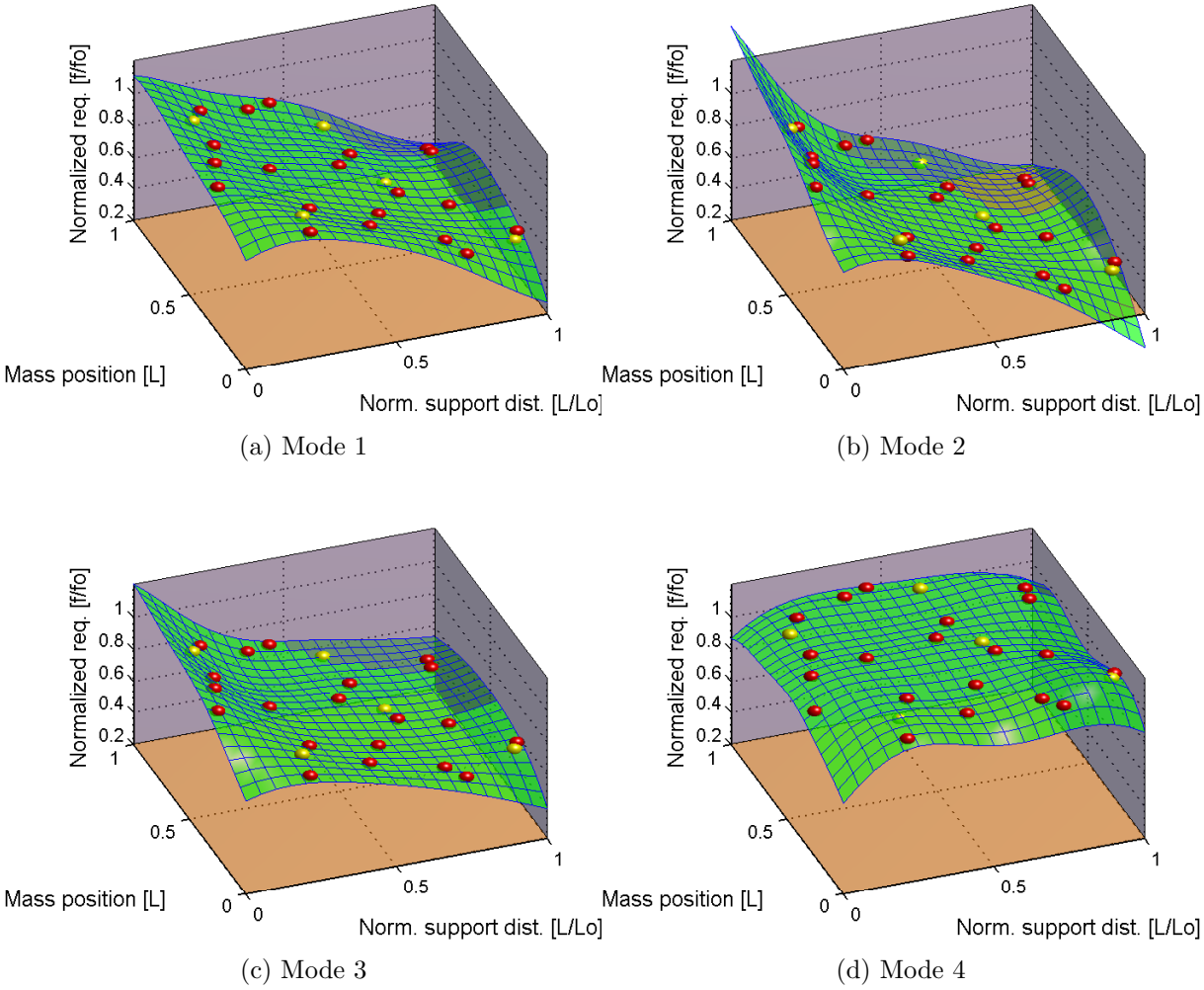

(a) Mode 1

(b) Mode 2

(c) Mode 3

(d) Mode 4

Figure 7.16: Frequency reference surface models of the experimental specimen.

In Figure 7.16, the reference surface models seems to be a good representation of the training points (red spheres). However, the approximate errors in some validation points (yellow spheres) are still considerably high. The errors at a particular validation point are obviously more than 1% as shown in Figure 7.17. This amount of error is quite significant for frequency response surface models. It will lead to poor prediction results in the damage detection phase, if the error is not considered. This means, these frequency reference surface models are not useful until the approximate error is fixed, for instance by using other approximation methods or by adding new support points.

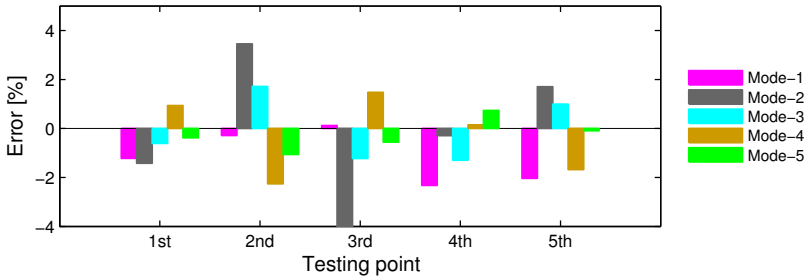

Figure 7.17: Approximate error of the frequency reference surface models .

The error might be caused by three suspicious aspects. The first aspect is the lack of support points. This is obvious for areas that have a limited number of training points while the surfaces are bumpy (Figure 7.16). For instance, in the region at mass position is approximately 0.8 and spring support distance is approximately 0.75. The second aspect is the irregularity of training points, where the chosen shape parameter is not suitable for all regions of the design space. An adaptive algorithm that can adjust the shape parameter can be applied to minimize the irregularity effect. The third aspect might be errors in input variables when the setup is changed from one to another, for instance, the accuracy of the spring's supports distance measurements. However, this presumption is ignored and the imperfect fit of the frequency reference surface model is assumed to be primarily caused by a lack of samples.

The approximation quality of the reference surface model may be improved by adding new observation data or by spreading the training points as regular as possible. In this case, the best action would be to consider validation points as additional training points. However, it should be noted that this improved model may still have a significant error in the regions far from any training points. This means that the damage identification by using the frequency reference surface model in this experimental study can only be performed in certain regions, particularly one that is close to support points. The detection phase by using the frequency reference surface model is presented in Section 7.8.

7.7.2 Wavelet Energy Reference Surface

In contrast to the frequency reference surface model, which does not consider the excitation force as an input variable, the wavelet energy reference surface model takes this variable into account. In this experimental study, the excitation force is an impulse force generated by a dropping ball. The duration of the measured signal should be similar for all tests in order to reduce the variation of signal's total energy. It can be done by

applying a triggering algorithm to the data acquisition system. The acceleration signals were recorded soon after the ball hit the force sensor until certain duration, in this case 10 seconds.

The first channel that contains force signal was used to calculate the impulse by using the Equation (7.3). The other channels that contain acceleration data were used to calculate the wavelet energy by using Equations (2.29), (2.30), and (2.31). The wavelet energy of each level is normalized to the signal's total energy to reduce the effect of different excitations.

The wavelet energy reference surface model in this experimental study contains three input variables, spring supports distance, mass position, and impulse force. Hence, it cannot be visualized using a 3D surface plot. Therefore, searching for the best approximation model will totally rely on the error quantification, in this case by using mean squared error (MSE).

The wavelet energy reference surface models were built by using the radial basis function approximation method. The optimum shape parameter α was obtained by iterations. The mean squared error of the wavelet energy reference surface models obtained from different shape parameters α is shown in Figure 7.18. The position of the sensor is shown in Figure 7.1.

The reference surface models with minimum mean squared error are considered the best wavelet energy reference surface models. These models will be used in the damage detection phase. However, individual error in all observation points should be observed before the reference surface model can be used for damage detection. In this case, the errors in the five validation points are still considerably high. The limit for the individual error in this experimental study is assumed 0.01%. This value is chosen by considering the results of the preliminary test.

Basically, the quality of the reference surface models can be improved by adding new training points. As such, in this experimental study, the five validation points were also used to train the reference surface models. It means all of the twenty-five observation points were used to train the model. Consequently, the improved reference surface models should only be used for damage identification at regions near to the training points.

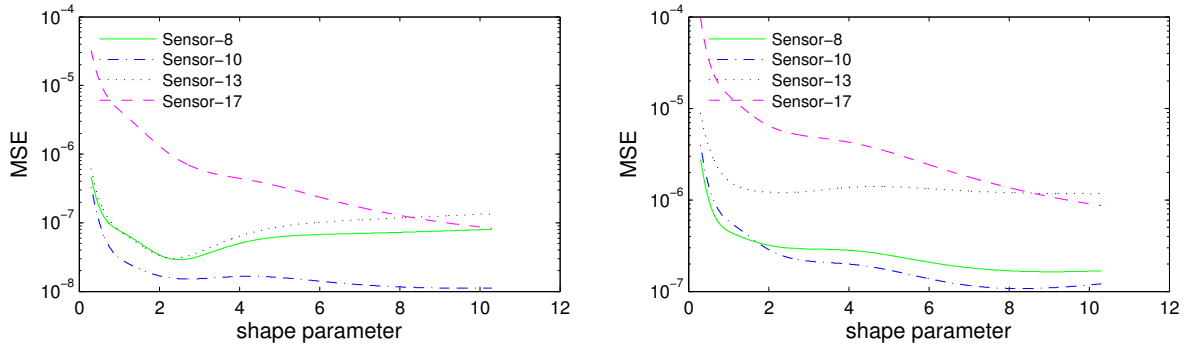

(a) WE level 1

(b) WE level 2

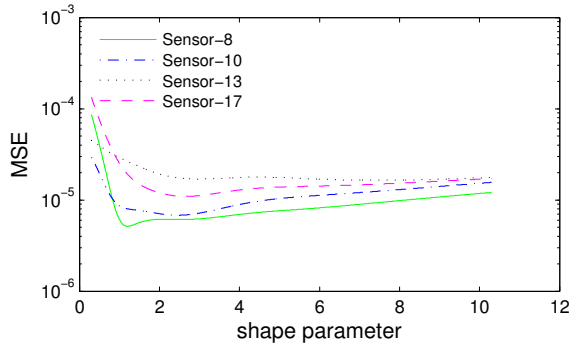

(c) WE level 3

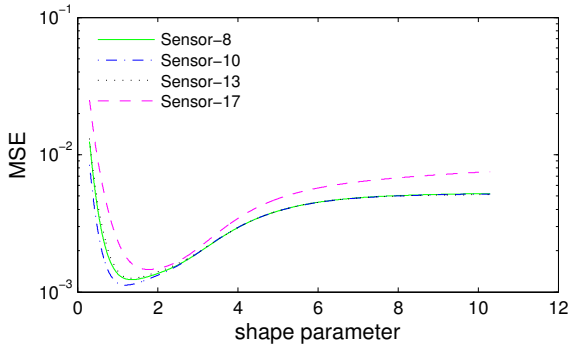

(d) WE level 4

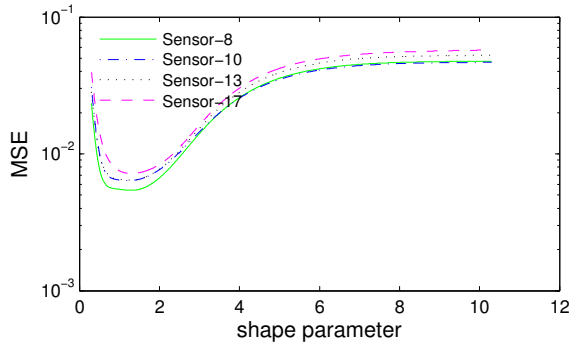

(e) WE level 5

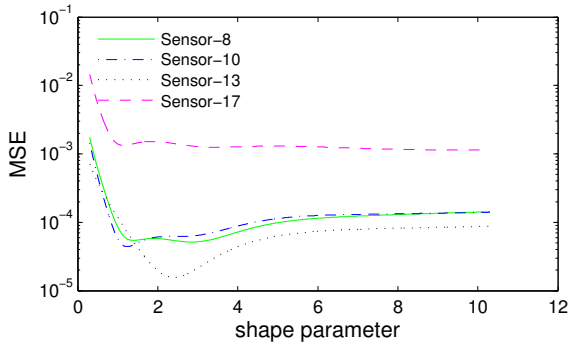

(f) WE level 6

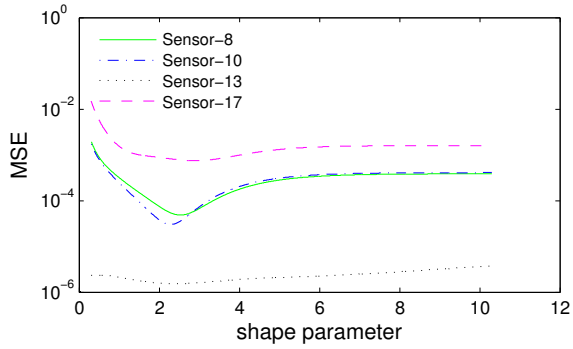

(g) WE level 7

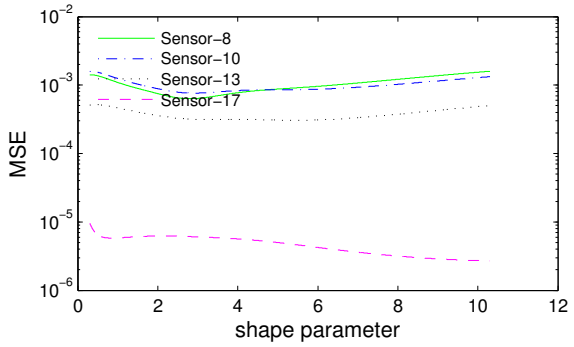

(h) WE level 8

Figure 7.18: Mean squared error (MSE) of wavelet energy reference surface models with difference shape parameters

7.7.3 SSI Reference Surface

Section 6.4.1.3 described that a base support point has to be defined first before other support points can be calculated. In this experimental study, the input value of the spring supports distance, mass position, and impulse force at 17.14 cm, 96.4 cm, and 25.36 N, respectively, is chosen as the base support point. The result of this experiment indicates that the input variable ranges, particularly the spring supports distance, were too wide. The twenty training points were not enough to build SSI reference surface models that adequately represent all design space. In this case, the approximate errors of some validation points are greater than 1%. The SSI reference surface model is improved by considering the validation points as training points.

7.8 Detection Phase

In this experimental study, the damage detection was performed for five different input variable values, which were called damage detection points (DP). In this case, the input value of the DP were coincided with the validation points in Figure 7.15. Three damage scenarios were assigned to the experimental model as is shown in Figure 7.9. The upper and lower bounds values were obtained by shifting the reference surface model. The shifting distance is 2σ that gives 95% confidence interval.

Damage identification using the frequency reference surface models is summarized in Figure 7.19. In the first damage scenario, the frequency reference surface models do not clearly show the damaged and undamaged conditions. Many damage detection points lie below the upper bound values. For instance, only one of the five damage detection points clearly indicates damaged condition by using the fourth eigen frequency reference surface model (Figure 7.19a). However, clearer indications were obtained in the second and third damage scenarios by observing the similar reference surface model (Figure 7.19b and (7.19b)). In these scenarios, all of the damage detection points lie above the upper bound values of the fourth eigen frequency reference surface model. Similar results are also obtained by observing the third eigen frequency reference surface model. In the third damage scenario, most of the frequency reference surface models can discriminate the damaged and undamaged conditions. However, the damage detection result by using the second eigen frequency reference surface model did not improve when the damage became more severe. Based on the typical mode shapes in the Figure 7.11, the second mode

seems to be only a rigid body motion. It is probably the reason for the insensitivity of the second eigen frequency reference surface model for the damage.

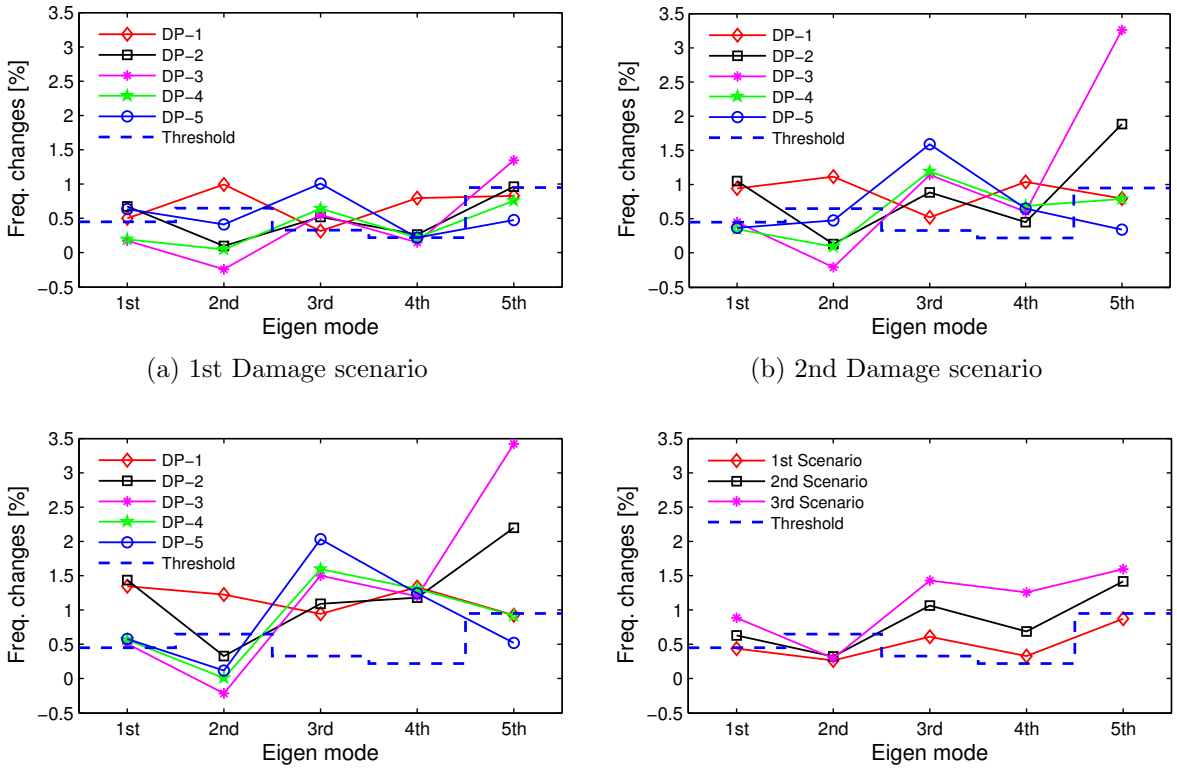

(a) 1st Damage scenario

(b) 2nd Damage scenario

(c) 3rd Damage scenario

(d) Mean value of all DPs

Figure 7.19: Detection phase using frequency reference surface model.

.

The damage detection results can be presented using a probability value. The probability of damage presence in the structure can be calculated using Equation (5.19). The damage probability of the first damage scenario is 42.24%. This value is obtained by considering the first five lowest eigen frequency reference surface models. The damage probability of the second and third damage scenarios are 96.95% and 98.57%, respectively. The damage probability assessment may be improved by understanding the behaviour of the structure. For instance, by ignoring the second eigen frequency, the damage probability of the first, second, and third damage scenarios become 75.72%, 99.27%, and 99.66%, respectively.

Figure 7.20 shows some of the results from the damage detection phase by using the wavelet energy reference surface models. Figure 7.20a depicts the change of WE-5 in the three different damage scenarios. In this Figure, the WE-5 increases with respect to damage severity for most of the damage detection points (DP). Only the DP-1 shows a

decreasing trend with respect to damage severity. Significant increments of the WE-5 are shown by the DP-2 and DP-3. This information was obtained from the signals measured by sensor 10 (S10 in Figure 7.1).

Figure 7.20b illustrates the change of wavelet energy decomposition level 7 (WE-7). In this wavelet energy level, a decreasing trend is shows by most of the damage detection points. A significant WE-7 change is shown by DP-3, DP-4, and DP-5. This information was also obtained by observing signals measured by sensor 10.

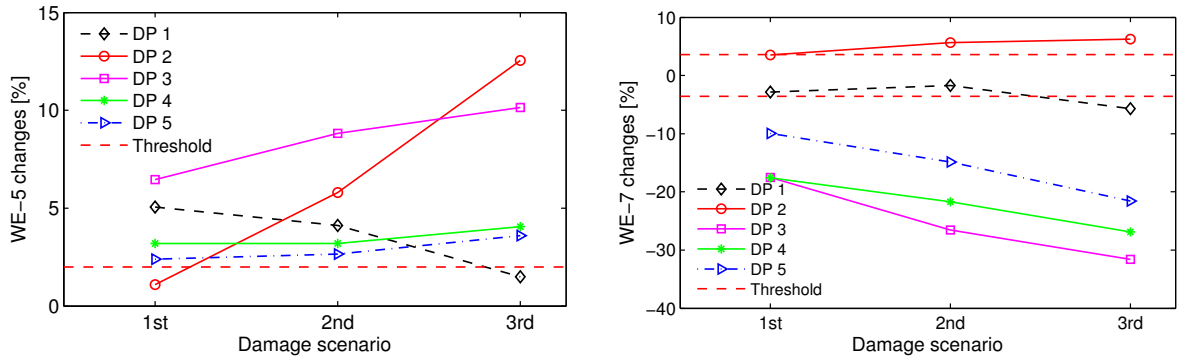

(a) WE-5 Sensor-10

(b) WE-7 Sensor-10

Figure 7.20: Detection phase using wavelet energy reference surface model.

According to the WE-5 and WE-7 reference surface models, the damage probability of the first damage scenario is 80.76%. This value is slightly higher when compared to the result of the eigen frequency reference surface models. The damage probability of the second and third damage scenarios are the same (98.37%).

The SSI reference surface model results 57% damage probability of the first and second damage scenarios. The damage probability in the third scenario increases to 76%. These results are obtained by analyzing signal of two acceleration sensors (S-9 and S-10). A better result may be obtained by considering more acceleration signals. In this case, the damage probability of the third damage scenario becomes 95% when the signals from six sensors are used. Similarly, the damage probability of the second damage scenario increases to 76%.

There are different characteristics between the frequency reference surface and wavelet energy reference surface models. In the frequency reference surface model, the frequency changes increase with respect to damage severity. In the wavelet reference surface models,

the changes may increase or decrease, when the damage condition of the structure becomes more severe.

7.9 Summary

The core of the reference surface-based system identification method is building the metamodels. Without a good metamodel, the damage identification may lead to erroneous results. Some observation points should be set aside for validation purposes to ensure that the reference surface model has good approximation for all input variable ranges.

The experimental model was prepared to observe the capability of the proposed damage detection method to identify damages in a physical structure. The experimental specimen was originally a 3300 mm length IPE-80 steel beam. The beam was modified by adding additional plates to its bottom flange. The damage was prescribed by removing the additional plates. Three variables were chosen as non-damaged variables, the support stiffness, impulse force, and the position of additional mass.

In this experimental study, the Latin hypercube sampling was used to choose twenty training points and five validation points. Unfortunately, the twenty training points were not enough to build reference surface models that can adequately represent the entire design space. The approximate errors for the five validation points are considerably high. i¿ Hence, the five validation points were also used to train the models. This means the reference surface models were built and validated with the same twenty-five training points. Consequently, the model should only be used for damage identification at input variables near to the supports points. In this study, the input variables of the damage detection points (DP) were same with the input variables of the 5 validation points. More validation or training points are required to make the reference surface models applicable for all intervals of input variables.

The result of this experimental study shows that the reference surface models are able to distinguish the three damage scenarios assigned to the structure. It indicates that the reference surface-based system identification method is a good approach for identifying damage in a structure with varying operational and experimental conditions. In a situation where there is plenty of observation data, such as a long-term monitoring system, the reference surface-based system identification method seems to be very useful.

Chapter 8

Conclusions and Recommendations for Further Research

8.1 Conclusions

This dissertation proposes the use of reference surface models for assessing damage in structures. The proposed method is a combination of the vibration-based damage identification and the response surface methodology. The reference surface-based system identification method enables the inclusion of effects from environmental and operational conditions in the damage detection procedures. The proposed method is considered as a very simple method to distinguish damaged and undamaged condition of a structure with varying environmental and operational conditions. By using particular damage indicators such as wavelet energy, reference surface models can be built using data from a single accelerometer sensor. However, the use of multiple sensors has positive impacts on the capability of the proposed damage detection method.

The core of the reference surface-based system identification method is the learning phase in which the reference surface models are trained and validated. The training is performed by using vibration-based damage indicator data of the healthy structure. The damage indicators are calculated from dynamic response signals of the structure. Probability theory is used to accommodate the response variations due to noise. The damage identification is done by comparing the current damage indicator values to the reference surface models.

The capability of the reference surface-based system identification method to detect damages in structures with arbitrary operational and environmental conditions is dependent on three major aspects:

1. The quality of the reference surface model.
   Quality in this context refers to how good the reference surface model is in approximating the vibration-based damage indicator value for a given environmental and operational conditions. The model quality depends on the number and distribution of training points. It also depends on the scattered data approximation method used.

2. The chosen vibration-based damage indicator
   The sensitivity and stability of the damage indicators have profound effects on the capability of the reference surface models to detect damage in structures. A higher sensitivity damage indicator leads to higher capability of the reference surface models, since it can deliver a greater gap between the damaged and undamaged conditions.

3. Level of noise
   Noise in this context does not only refer to the noise that comes from the measurement equipments or signal processing, but also to the variation of response due to the contribution of variables that are not included in the reference surface models. The level of noise significantly impacts the capability of the reference surface model to detect damage, particularly in the early damage stage.

The proposed system identification method has been applied to the Finite Element model of the Erfttal-Brücke, a high-speed railway bridge near Cologne, Germany. The bridge was excited by moving loads of the ICE train model. Train speed and temperature were chosen as operational and environmental variables, respectively. The proposed method showed good performance in discriminating between damaged and undamaged scenarios. The proposed method was still able to distinguish these two scenarios if the certain level of zero mean random noise (up to 5% of the max. amplitude) were added to the acceleration signals.

The Gaussian random noise used in the numerical simulation study might be different from the noise in a physical structure. An experimental model was prepared to observe the capability of the proposed method to identify damage in a real physical structure. Support stiffness, impulse force, and mass position were chosen as non-damaged variables. The results showed that the proposed method was capable of identifying the three damage scenarios. Due to lack number of training points, the reference surface models that have been developed for the experimental model does not have a good approximation in some regions of the input variables, particularly near to boundary. However, the approximate

error in the support points is very small. This means that at the moment, the reference surface models are only applicable for areas close to the support points. However, by adding new training and validation points, the reference surface models can be improved to cover all ranges of the design space.

Basically, the usage of multiple types reference surface models may increase the opportunity to detect damages in a broader spectrum of damage severity, as all types of reference surface models have benefit and drawbacks. For instance, in some cases, the frequency response surface models are not sensitive to small local damage. However, its sensitivity grows when the damage becomes more severe. On the other hand, the wavelet energy reference surface model works much better for small changes in the structure when compared to the frequency model. However, its sensitivity does not has a monotonic trend with respect to damage severity. Hence, by having multiple types reference surface models, the chance of detecting damage in the structure becomes greater.

8.2 Recommendations for Further Research

The results of this study indicate that the reference surface-based system identification method seems to be a robust approach to be applied in long time structural health monitoring systems where the operational and environmental conditions vary with time. However, the proposed system-identification method requires further investigation and improvement for the following items:

- The basic assumption during the learning phase is that there is no damage in the structure. This presumption might not be correct, particularly for old structures. A method is required to assess the validity of this assumption. This method is essential for the application of the reference surface-based system identification method to old structures.
- In some particular cases, the output variable values' gap between two neighboring regions of the reference surface model is too high. The meta-model may fail to approximate the training points in the lower output region. This problem may be overcome by dividing the input variables ranges into some blocks with respect to the output variable values and then independent meta-models are built for every block. An algorithm is needed to automatically create the blocks, build meta-models, and combine them later by considering the continuity within the borders.

- The proposed system identification method can be extended to damage localization by using cross information between the physical and the finite element model of the structure. The finite element model is calibrated through model updating.
- The capability of the reference surface models to detect damage might be improved by reducing the variability of the dynamic response signals for instance by using signal filtering.
- It is necessary to assess the reliability of the reference surface-based system identification by considering various types of structures and damages.

Appendix A

Experimental Tools

A.1 Beam's support

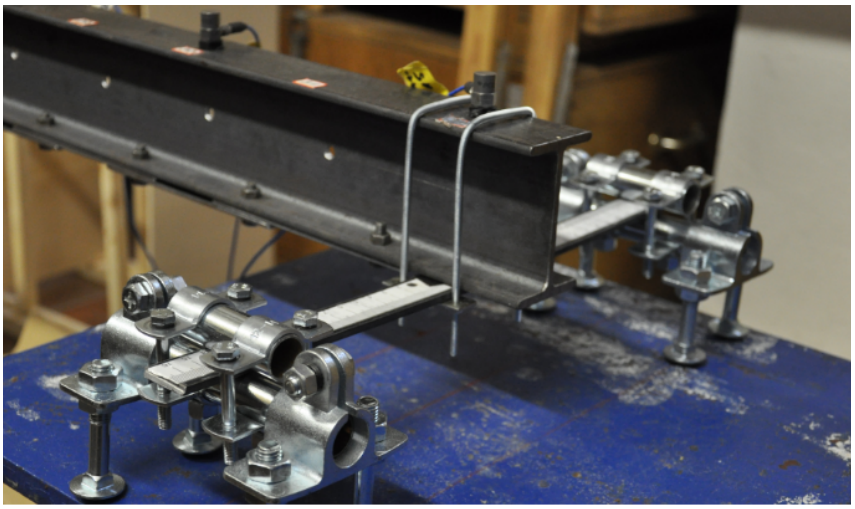

Figure A.1: Spring support: The spring stiffnes is modified by dragging the supports

A.2 Additional mass

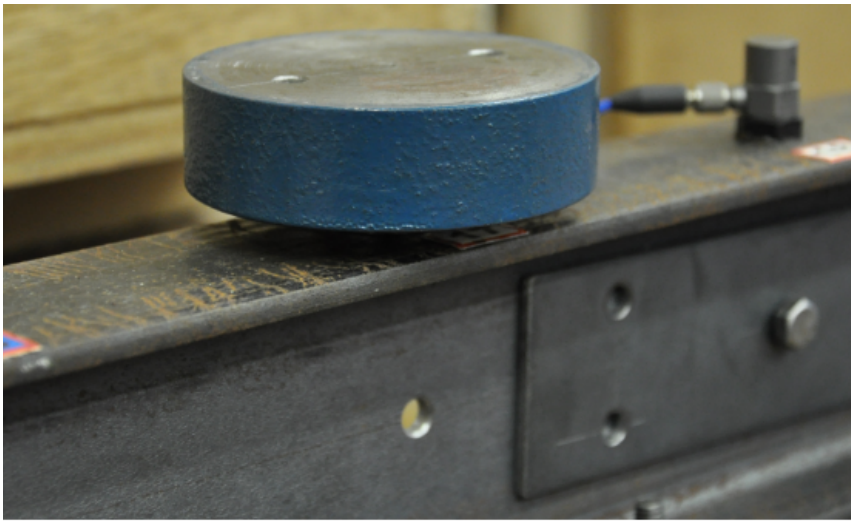

Figure A.2: Additional concentrated mass

A.3 Accelerometer

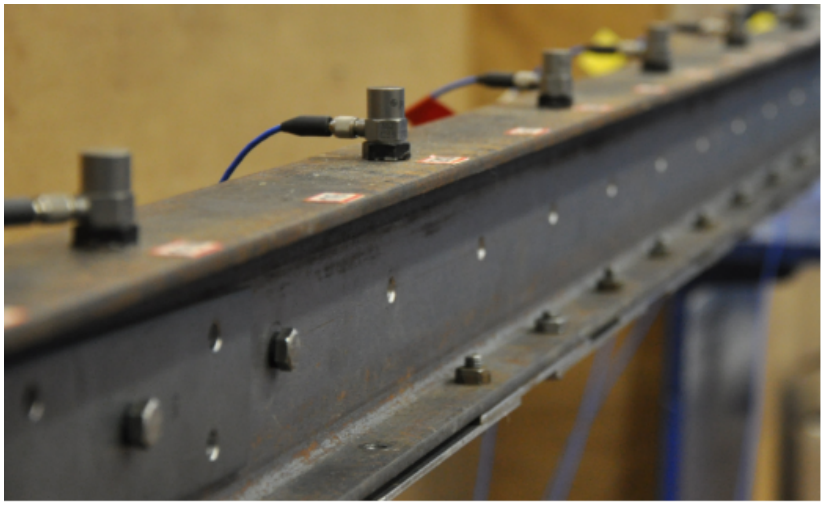

Figure A.3: Accelerometer sensor placement

References

Ahmad, S., Zabel, V. & Brehm, M. (2011). Vibration-based detection of structural damage in a railway bridge - a comparative study. *In Proc. International Conference on Structural Dynamics (EURODYN), Leuven, Belgium*. 54, 66, 80

Allemang, R.J. (2003). The modal assurance criterion - twenty years of use and abuse. *Sound and Vibration*, **37(8)**, 14–21. 32

Allemang, R.J. & Brown, D.L. (1982). A correlation coefficient for modal vector analysis. *In Proc. 1st International Modal Analysis Conference*. 32, 33

Balmès, È., Basseville, M., Mevel, L. & Nasser, H. (2008). Handling the temperature effect in vibration monitoring of civil structures: A combined subspace-based and nuisance rejection approach. *Control Engineering Practice*. 52

Basseville, M., Abdelghani, M. & Benveniste, A. (2000). Subspace-based fault detection algorithms for vibration monitoring. *Automatika*, **36**, 101–109. 18, 22

Bathe, K.J. (1982). *Finite Element Procedures in Engineering Analysis*. Prentice-Hall Inc., New Jersey, USA. 8

Begg, R.D., MacKenzie, A.C., Dodds, C.J. & Loland, O. (1976). Structural integrity monitoring using digital processing of vibration signals. *in Proc. 9th Annual Offshore Tech. Conf*, **-**, 305–311. 7

Box, G.E.P. & Draper, N.R. (1987). *Empirical Model-Building and Response Surface*. John Wiley & Sons, New York. 39

Box, G.E.P. & Wilson, K.B. (1951). On the experimental attainment of optimum conditions. *Journal of The Royal Statistical Society, Series B*, **13**, 1–45. 35

Brehm, M. (2011). Vibration-based model updating: Reduction and quantification of uncertaities. 70

Brehm, M. & Zabel, V. (2008). Comparison of modal and wavelet based damage indicators. *In Proc. International Conference on Noise and Vibration Engineering (ISMA), Leuven, Belgium*. 10

Brehm, M., Zabel, V. & Cantieni, R. (2009). Modelanpassung einer eisenbahnbrücke für den hochgeschwindigkeitsverkehr. *In VDI-Berichte - Baudynamik*, **2063**, 403–4018. 69

Breitkopf, P., Naceur, H., Rassineux, A. & Villon, P. (2005). Moving least squares response surface approximation: formulation and metal forming applications. *Computer & Structures*, **83**, 1411–1428. 45

Bucher, C.G. (1990). A fast and efficient response surface approach for structural reliability analysis. *Structural Safety*, **7(1)**, 57–66. 35

Buhmann, M.D. (2004). *Radial Basis Functions Theory and Implementation*. Cambridge University Press, Cambridge. 41, 42

Cantieni, R., Brehm, M., Zabel, V., Rauert, T. & Hoffmeister, B. (2009). Ambient testing and model updating of a filler beam bridge for highspeed trains. *In Proceeding of 7th European conference on structural dynamics (EURODYN), July 7-9 Southhampton, UK*. 69

Cornwell, P., Doebling, S.W. & Farrar, C.R. (1999a). Application of strain energy damage detection method to plate-like structures. *Journal of Sound and Vibration*, **224(2)**, 359–374. 10

Cornwell, P., Farrar, C.R., Doebling, S.W. & Sohn, H. (1999b). Environmental variability of modal properties. *Experimental Techniques*, **23(6)**, 45–48. 3, 51

Daraemaeker, A., Reynders, E., de Roeck, G. & Kullaa, J. (2008). Vibration-based structural health monitoring using output-only measurements under changing environment. *Mechanical Systems and Signal Processing*, **22**, 34–56. 52

Daubechies, I. (1992). *Ten Lectures on Wavelets*. Society for Industrial and Applied Mathematics (SIAM), Philadelphia. 10, 11, 13

De Clerk, J.P. & Avitable, P. (1998). Development of several new tools for pre-test evaluation. *Proceedings of the 16th International Modal Analysis Conference*, 1272–1277. 29

Doebling, S.W., Farrar, C.R. & Prime, M.B. (1998). A summary review of vibration-based damage identification methods. *Shock Vibration Digest*, **30**, 91–105. 8

Dynardo GmbH & Bauhaus University Weimar (2009). Slang - the structural language. 15, 70, 80

Egmont-Petersen, M., de Ridder, D. & Handels, H. (2002). Image processing with neural networks - a review. *Pattern recognition*, **35**, 2279–2301. 46

Ewins, D.J. (2000). *Modal Analysis Theory, Practice,and Applications*. Research Studies Press, Philadelphia. 32, 33, 34

Farrar, C.R., Baker, W.E., Cone, T.M., Darling, T.A., T. W. Duffey & Eklund, A., A. Migliori (1994). Dynamic characterization and damage detection in the i-40 bridge over rio grande. *Los Alamos National Laboratory Report: LA-12767-MS*. 51

Fasshauer, G.E. (2007). *Meshfree Approximation Method with MATLAB*. World Scientific, London. 41, 42

Forrester, A.I.J., Sobester, A. & Keane, A.J. (2008). *Engineering Design Via Surrogate Modeling : A practical guide*. John Wiley & Sons, Chicester. 49

Gabor, D. (1946). Theory of communication. *Journal IEEE*, **93(3)**. 11

Gao, R.X. & Yan, R. (2009). *Wavelets: Theory and Applications for Manufacturing*. Springer, New York. 11

Giunta, A.A., Wojtkiewicz Jr., S.F. & Eldred, M.S. (2003). Overview of modern design of experiments methods for computational simulations. *AIAA Paper*, **649**, 1–17. 36, 37

Grossmann, A. & Morlet, J. (1984). Decomposition of functions into wavelets of constant shape, and related transforms. *Lecture on recent results, Mathematics and Physics*. 11

Hagan, M.T., Demuth, H.B. & Beale, M. (1996). *Neural Networks Design*. PWS Publishing, Boston. 47

Hardy, R.L. (1971). Multiquadric equations of topography and other irregular surfaces. *J. Geophys. Res*, **76**, 1905–1915. 41

Hurtado, J.E. & Alvarez, D.A. (2001). Neural-network-based reliability analysis: a comparative study. *Computer methods Appl. Mech. Engrg*, **191**, 113–132. 47

Johnson, M.E., Moore, L.M. & Ylvisakei, D. (1990). Minimax and maximin distance design. *Journal of Statistical Planning and Inference*, **26**, 131–148. 38

Kammer, D.C. (1991). Sensor placement for on-orbit modal identification and correlation of large space structures. *Journal of Guidance, Control and Dynamics*, **14(2)**, 251–259. 28, 29, 30

Keane, A.J. & Nair, P.B. (2005). *Computational Approaches to Aerospace Design: The Pursuit of Excellent*. John Wiley & Sons, Chichester. 37

Knill, D.L., Giunta, A.A., Baker, C.A., Grossman, B., Mason, W.H., Haftka, R.T. & Watson, L.T. (1998). *Response surface models combining linear and Euler aerodynamics for HSCT design*. American Institute of Aeronautics and Austonautics, Inc., Virginia. 35

Lancaster, P. & Salkauskas, K. (1981). Surfaces generated by moving least squares methods. *Mathematics of Computation*. 45

Lancaster, P. & Salkauskas, K. (1986). *Curve and Surface Fitting: An Introduction*. Academic Press, London. 45

Levin, D. (1998). The approximation power of moving least-squares. *Mathematics of Computation*. 45

Li, D.S., Li, H.N. & Fritzen, C.P. (2007). The connection between effective independence and modal kinetic energy methods for sensor placement. *Journal of Sound and Vibration*, **305**, 945–955. 28, 29

Maia, N.M.N. & Silva, J.M.M. (1997). *Theoretical and Experimental Modal Analysis*. Research studies Press, Baldock, UK. 32, 34

Mallat, S.G. (1989). A theory for multiresolution signal decomposition: The wavelet representation. *IEEE Transactions on Pattern Analysis and Machine Intelligence*, **25**, 47–68. 13, 15, 80

Mallat, S.G. (1998). *A wavelet tour of signal processing*. Academic Press, San Diego, USA. 12

McKay, M.D., Beckman, R.J. & Conover, W.J. (1979). A comparison of three methods for selecting values of input variables in the analysis of output from a computer code. *Technometrics*, **21**, 239–245. 37

Mengelkamp, G. (2003). Entwicklung einer intelligenten struktur - eine kombination globaler und lokaler verfahren zur schadendiagnose. xiii, 18, 23, 24, 25

Metropolis, M. & Ulam, S. (1949). The monte carlo method. *Journal of American Statistical Association*, **44(247)**. 37

Most, T. (2008). An adaptive response surface approach for reliability analysis of discontinuous limit state functions. *In Proc. International probabilistic workshop, Darmstadt, Germany.*. 35

Myers, R.H., Montgomery, D.C. & Anderson-Cook, C.M. (2007). *Response Surface Methodology: Process and Product Optimization Using Designed Experiment*. John Wiley & Sons, New Jersey. 35

Newland, D.E. (1993). *An Introduction to Random Vibrations, Spectral and Wavelet Analysis*. Longman, Singapore. 11

Overschee, P.V. & Moor, B.D. (1996). *Subspace Identification for Linear Systems: Theory - Implementation - Application*. Kluwer Academic Publisher, Boston/London/Dordrecht. 18

Owen, B. (1994). Controlling correlations in latin hypercube samples. *Structural Safety*, **25**, 47–68. 38

Pandey, A.K., Biswas, M. & Samman, M.M. (1991). Damage detection from changes in curvatures mode shape. *Journal of Sound and Vibration*, **145(2)**, 321–332. 10

Papadopoulos, M. & Garcia, E. (1998). Sensor placement methodologies for dynamic testing. *AIAA Journal*, **36(2)**, 256–263. 29

Papadrakakis, M., Papadopoulos, V. & Lagaros, N.D. (1996). Structural reliability analysis of elastic-plastic structures using neural networks and monte carlo simulation. *Computer Methods in Applied Mechanics and Engineering*, **136(1)**, 145–163. 47

Peeters, B. (2000). *System Identification and Damage Detection in Civil Engineering*. PhD Thesis - Katholieke Universiteit Leuven, Belgien. 18

Peeters, B. & De Roeck, G. (2001). One year monitoring of the z24-bridge: Environmental effects versus damage evens. *Earthquake Engineering and Structural Dynamics*, **30**, 149–171. 3, 51

Poggio, T. & Girosi, F. (1990). Regularization algorithms for learning that are equivalent to multilayer networks. *Science*, **247**, 978–982. 44

Prevosto, M., Olagnon, M., Benveniste, A., , Basseville, M. & Le Ve, G. (1991). State space formulation: A solution to modal parameter estimation. *Journal of Sound and Vibration*, **148(2)**, 329–342. 18

Ren, W. & Sun, Z. (2008). Structural damage identification by using wavelet entropy. *Engineering Structures*. 10

Reynders, E., Schevenels, M. & De Roeck, G. (2011). Macec - a matlab toolbox for experimental and operational modal analysis. 103, 108

Reynier, M. & Abou-Kandil, H. (1999). Sensor location for updating problems. *Mechanical Systems and Signal Processing*, **13(2)**, 297–314. 28

Roux, W.J., Stander, N. & Haftka, R.T. (1998). Response surface approximations for structural optimization. *International Journal for Numerical Methods in Engineering*, **42**, 517–534. 35

Rytter, A. (1993). *Vibration Based Inspection of Civil Engineering Structures*. Denmark. 8, 67

Sacks, J., Welch, W.J., Mitchell, T.J. & Wynn, H.P. (1989). Design and analysis of computer experiments. *Journal of The American Statistical Assosiation*, **11**, 674–693. 37

Salawu, D.S. (1997). Detection of structural damage through change in frequency: a review. *Engineering Structures*. 9

Schueremans, L. & Van Gemert, N.D. (2005). Benefit of splines and neural networks in simulation based structural reliability analysis. *Structural Safety*, **27**, 145–163. 47

Schwarz, B., Richardson, M. & Avitabile, P. (2002). Locating optimal references for modal testing. *In Proc. of 20th International Modal Analysis Conference*. 28, 29

Shannon, C.E. & Weaver, W. (1949). *The Mathematical Theory of Communication*. University of Illinois, USA. 17

Sohn, H. (2008). Effects of environmental and operational variability on structural health monitoring. *Phil. Trans. R. Soc. A*, **365**, 539–560. 3, 52

Sohn, H., Dzwonczyk, M., Straser, E.G., Kiremidjian, A.S., Law, K.H. & Meng, T. (1999). An experimental study of temperature effects on modal parameters of the alamosa canyon bridge. *Earthquake Eng. Struct. Dyn.*, **28**, 879–897. 3, 51

Sohn, H., Worden, K., & Farrar, C.R. (2002). Statistical damage classification under changing environmental and operational condition. *Journa of Intelligent Material Systems and Structures*, **13**, 561–574. 52

Stubbs, N., Kim, J.T. & Topole, K. (1992). An efficient and robust algorithm for damage localization in offshore platforms. *Proceeding of the ASCE Tenth Structures Congress*, **-**, 543–546. 10

Sun, Z. & Chang, C.C. (2002). Structural damage assessment based on wavelet packet transform. *Journal of Structural Engineering*, **128**, 1354–1361. 10

Udwadia, F.E. (1994). Methodology for optimum sensor locations for parameter identification in dynamic system. *Journal of Engineering Mechanics*, **120(2)**, 368–390. 28

Upton, G. & Cook, I. (2008). *A dictionary of statistics*. Oxford University Press, Oxford. 60

Vandiver, J.K. (1977). Detection of structural failure on fix platforms by measurements of dynamic response. *Journal of Petroleum Technology*, **293**, 305–310. 7

Viberg, M. (1995). Subspace-based methods for the identification of linear time-invariant systems. *Automatica*, **31(12)**, 1835–1851. 18

Waters, T.P. (1995). *Finite Element Model Updating Using Measured Frequency Response Function*. United Kingdom. 34

Wendland, H. (2005). *Scattered Data Approximation*. Cambridge University Press, Cambridge. 41

Wojnarowski, M.E., Stiansen, S.G. & Reddy, N.E. (1977). Structural integrity evaluation of a fixed platform using vibration criteria. *in Proc. 9th Annual Offshore Tech. Conf*, **-**, 247–256. 7

Yao, L., Sethares, W.A. & Kammer, D.C. (1993). Sensor placement for on-orbit modal identification via a genetic algorithm. *AIAA Journal*, **31(10)**, 1922–1928. 28

Zabel, V. (2003). *Applications of Wavelet Analysis in System Identification.*. PhD Thesis - Bauhaus University Weimar, Germany. 10, 11

Zabel, V., Brehm, M. & Nikulla, S. (2010). The influence of temperature varying material parameters on the dynamic behavior of short span railway bridge. *In Proc. In-*

ternational Conference on Noise and Vibration Engineering (ISMA), Leuven, Belgium. 74